

UNIVERSITÀ DI PARMA

UNIVERSITÀ DEGLI STUDI DI PARMA

DOTTORATO DI RICERCA IN
SCIENZA E TECNOLOGIA DEI MATERIALI

CICLO XXXI

Dynamic Polyolefin Networks

Coordinatore:
Prof. Enrico Dalcanale

Tutore:
Prof. Roberta Pinalli
Dr. Jérôme Vachon

Dottorando: Jonathan Tellers

Anni 2015/2018



This work was supported by the Marie Skłodowska-Curie project: SUPRAmolecular polyolefins as oxygen BARRIER materials (SUPRABARRIER), which is funded through the European Union Horizon 2020 Program (H2020-MSCA-ITN-2014) under the Grand Agreement No. 642929.

The financial support from SABIC is gratefully acknowledged.

Dedication

Dedicated to my dad, who always tried to teach me that if you do not do things right, you should not do them at all, to my mum, for raising me and supporting me all the way up to this spot, even when I was a pain in the ass, and to my brother, for being a great inspiration and motivation for me to chase this dream.

Declaration

I declare that this thesis has been composed solely by myself and that it has not been submitted, in whole or in part, in any previous application for a degree. Except where states otherwise by reference or acknowledgment, the work presented is entirely my own. I further declare that all experiments and analyses done were performed by me or under my supervision.

Contents

Summary **1**

1 Fundamentals **5**
1.1 Motivation - Adaptable Polyolefins Networks 5
1.2 Supramolecular Chemistry 6
1.3 Adaptable Polymer Networks 9
1.4 Dynamic Mechanical Thermal Analysis 17

2 ODIN, a Novel Sextuple Hydrogen Bonding Motif **27**
2.1 A New Hydrogen Bonding Motif 29
2.2 Supramolecular Polymer Network Using Sextuple Hydrogen Bonding 35
2.3 Conclusions 37
2.4 Experimental Section 38
References 43
Appendix A 47

3 Dynamic Cross-Linking of Polyolefins *via* Hydrogen Bonding **51**
3.1 Dynamic Cross-Linking of Polyethylene *via* Sextuple Hydrogen Bonding Array 52
3.2 Dynamic Cross-Linking of Polypropylene *via* Sextuple Hydrogen Bonding Array 70
3.3 Conclusions 75
3.4 Experimental Section 76
References 81

Appendix B 88

4 Cavitand Functionalized Polyethylene **97**

4.1 Design and Synthesis of a Suitable Cavitand 98

4.2 Synthesis and Properties of Cavitand Functional Polymer Networks 99

4.3 Conclusions 105

4.4 Experimental 105

References 111

Appendix C 112

5 Polyethylene Vitrimers **117**

5.1 Functional Polyethylene for Vitrimer Synthesis 119

5.2 Vinylogous Urethane PE Vitrimers 121

5.3 DTA cross-linked PE-MA 135

5.4 Experimental Section 141

References 147

Appendix D 152

6 Epilogue **163**

6.1 Afterword 163

6.2 Way forward 165

References 167

Acknowledgements **169**

List of Publications **171**

Nomenclature

ODIN	1-(7-oxo-7,8-dihydro-1,8-naphtiridin-2-yl)urea 1
CAN	covalent adaptable network 1
D	donor 1
A	acceptor 1
PP	polypropylene 1
PE	polyethylene 1
PE-HEMA	poly (ethylene-*co*-(2-hydroxethyl methacrylate)) 2
DSC	differential scanning calorimetry 2
DMA	dynamic mechanical analysis 2
VTIR	variable temperature infrared spectroscopy 2
$\mathbf{K_a}$	association constant 2
UPy	ureidopyrimidone 2
η_{sp}	specific viscosity 2
$\mathbf{T_g}$	glass transition 2
E'	storage modulus (tension) 3
FTIR	Fourier transformed infrared spectroscopy 3
ACAC	acetylacetonate 3
MA	maleic anhydride 3
LPC	cross-links per chain 3
$\mathbf{E_a}$	activation energy 4
$\mathbf{M_n}$	number average molecular weight 4

DNA	deoxyribonucleic acid	6
PS	polystyrene	13
WLF	Williams–Landel–Ferry	
AFM	atomic force microscopy	13
$\mathbf{T_v}$	topology freezing temperature	15
$\mathbf{T_m}$	melting temperature	17
(HD)PE	high density polyethylene	17
DMTA	dynamic mechanical thermal analysis	17
ϵ	strain	17
σ	stress	18
E*	complex modulus (tension)	18
E"	loss modulus (tension)	18
Tan δ	tangent of delta	18
TOC-graphic	table of content graphic	
Napy	naphthyridine	28
NMR	nuclear magnetic resonance	32
$\mathbf{M_w}$	weight average molecular weight	35
SCXRD	single crystal X-ray diffraction	37
DMSO-d_6	dimethyl sulfoxide-d_6	38
ppm	parts per million	38
HDI	hexamethylene diisocyanate	41
EVOH	ethylene vinyl alcohol	52
HEMA	2-hydroxyethyl methacrylate	53
HTNMR	high temperature nuclear magnetic resonance	53
GPC	gel permeation chromatography	53
SCB	short chain branching	53
$X_\mathbf{c}$	degree of crystallinity	55
(LD)PE	low density polyethylene	55

DBTDL dibutyltin dilaurate . . . 55
EA elemental analysis . . . 55
TCE-d_2 tetrachloroethane-d_2 . . . 56
G' storage modulus (shear) . . . 63
G" loss modulus (shear) . . . 63
TGA thermogravimetric analysis . . . 64
OTR oxygen transmission rate . . . 68
WVTR water vapor transmission rate . . . 68
PP-MA polypropylene-*graft*-(maleic anhydride) . . . 70
TC thermal conductivity . . . 77
T_c crystallization temperature . . . 77
DMF dimethylformamide . . . 99
TCE tetrachloroethane . . . 102
PTFE polytetrafluoroethylene . . . 102
H_m melting enthalpy . . . 106
DCM dichloromethane . . . 109
DTA 4,4'-dithiodianiline . . . 118
PE-MA polyethylene-*graft*-(maleic anhydride) . . . 118
XYDIA *m*-xylylenediamine . . . 119
PACHE poly(ethylene-co-2-[methacryloyloxy]ethyl acetoacetate-co-2-hydroxyethyl methacrylate) . . . 119
DMAP 4-(dimethylamino)pyridine . . . 120
TAEA tris(2-aminoethyl)amine . . . 122
WAXD wide-angle X-ray scattering . . . 129
G* complex modulus (shear) . . . 130
τ characteristic relaxation time . . . 133
η viscosity . . . 133
Đ dispersity . . . 136

Summary

Conventional thermoplastics such as polyethylene (PE) and polypropylene (PP) are known for being easily processable, lightweight, robust, and low-cost materials. Some of their flaws include low wear, chemical, and solvent resistance. To overcome these flaws, it is common practice to cross-link these materials by means of irradiation, peroxide, or other chemical methods. While significantly improving the material properties, this presents the inherent downside that these cross-linked thermosets are no longer processable. To circumvent this issue, dynamic cross-links can be introduced, which either adapt or dissociate upon applying a stress.

The objective of this thesis was to first evaluate existing tools for the dynamic cross-linking of polymeric materials and, where possible, improve or provide new tools suitable to obtain adaptable polyolefin networks. Then, the implications of these dynamic cross-links for the material properties were elucidated, analyzing the dynamic mechanical and relaxation behavior, as well as investigating how these new properties relate to real world applications. To achieve this, dynamic cross-links based on multiple hydrogen bonding units, aromatic stacking of CAVITANDS, and a sub class of covalent adaptable networks (CANs), referred to as VITRIMERS, have been studied.

To provide additional tools for the dynamic cross-linking of polymers, a new multiple hydrogen bonding motif capable of reversible association was developed and described in Chapter 2. This motif, namely 1-(7-oxo-7,8-dihydro-1,8-naphtiridin-2-yl)urea (ODIN), is readily synthesized in two steps. X-ray crystallography revealed that its dimer is comprised of two regular and two bifurcated hydrogen bonds, resulting in a total of six hydrogen bonds. By alternating the arrangement of donor (D) and acceptor (A) moieties, a motif with a greater number of hydrogen bonds than the fields most commonly used

motif ureidopyrimidone (UPy), but with a lower association constant (K_a), can be obtained. Thereby, ODIN combines the directionality of multiple hydrogen bonding that provides increased resistance towards water with a relatively weak K_a of $4{\cdot}10^4$ M^{-1} (in $CHCl_3$). The weak K_a presents advantages when these moieties are embedded into apolar polymers, because the apolar polymer matrix stabilizes the dimer. For an inherently stronger motif (higher K_a), this could lead to processing issues. To demonstrate the potential of reversible cross-linking with this new multiple hydrogen bonding motif, liquid tri-functional JEFFAMINE T3000 bearing pendant amines was reacted with an isocyanate functionalized ODIN derivative, resulting in the moldable suprapolymer JEFFODIN. The specific viscosity (η_{sp}) of this suprapolymer dissolved in chloroform increased significantly faster with concentration compared to the non-functional oligomeric chains. The reversible nature of this cross-linking was apparent from variable temperature infrared spectroscopy (VTIR), based on the reduced intensity and shift of bands involved in hydrogen bonding.

In Chapter 3 the sextuple hydrogen bonding motif ODIN is used for the dynamic cross-linking of PE. By reacting ODIN bearing an aliphatic isocyanate with poly (ethylene-*co*-(2-hydroxethyl methacrylate)) (PE-HEMA), multiple hydrogen bonding array functionalized PEs with an ODIN content ranging from 1 to 6 mol% were obtained. Compared to the pristine material, the obtained PE-HEMA-ODIN had increased tensile strength, stiffness, gas and water barrier properties, and a remarkably increased melt strength evident from the observed plateau modulus after melting. The formation of a network structure was revealed by a significant increase in glass transition (T_g) and shear and tensile storage moduli. The apolar PE matrix was found to stabilize the new hydrogen bonding motif, because in contrast to the supramolecular polymer described in Chapter 2, no substantial dissociation of hydrogen bonds was observed up to 175 °C. The adaptable nature of the hydrogen bonding system was revealed *via* stress relaxation measurements and compression molding of thin films and sample strips. In comparison to UPy functionalized polymers, the fields most commonly employed multiple hydrogen bonding motif, differential scanning calorimetry (DSC) cycling and isothermal dynamic mechanical analysis (DMA) measurements found that

the thermal degradation of ODIN polymers occurred at 190 °C, which is about 40 °C higher than the degradation temperature determined for UPy polymers. At these temperatures the degradation mechanism involves a permanent cross-linking resulting in an increased storage modulus (tension) (E') during the isothermal DMA measurement performed at 190 °C. Due to the improved thermal stability of ODIN the concept could be extended to maleic anhydride (MA) functional PP, a polymer that usually melts above the degradation temperature of the UPy motif.

An alternative method to reversibly cross-link PE is investigated in Chapter 4, relying on the solvophobic reversible association of a quinoxaline CAVITAND in kite conformation with an K_a of 5 – $8.5 \cdot 10^4$ M^{-1} (in $CHCl_3$). Firstly, the CAVITAND was functionalized with an isocyanate group at the lower rim so that functionalization of a hydroxy or amine containing polymer can be readily achieved. Subsequently, this functional CAVITAND was reacted with PE-HEMA, and the resulting polymer was characterized by ^{1}H-NMR, DSC, and FOURIER transformed infrared spectroscopy (FTIR). Films with varying amounts of CAVITAND, obtained by solution casting and slow evaporation, were tested for their oxygen barrier properties, which were found lacking due to a severely reduced crystallinity and increased free volume as a result of introducing the bulky side group. Most significantly, the isocyanate functional CAVITAND provides a tool to easily introduce CAVITANDS into polymers, or to attach further functionality.

VITRIMERS are an emerging class of permanently cross-linked materials, that are dynamic because these cross-links can undergo thermally triggered exchange reactions. As a consequence, the network density is constant, but the materials are still malleable when the exchange reactions are fast enough. In Chapter 5, the introduction of exchangeable cross-links based on vinylogous urethanes and disulfides in PE is described, both in solution and in the melt. This is achieved by employing a suitable macromer precursor with pendant acetylacetonate (ACAC) or MA groups together with multifunctional amine cross-linkers. The focus was laid on reactive extrusion to demonstrate an industrially relevant, easy to up-scale pathway to PE VITRIMERS. A particular importance was placed on the varying amount of cross-links per chain (LPC), which could be controlled by varying the

number average molecular weight (M_n) and mol% of ACAC of the precursor polymer. Only after a sufficient amount of LPC to form a network structure were employed (>1.9 LPC), materials became insoluble with a maximum gel fraction of 65.3±4.4 %, and relaxation was controlled by the exchange kinetics following an ARRHENIAN dependence on temperature. Compared to vinylogous urethane VITRIMERS based on short chain oligomers, an almost twice as large activation energy (E_a) of 108±2 kJ·mol^{-1} was determined due to the reduced density of reactive groups in the polymer matrix. By repeated tensile tests and extrusion processing of the material, recyclability of up to four times could be demonstrated for a network with 2.6 LPC.

In closing, three methods to dynamically cross-link polyolefins were described, namely multiple hydrogen bonding, solvophobic interactions, and dynamic exchange reactions. Using a functional CAVITAND to obtain these systems appears to be the least appealing due to the synthetic effort involved and substantial size of the functional motif. In fact, the synthetic effort stopped an exhaustive investigation into the mechanical implications of the functional polymers simply due to the lack of sufficient material. Multiple hydrogen bonding and exchangeable cross-links were both effective tools to develop dynamic PE networks. The increased thermal stability and melt strength of these functional PE is useful for applications where high temperatures are used. Also, simply extruding materials with dynamic cross-links eliminates the need for "after the fact" static cross-linking. Implementing the VITRIMER technology into existing production can be readily done. Firstly, the precursor *co*-polymer can be prepared by catalyst free radical polymerization using methods employed for the production of PE. Secondly, the synthesis of the VITRIMER requires only one step that can be carried out inside the extruder, so that direct injection molding after synthesis is an option, combining processability of thermoplastics with thermoset resilience.

Chapter 1

Fundamentals

1.1 Motivation - Adaptable Polyolefins Networks

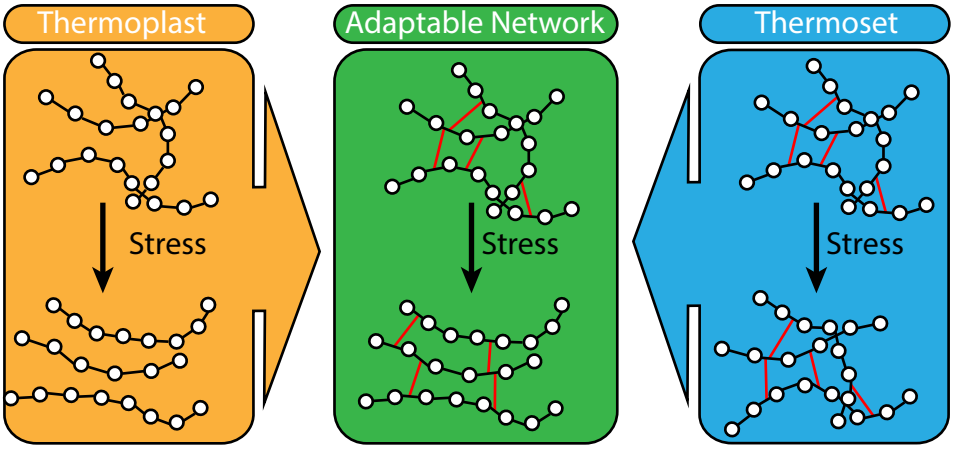

Figure 1.1: Illustration of the typical response to an exterior stress of thermoplastics, thermosets, and adaptable polymers in the melt.

Polyolefins are typically polymers made up of a carbon backbone chain with high molecular weight that are entangled or partially crystalline. Being thermoplastic, their main advantage is that they can be reshaped repeatedly by melting or softening at higher temperature, followed by subsequent hardening upon cooling when the new desired shape is obtained, usually a process that can take place within seconds.[1] For demanding applications, cross-linking of these long chain species or use of highly cross-linked polymer networks like BAKELITE[2] is common. These materials have greater dimen-

sional stability, are insoluble, and have increased resistance to abrasion and wear compared to thermoplastics. Their main disadvantage is that once cross-links are in place, the morphology is set, requiring that they have to be cured inside the mold.

For the last decades, there has been a growing research interest in materials that combine the processability of thermoplastic polymers such as PE and PP with the superior mechanical performance of thermosets by introducing dynamic cross-links that are frozen at process-, but active at elevated temperatures (Figure 1.1).[3–6] These materials promise that all thermoset polymers employed in demanding environments will be recyclable. This is a much needed change, as also political entities such as the European Commission are pushing for all plastic packaging to be recyclable by as early as 2030.[7]

1.2 Supramolecular Chemistry

According to Jean-Marie Lehn, one of the recipients of the Nobel Prize awarded in the field of supramolecular chemistry in 1987,[8] "Supramolecular chemistry has been defined as **chemistry beyond the molecule**, as it aims at designing and implementing functional chemical systems based on molecular components held together by noncovalent intermolecular forces".[9] Despite the relatively weak nature of these noncovalent interaction (excluding ionic bonding), they exert a huge influence in nature acting in unison to self-assemble complex structures.[10,11]

Specifically, ion-dipole and dipole-dipole interactions, hydrogen bonding, metal coordination, hydrophobic forces, van der Waals forces, π-π interactions, and electrostatic effects are considered as supramolecular interactions. The arguably most prominent type of supramolecular interaction is a special type of dipole-dipole interactions, the hydrogen bonds. Their importance is famously highlighted on the example of deoxyribonucleic acid (DNA), where complimentary base pairs (purines and pyrimidines) allow for the reversible assembly of two sugar phosphate strands, a mechanism of utmost importance for the storage of information in organisms.[11]

The main motivation to pursue supramolecular chemistry stems from the

Table 1.1: Functional groups that can form hydrogen bonds, arranged by element.

Element	Donors	Donor str.	Acceptors	Acceptor str.
fluorine	F–**H**	very strong	$\mathbf{F}^-$	very strong
			F–H	strong
oxygen	O–**H** (in an acid)	strong	$^-$**O**–P, $^-$**O**–S, $^-$**O**–C	strong strong
oxygen	O–**H** (in water, or alcohols)	medium	**O**=P, **O**=S, **O**=C, H_2**O**, H–**O**–C, C–**O**–C	medium-strong medium
nitrogen	N^+–**H**	strong	C=**N**–C	medium
nitrogen	N–**H**	medium	**N**$(R)_3$	medium
sulfur	S–**H**	weak	**S**=C	medium-weak
carbon	C–**H**	weak	π-electrons	weak

desire to explore and understand the self-assembled systems in biology such as DNA, and to use the thereby acquired knowledge in the synthesis of artificial complimentary molecules able to assemble in desired structures.[12–15]

1.2.1 Hydrogen Bonding and Multiple Bonding Groups

A hydrogen bond describes the non-covalent interaction between two partially charged hydrogen bonding donor (D) (partially negative) and acceptor (A) (partially positive) species, with the name-giving example being between a proton and oxygen in e.g. water. Some of the typical examples of functional groups taking part in hydrogen bonding and their relative strength are summarized in Table 1.1.[16]

Multiple hydrogen bonding occurs in a class of molecules where more than one hydrogen bond arranged in an array work together to form an assembled species with either itself (homo-dimerization), or with another complimentary molecule (hetero-dimerization). The most well-known example of these types of molecules are found in DNA,[11] where complimentary base pairs mostly directed by hydrogen bonding assemble to connect the strands of the DNA. The tendency of these molecules to assemble is captured by the K_a, which is defined by the rate of association of dimers divided by the rate of dissociation

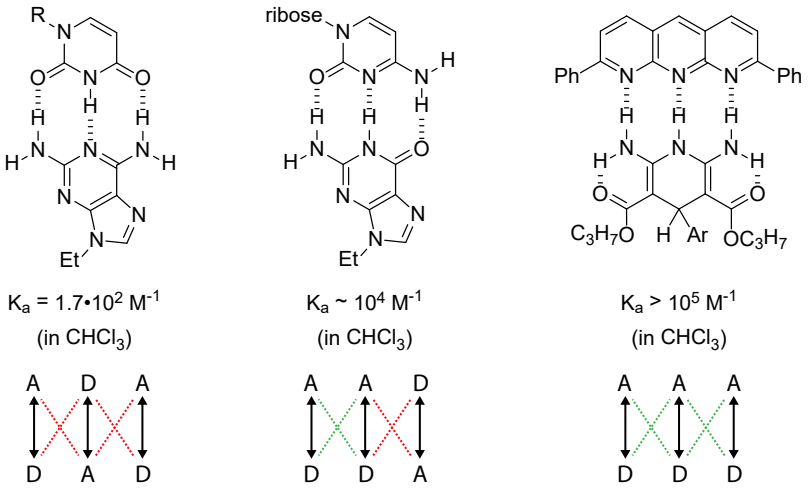

Figure 1.2: Examples of triple hydrogen bonding pairs, their K_a in $CHCl_3$,[18] and their arrangement of donor (D) and acceptor (A) groups according to Jorgensen.[19]

(Eq. 1.1). Consequently, the association is reversible and dissociation can be triggered by external stimuli such as temperature.[17]

$$K_a = \frac{k_{Ass}}{k_{Diss}} \tag{1.1}$$

For the design of these molecules not only the number of hydrogen bonds, but also the arrangement of D and A moieties is important. This concept was first captured by Jorgensen *et al.*, who found that for molecules with the same amount of hydrogen bonding groups, favorable and unfavorable cross-interactions between D and A moieties not directly opposite to each other have a big influence on K_a. For example, for complimentary molecules with an array of three hydrogen bonds, there are three possible arrangements that result in either none, one, or two beneficial cross-interactions (AAA–DDD; AAD–DDA; ADA–DAD), each increasing the association tendency of the respective molecule (see Figure 1.2).

1.2.2 Cavitands

Cavitands are a class of cage molecules that are mainly known for their excellent complexation capabilities in host-guest chemistry.[20,21] One of

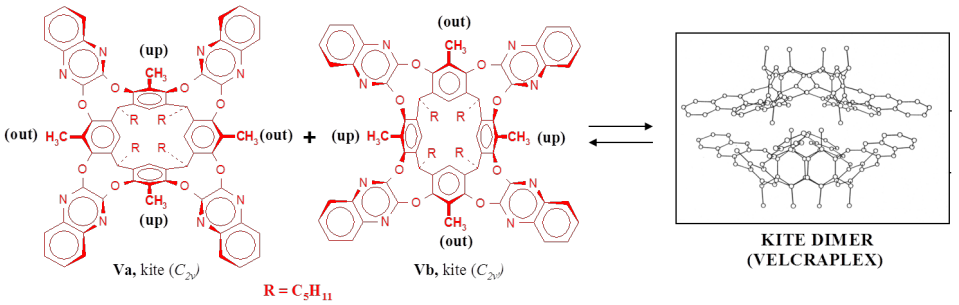

Figure 1.3: Dimerization of quinoxaline kite cavitand with related crystal structure.

the most prominent CAVITANDS is the 4-quinoxaline CAVITAND (structure in Figure 1.3).[22] Generally, two configurations of this CAVITAND are differentiated, the "vase" form with four quinoxaline flaps in axial position (aaaa) and the "kite" form with four quinoxaline flaps in equatorial position (eeee).[22,23] As a kite, this CAVITAND can interact with itself in such a way that it forms dimers, thanks to a combination of VAN DER WAALS and π-π interactions. The K_a of this system was found to be $8.5 \cdot 10^4$ M^{-1} in chloroform.[24] The reversible association of these dimers allows for the assembly of polymeric structures,[25,26] showing potential for the use of kite CAVITANDS as reversibly chain extending or cross-linking moieties similar to multiple hydrogen bonding motifs.

1.3 Adaptable Polymer Networks

Polymer networks are per definition a single, highly connected molecule, obtained by cross-linking of either small multi-functional molecules, or interconnected functional main chain polymers. Originally, only one type of polymer networks, thermosetting plastics that after synthesis cannot be reshaped or remolded, were known. In recent years, a new class of networks called adaptable polymer networks emerged. These are networks in which cross-links are adaptable, making reprocessing of the cross-linked polymers possible.

Adaptable polymer networks can be further divided into two sub-classes, which are supramolecular networks and CANs. Supramolecular networks

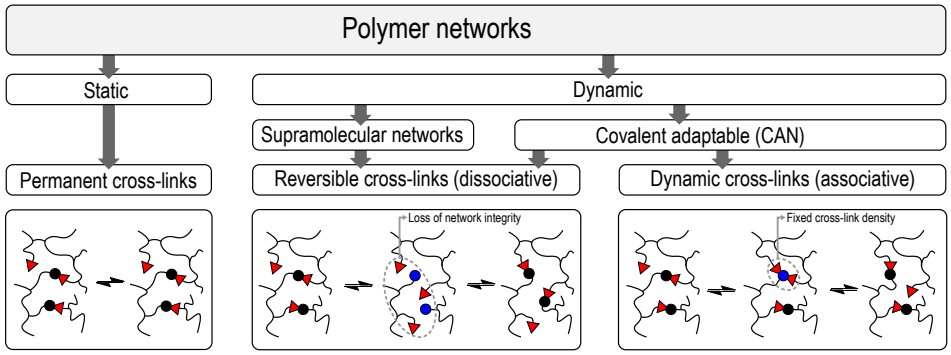

Figure 1.4: Classes of polymer networks and illustration showcasing the fundamental difference between permanent, reversible, and dynamic covalent networks.

make use of non-covalent interactions that provide cross-linking sites, whereas CANs are made up of reactive covalent bonds. Two types of CANs are recognized based on their exchange mechanism, dissociative and associative. Dissociative CANs are fully reversible networks, as cross-links dissociate from each other which is accompanied by a loss of the network integrity. Typical examples include Diels-Alder networks. On the other hand, associative CANs adapt according to an associative mechanismn. Since exchanges of cross-links only occur after a new cross-link is formed, the network integrity is kept intact due to a fixed cross-link density. It may be noted here, that supramolecular networks and dissociative CAN are both a type of reversible network, and it also makes sense to group polymer networks based on their network characteristics and not their type of cross-links. An overview of the types of polymer networks and an illustration of the fundamental difference between the cross-linking mechanisms is shown in Figure 1.4. Supramolecular polymer networks and a special type of associative CAN called Vitrimers will be further discussed due to their relevancy for this thesis.

1.3.1 Supramolecular Polymers and Polymer Networks

Supramolecular polymers are materials in which monomers and macromers assemble to larger superstructures thanks to highly directive, reversible interactions between themselves. Per definition, these interaction have to

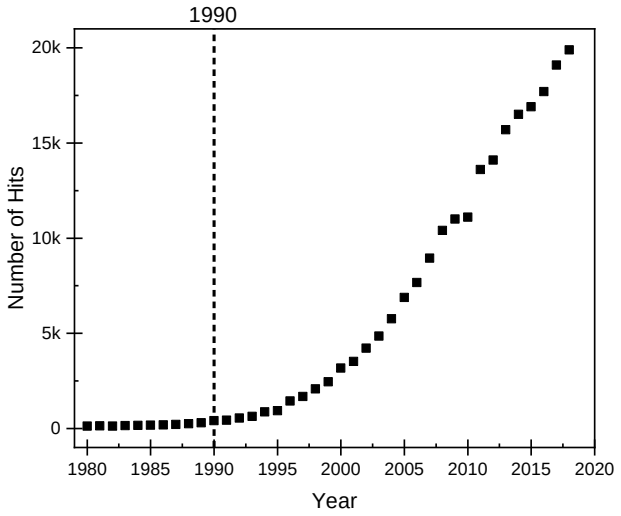

Figure 1.5: Number of hits on Google Scholar for the search term "Supramolecular Polymer" since 1980. Survey conducted on 01-07-2018. Counts for 2018 projected considering the count rate when survey was conducted.

be strong enough to impart polymeric properties in solution and in bulk.[27] All of the non-covalent interactions listed in 1.2 are suitable, but they need to be directed and strong enough so that the assembly is thermodynamically favored. Directionality and increased interaction strength are usually achieved by combining multiples of the same type of interaction, as is the case with multiple hydrogen bonding and Cavitands described in section 1.2.1 and 1.2.2, respectively. The most common strategies include the use of complimentary hetero- or homo multiple hydrogen bonding dimers,[5,28,29] metal-ligand coordination,[30–33] host-guest interactions,[34–38] or a combination of multiple types of interactions.[39]

After the first publication of a supramolecular polymer employing multiple hydrogen bonding in 1990 by Lehn *et al.*,[40] the interest in the field of supramolecular polymers has been on a steady increase (see Figure 1.5). One elegant example showcasing how commodity plastics could be assembled from short chain macromers was published by Meijer *et al.*, which reacted oligomers of poly(ethylene/butylene) bearing reactive OH end groups with

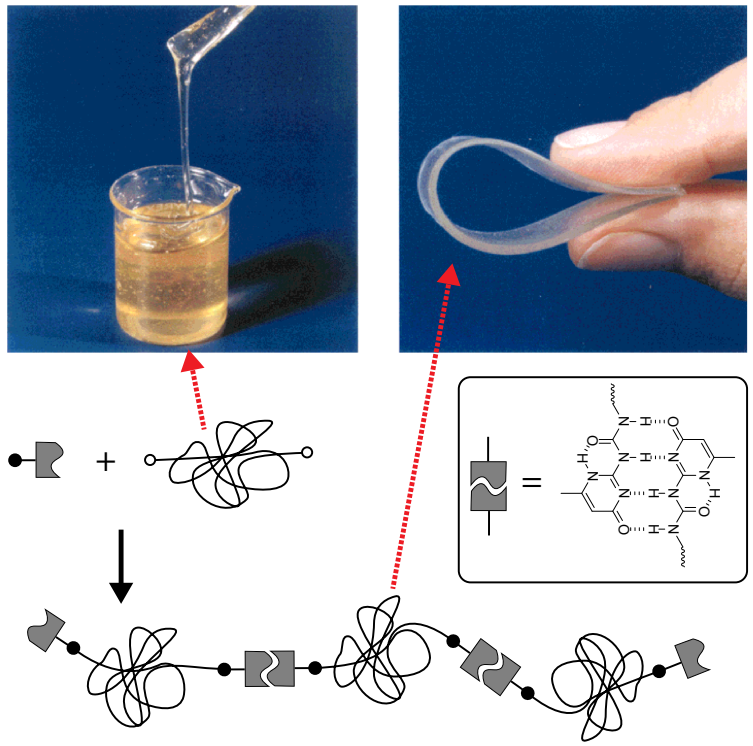

Figure 1.6: Poly(ethylene/butylene) with OH end groups (top left), poly(ethylene/butylene) functionalized with UPy (top right). The schematic shows the functionalization of telechelic polymers with UPy. The arrows indicate which schematic represents the material in the picture. Figure adapted from literature with permission.[5]

the quadruple hydrogen bonding motif UPy. The UPy motif is able to homo-dimerize and can therefore be used to connect the macromers with each other. As illustrated in Figure 1.6, the highly viscous polymer with OH end groups becomes plasticized after introduction of UPy, a result of the concatenation of monomers.[5] This represents a substantial change in material properties at room temperature. Upon heating however, melt viscosity was found to drop drastically, allowing for easy processing of the material, which showcases the potential of this strategy.

In the above case, using telechelic macromolecules led to formation of linear polymers through chain extension. However, the same principle can be employed to obtain cross-linked network structures, requiring more than two

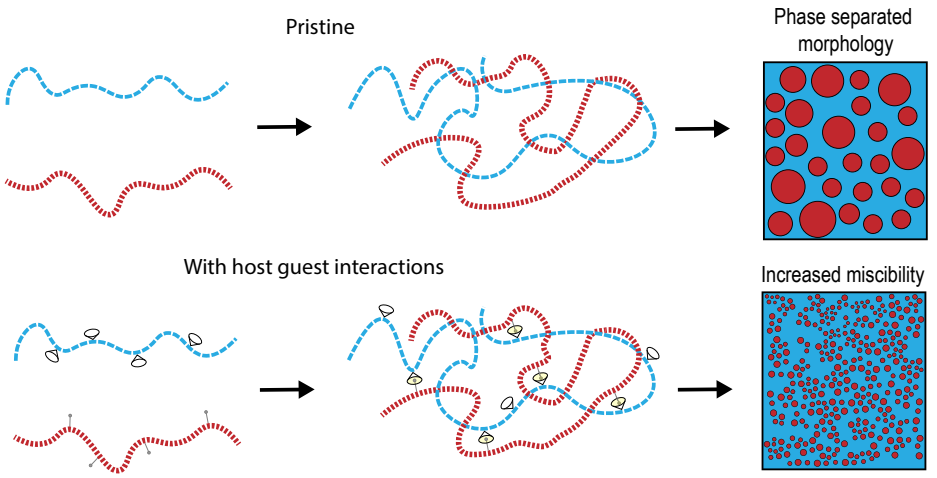

Figure 1.7: Illustration of the concept to compatibilize immiscible polymers by using host guest interaction.

connection points. By using either branched monomers,[41,42] or polymers with functional side chains,[29,36] supramolecular networks with properties of cross-linked material like e.g. epoxy resins can be obtained, with the added benefit of reprocessability of the materials.[42] This method is also suitable to compatibilize polymers, introducing complimentary moieties on two different, usually immiscible, polymers. For example, side chain functionalization of polystyrene (PS) with a tetraphosphonate cavitand (host) and of a methacrylate polymer with methylpyridinium (guest), resulted in an improved miscibility between the two polymers, evident from the improved morphology observed *via* atomic force microscopy (AFM).[36] A similar feat was achieved by using complimentary multiple hydrogen bonding heterodimers UG and DAN. These dimers hardly self-dimerize, but have a high affinity towards each other. By functionalizing two polymers, miscibility was achieved largely avoiding phase separation.[29,43] The concept is illustrated in Figure 1.7, exemplified for the host guest approach.

1.3.2 Vitrimers

Vitrimers are a type of associative CAN, in which thermally triggered exchange reactions of cross-links facilitate network rearrangement, making

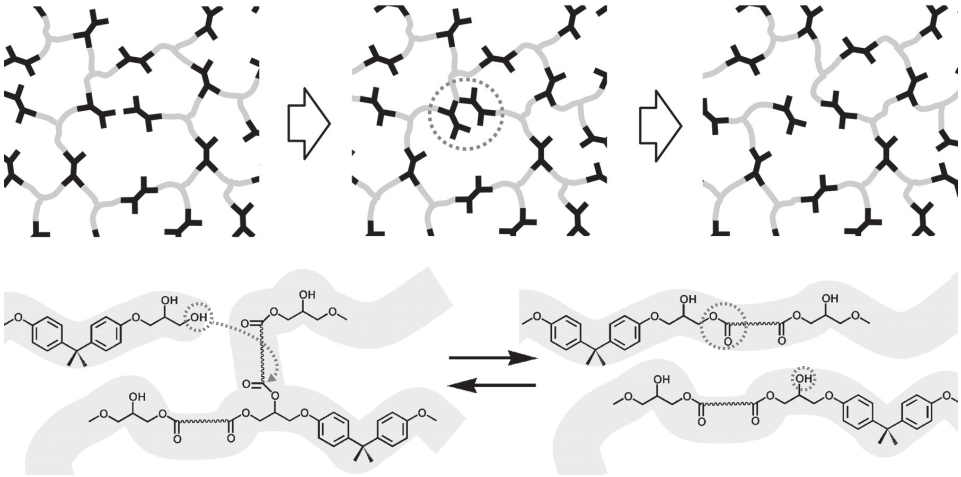

Figure 1.8: Transesterification reaction reshuffling cross-link in a polyester epoxy resins. Reproduced with permission from literature.[46]

macroscopic reshaping possible.[44–51] Pioneered by LEIBLER *et al.*, the earliest examples of VITRIMERS were exclusively based on the transesterification chemistry.[44–46,49,52–55] LEIBLER found, that with residual amounts of Zn(II) catalyst present inside the polyester matrix, the thermoset proved to be malleable at elevated temperatures.[44–46] Malleability is provided by transesterification reactions occurring in the network, where free hydroxy groups perform a nucleophilic attack on the ester groups, resulting in reshuffling of the bonds that make up the cross-links (see Figure 1.8).

If a stress is applied to the system, cross-links will rearrange until the stress relaxes and a new shape is obtained. The relaxation process is therefore controlled by the reaction kinetics and consequently the viscosity in the melt decreases following the ARRHENIUS law. This is a distinct difference compared to conventional polymers such as PS, where the viscosity drops abruptly after reaching the T_g (see Figure 1.9).[46,56] This property is similar to that of vitreous silica, hence the origin of the name VITRIMERS. Because new cross-links are only formed after association of another functional group with the existing cross-link, VITRIMERS keep a constant cross-link density and the network integrity stays intact.[47] Both of the aforementioned points distinguish VITRIMERS from supramolecular polymers described in 1.3.1, which lose their connectivity at elevated temperatures leading to

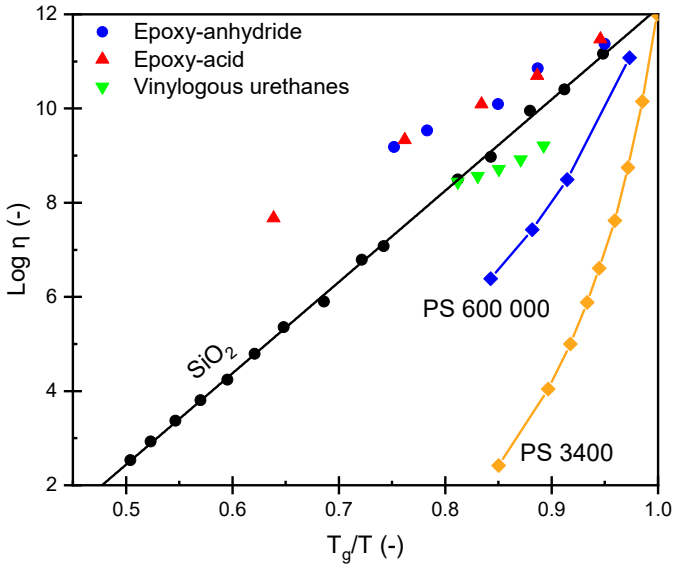

Figure 1.9: ANGELL fragility plot, showing the viscosity as a function of the inverse temperature, scaled with T_g (or T_v for VITRIMERS when $T_v > T_g$). Thermoplastics such as PS[57] are characterized with a narrow T_g, and thus a very fast decrease in viscosity near T_g. In contrast, VITRIMERS (epoxy-anhydride based, epoxy-acid based[46] and vinylogous urethanes[48]) show an ARRHENIUS like dependence of the viscosity, which results in a gradual viscosity decrease similar to vitreous silica.[58] - Published by The Royal Society of Chemistry.[47]

de-polymerization and different relaxation properties in the melt.

Two temperatures characterize the major transitions occurring inside a VITRIMER network. One is the well-known T_g, associated with the onset of large chain movement of the polymer backbone. Below T_g, the material behaves like a hard glassy solid, whereas above, the material is soft and rubber like. The other temperature is related to the exchange reactions of the VITRIMER network. Until exchange reactions become fast enough, the network is set, and the topology cannot change. This temperature is denoted as topology freezing temperature (T_v), and the established convention is to place T_v at the solid to liquid transition point where a viscosity of 10^{12} Pa·s is reached.[46,59]

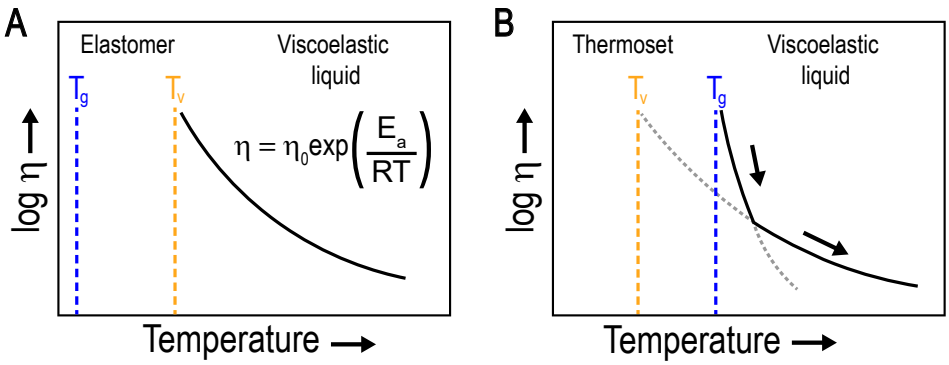

Figure 1.10: Representation of the viscoelastic behavior of VITRIMERS with **A**: A T_g lower than T_v. Upon heating, the VITRIMER evolves from a glassy solid ($T < T_g$) to an elastomer ($T_g < T < T_v$) to a viscoelastic liquid ($T > T_v$) that follows the ARRHENIUS law. **B**: A hypothetical T_v is situated well below T_g. Upon heating, the VITRIMER evolves from a glassy solid to a viscoelastic liquid with a viscosity that is first controlled through diffusion (WLF law) and then by the exchange kinetics (ARRHENIUS) - Reproduced from a publication by The Royal Society of Chemistry.[47]

The relative position of these two temperatures has implications for the viscosity profile of VITRIMERS, and can be illustrated neatly with the scheme presented in Figure 1.10.[47] In the first case, seen in Figure 1.10 **A**, the T_g is situated below T_v, and the VITRIMER will first behave like a glassy solid below T_g, then like an elastomer above T_g, and finally, when T_v is reached, the viscosity will decline following the ARRHENIUS law because viscosity is predominantly controlled by the exchange reactions. In the second case, illustrated in Figure 1.10 **B**, the T_v has a relative placement below T_g, representing fast exchange reactions in a rigid matrix. This will cause the material to essentially behave like a thermoset, because even if T_v is reached, exchange reactions will not take place because of the limited movement below T_g. After passing the T_g, exchange reactions are already fast, and the viscosity will first decrease sharply due to motion of the polymer chains following the WILLIAMS–LANDEL–FERRY (WLF) law (diffusion controlled).[60] After raising the temperature further, the viscosity will again be dominated by the exchange reactions, showing the typical ARRHENIAN decline. This latter case was recently observed for the first time by GUAN *et al*, who studied the exchange reactions of silyl ether embedded

inside a PS matrix.[61] In case of semi-crystalline polymers, also the melting temperature (T_m) has to be considered. For sufficiently crystalline polymers, T_m will have a similar influence as T_g, below which the topology is frozen due to the physical connections provided by the crystals inhibiting the exchange reactions.

Following the initial exploration of transesterification chemistry, a multitude of different exchange chemistries have been explored for the preparation of VITRIMERS and VITRIMER-like materials, such as disulfide metathesis,[50,62] transcarbonation,[51] imine amine exchange,[63] silyl ether exchange,[61] vinylogous transamination,[48,64–67] olefin metathesis,[68,69] transalkylation of triazolium[70] and trialkylsulfonium salts,[71] and boronic ester transesterification and metathesis,[72,73] some of which have been discussed in a recent review.[47] Only few of these chemistries have been used to functionalize commercial plastics. The viscostiy and melt strength of poly(butylene terephthalate) and high density polyethylene ((HD)PE) were tuned making use of the transesterification and boronic ester chemistry,[49,74] which also reduced creep and improved the dimensional stability of the latter.[72] Silyl ether chemistry was used to design a PS VITRIMER.[61]

An overview of potential applications for VITRIMERS is given by XIS *et al.*.[75] VITRIMERS promise to affect the landscape of thermosets significantly, potentially leading into a future in which all polymers are recyclable and land-filling/incineration will be significantly reduced.[6,76,77]

1.4 Dynamic Mechanical Thermal Analysis

In this section, the major informations that can be obtained from dynamic mechanical thermal analysis (DMTA) of polymers will be briefly mentioned. DMTA is a technique most useful for the polymer chemist to detect motions and transitions occurring inside the polymer matrix. In DMTA, the response of a polymer subjected to a small oscillatory (sinusoidal) strain (ϵ) is monitored (see Figure 1.11). The ϵ has to be small enough so that the displacement is fully reversible, which is referred to as the linear viscoelastic regime of the polymer. A related familiar experiment that probes the mechanical response is the measurement of stress-strain curves. The slope of

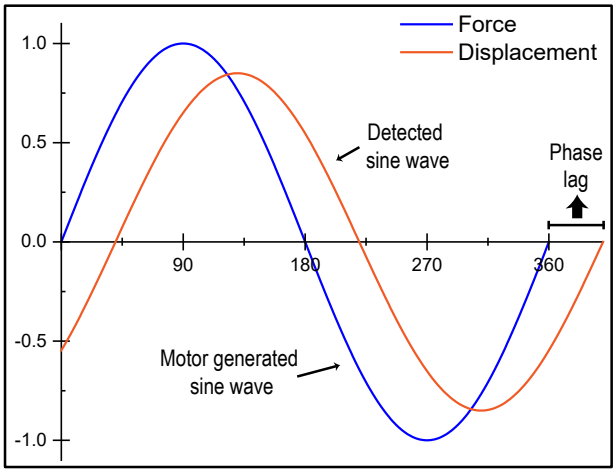

Figure 1.11: The DMA supplies an oscillatory force, causing a sinusoidal stress to be applied to the sample, which generates a sinusoidal strain. By measuring both the amplitude of the deformation at the peak of the sine wave and the lag between the stress and strain sine waves, quantities like the modulus, the viscosity, and the damping can be calculated.

the initial part of the stress-strain curve is the YOUNG's modulus, which is essentially the ratio between the applied ϵ and the resulting stress (σ).

In DMTA, the observed modulus is referred to as complex modulus (tension) (E*). The YOUNG's modulus and E* are not exactly the same, and there is usually a phase lag between the applied σ and the observed ϵ (see Figure 1.11). For an ideal solid the ϵ curve would be exactly in phase with the σ curve, whereas for a purely viscous liquid a phase lag of 90° would be observed. The E* can be separated into an in phase (elastic) and out of phase (viscous) response (equation 1.2). The real part referred to as the storage modulus (tension) (E') represents the elastic response of the material and is described by equation 1.3. The imaginary part called loss modulus (tension) (E") represents the viscous response of the material and is described by equation 1.4. The ratio of E" and E' is the tangent of delta (Tan δ) (equation 1.5), and is often referred to as damping, or the ability of the material to lose energy as heat.[78]

$$E^* = E' + iE'' \tag{1.2}$$

$$E' = \frac{\sigma_0}{\epsilon_0} \cdot \cos\delta \tag{1.3}$$

$$E'' = \frac{\sigma_0}{\epsilon_0} \cdot \sin\delta \tag{1.4}$$

$$\text{Tan } \delta = \frac{E''}{E'} \tag{1.5}$$

In contrast to conventional stress-strain tests, DMTA allows to easily test multiple frequencies and temperatures. For example, applying a sine wave every second, ergo a frequency of 1 Hz, allows to obtain a data point every second. For reasonably slow temperature changes (conventionally 3 $K \cdot min^{-1}$), a detailed modulus vs temperature curve can be obtained. An idealized DMTA scan of the E' as a function of temperature is illustrated in Figure 1.12, showcasing the influence of different polymer motions on the observed E'.[78]

Relaxations are conventionally numbered in Greek letters starting from high temperatures. Therefore, in semi-crystalline polymers, T_α corresponds to the melting temperature. Thermosets, thermoplastics, rubbers, and adaptable networks all show very different and characteristic temperature responses, and DMTA provides and excellent tool to distinguish between them. The monitoring of transitions is also important to assess whether the material in question can be used within a certain temperature operating range without major changes in properties.[78] Most critically, the operating range of most polymeric sample is defined at either below or above T_g, where large scale chain motions drastically change the polymer properties. It should be noted that DMTA is generally quoted as the most sensitive method for the determination of the T_g, showcasing its importance for the material scientist.[78,79]

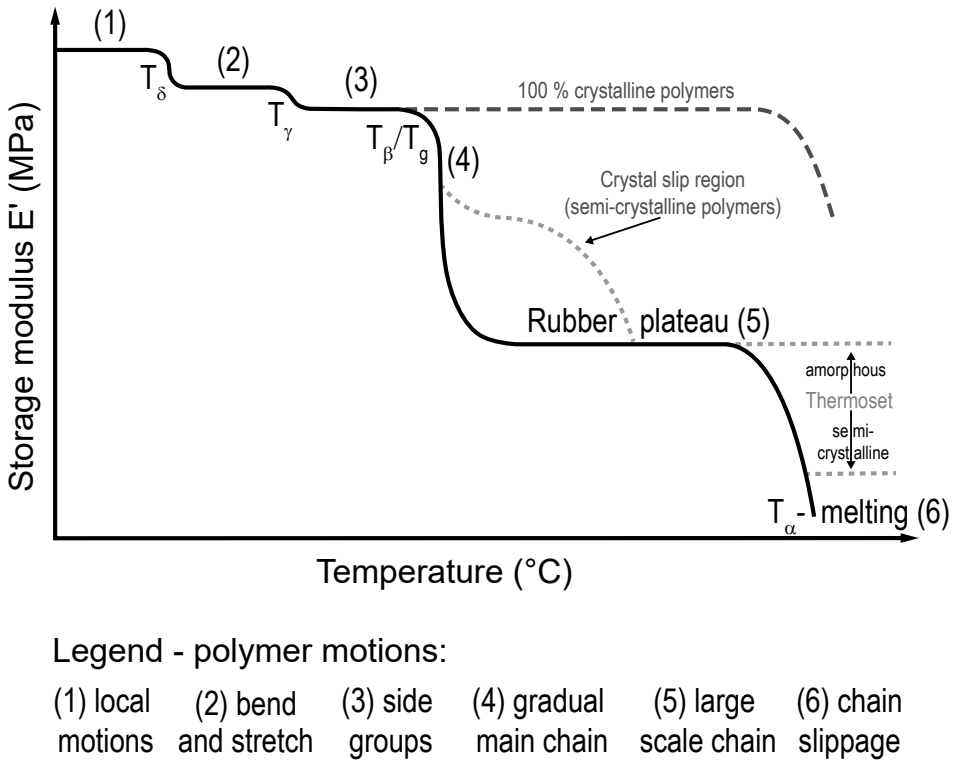

Figure 1.12: An idealized DMTA graph illustrating the effect of various molecular relaxations on the E' – Figure adapted from literature.[78]

References

[1] M Razavi-Nouri, *Iran. J. Chemcial Eng.* **2012**, *9*, 60–68.

[2] L. H. Baekeland, *Ind. Eng. Chem.* **1909**, *1*, 149–161, DOI 10.1021/ie50003a004.

[3] C. L. Lewis, K. Stewart, M. Anthamatten, *Macromolecules* **2014**, *47*, 729–740, DOI 10.1021/ma402368s.

[4] M. Staropoli, A. Raba, C. H. Hövelmann, M.-S. Appavou, J. Allgaier, M. Krutyeva, W. Pyckhout-Hintzen, A. Wischnewski, D. Richter, *J. Rheol. (N. Y. N. Y).* **2017**, *61*, 1185–1196, DOI 10.1122/1.5001059.

[5] B. J. B. Folmer, R. P. Sijbesma, R. M. Versteegen, J. A. J. Van Der Rijt, E. W. Meijer, *Adv. Mater.* **2000**, *12*, 874–878, DOI 10.1002/1521-4095(200006)12:12<874::AID-ADMA874>3.0.CO;2-C.

[6] L. Imbernon, S. Norvez, L. Leibler, *Macromolecules* **2016**, *49*, 2172–2178, DOI 10.1021/acs.macromol.5b02751.

[7] European Commission, First-ever Europe-wide strategy on plastics, **2018**.

[8] Nobel Media AB 2014, Press Release: The 1987 Nobel Prize in Physics, **2014**.

[9] J.-M. Lehn, *Chem. Soc. Rev.* **2017**, *46*, 2378–2379, DOI 10.1039/C7CS00115K.

[10] A. Klug, *Angew. Chemie Int. Ed. English* **1983**, *22*, 565–582, DOI 10.1002/anie.198305653.

[11] J. D. Watson, F. H. Crick, *Nature* **1953**, *171*, 737–738, DOI 10.1038/171737a0.

[12] S. P. Newton, J. F. Stoddart, W. Hayes, *Supramol. Sci.* **1996**, *3*, 221–236, DOI 10.1016/S0968-5677(96)00063-6.

[13] S. C. Zimmerman, P. S. Corbin, *Struct. Bond.* **2000**, *96*, 63–94, DOI 10.1007/3-540-46591-X_3.

[14] G. M. Whitesides, J. P. Mathias, C. T. Seto, *Science* **1991**, *254*, 1312–1319, DOI 10.1126/science.1962191.

[15] D. Philp, J. Fraser Stoddart, *Angew. Chemie (International Ed. English)* **1996**, *35*, 1154–1196, DOI 10.1002/anie.199611541.

[16] G. A. Jeffrey, W. Saenger, *The Importance of Hydrogen Bonds*, Springer Berlin Heidelberg, Berlin, Heidelberg, **1994**, DOI 10.1007/978-3-642-85135-3_1.

[17] S. Sivakova, S. J. Rowan, *Chem. Soc. Rev.* **2005**, *34*, 9, DOI 10.1039/b304608g.

[18] S. K. Yang, S. C. Zimmerman, *Isr. J. Chem.* **2013**, *53*, 511–520, DOI 10.1002/ijch.201300045.

[19] W. L. Jorgensen, J. Pranata, *J. Am. Chem. Soc.* **1990**, *112*, 2008–2010, DOI 10.1021/ja00161a061.

[20] D. J. Cram, *Science* **1983**, *219*, 1177–1183, DOI 10.1126/science.219.4589.1177.

[21] D. J. Cram, *Angew. Chemie Int. Ed. English* **1986**, *25*, 1039–1057, DOI 10.1002/anie.198610393.

[22] J. R. Moran, J. L. Ericson, E. Dalcanale, J. A. Bryant, C. B. Knobler, D. J. Cram, *J. Am. Chem. Soc.* **1991**, *113*, 5707–5714, DOI 10.1021/ja00015a026.

[23] F. Lagugné-Labarthet, Y. Q. An, T. Yu, Y. R. Shen, E. Dalcanale, D. K. Shenoy, *Langmuir* **2005**, *21*, 7066–7070, DOI 10.1021/la050821n.

[24] D. J. Cram, H. J. Choi, J. A. Bryant, C. B. Knobler, *J. Am. Chem. Soc.* **1992**, *114*, 7748–7765, DOI 10.1021/ja00046a022.

[25] L. Pirondini, A. G. Stendardo, S. Geremia, M. Campagnolo, P. Samorì, J. P. Rabe, R. Fokkens, E. Dalcanale, *Angew. Chemie - Int. Ed.* **2003**, *42*, 1384–1387, DOI 10.1002/anie.200390355.

[26] H. Ihm, J. S. Ahn, S. L. Myoung, H. K. Young, K. Paek, *Org. Lett.* **2004**, *6*, 3893–3896, DOI 10.1021/ol048539f.

[27] L Brunsveld, B. J. B. Folmer, E. W. Meijer, R. P. Sijbesma, *Chem. Rev.* **2001**, *101*, 4071–4098, DOI 10.1021/cr990125q.

[28] F. H. Beijer, R. P. Sijbesma, H. Kooijman, A. L. Spek, E. W. Meijer, *J. Am. Chem. Soc.* **1998**, *120*, 6761–6769, DOI 10.1021/ja974112a.

[29] T. Park, S. C. Zimmerman, S. Nakashima, *J. Am. Chem. Soc.* **2005**, *127*, 6520–6521, DOI 10.1021/ja050996j.

[30] M. D. Hossain, T. Sato, M. Higuchi, *Chem. - An Asian J.* **2013**, *8*, 76–79, DOI 10.1002/asia.201200668.

[31] F. Schlütter, A. Wild, A. Winter, M. D. Hager, A. Baumgaertel, C. Friebe, U. S. Schubert, *Macromolecules* **2010**, *43*, 2759–2771, DOI 10.1021/ma902110v.

[32] G. Schwarz, I. Haßlauer, D. G. Kurth, *Adv. Colloid Interface Sci.* **2014**, *207*, 107–120, DOI 10.1016/j.cis.2013.12.010.

[33] M. Schütte, D. G. Kurth, M. R. Linford, H. Cölfen, H. Möhwald, *Angew. Chemie - Int. Ed.* **1998**, *37*, 2891–2893, DOI 10.1002/(SICI)1521-3773(19981102)37:20<2891::AID-ANIE2891>3.0.CO;2-7.

[34] Y. Liu, Y. Yu, J. Gao, Z. Wang, X. Zhang, *Angew. Chemie - Int. Ed.* **2010**, *49*, 6576–6579, DOI 10.1002/anie.201002415.

[35] F. Tancini, E. Dalcanale in *Supramol. Polym. Chem.* Wiley-VCH Verlag GmbH & Co. KGaA, Weinheim, Germany, **2012**, pp. 71–93, DOI 10.1002/9783527639786.ch4.

[36] M. Dionisio, L. Ricci, G. Pecchini, D. Masseroni, G. Ruggeri, L. Cristofolini, E. Rampazzo, E. Dalcanale, *Macromolecules* **2014**, *47*, 632–638, DOI 10.1021/ma401506t.

[37] D. Garozzo, G. Gattuso, F. H. Kohnke, A. Notti, S. Pappalardo, M. F. Parisi, I. Pisagatti, A. J. White, D. J. Williams, *Org. Lett.* **2003**, *5*, 4025–4028, DOI 10.1021/ol035310b.

[38] G. Gattuso, A. Notti, A. Pappalardo, M. F. Parisi, I. Pisagatti, S. Pappalardo, D. Garozzo, A. Messina, Y. Cohen, S. Slovak, *J. Org. Chem.* **2008**, *73*, 7280–7289, DOI 10.1021/jo801202h.

[39] H. Hofmeier, U. S. Schubert, *Chem. Commun.* **2005**, *0*, 2423–2432, DOI 10.1039/b419171d.

[40] C. Fouquey, J. M. Lehn, A. M. Levelut, *Adv. Mater.* **1990**, *2*, 254–257, DOI 10.1002/adma.19900020506.

[41] D. W. Balkenende, R. A. Olson, S. Balog, C. Weder, L. Montero De Espinosa, *Macromolecules* **2016**, *49*, 7877–7885, DOI 10.1021/acs.macromol.6b01491.

[42] D. W. R. Balkenende, C. A. Monnier, G. L. Fiore, C. Weder, *Nat. Commun.* **2016**, *7*, 1–9, DOI 10.1038/ncomms10995.

[43] T. Park, S. C. Zimmerman, *J. Am. Chem. Soc.* **2006**, *128*, 11582–11590, DOI 10.1021/ja0631854.

[44] M. Capelot, D. Montarnal, F. Tournilhac, L. Leibler, *J. Am. Chem. Soc.* **2012**, *134*, 7664–7667, DOI 10.1021/ja302894k.

[45] M. Capelot, M. M. Unterlass, F. Tournilhac, L. Leibler, *ACS Macro Lett.* **2012**, *1*, 789–792, DOI 10.1021/mz300239f.

[46] D. Montarnal, M. Capelot, F. Tournilhac, L. Leibler, *Science* **2011**, *334*, 965–968, DOI 10.1126/science.1212648.

[47] W. Denissen, J. M. Winne, F. E. Du Prez, *Chem. Sci.* **2015**, *7*, 30–38, DOI 10.1039/c5sc02223a.

[48] W. Denissen, G. Rivero, R. Nicolaÿ, L. Leibler, J. M. Winne, F. E. Du Prez, *Adv. Funct. Mater.* **2015**, *25*, 2451–2457, DOI 10.1002/adfm.201404553.

[49] Y. Zhou, J. G. Goossens, R. P. Sijbesma, J. P. Heuts, *Macromolecules* **2017**, *50*, 6742–6751, DOI 10.1021/acs.macromol.7b01142.

[50] A. Ruiz de Luzuriaga, R. Martin, N. Markaide, A. Rekondo, G. Cabañero, J. Rodríguez, I. Odriozola, *Mater. Horiz.* **2016**, *3*, 241–247, DOI 10.1039/C6MH00029K.

[51] R. L. Snyder, D. J. Fortman, G. X. De Hoe, M. A. Hillmyer, W. R. Dichtel, *Macromolecules* **2018**, *51*, 389–397, DOI 10.1021/acs.macromol.7b02299.

[52] F. I. Altuna, V. Pettarin, R. J. J. Williams, *Green Chem.* **2013**, *15*, 3360, DOI 10.1039/c3gc41384e.

[53] K. Yu, P. Taynton, W. Zhang, M. L. Dunn, H. J. Qi, *RSC Adv.* **2014**, *4*, 48682–48690, DOI 10.1039/C4RA06543C.

[54] J. P. Brutman, P. A. Delgado, M. A. Hillmyer, *ACS Macro Lett.* **2014**, *3*, 607–610, DOI 10.1021/mz500269w.

[55] G. B. Lyon, L. M. Cox, J. T. Goodrich, A. D. Baranek, Y. Ding, C. N. Bowman, *Macromolecules* **2016**, *49*, 8905–8913, DOI 10.1021/acs.macromol.6b01281.

[56] C. A. Angell, *Science* **1995**, *267*, 1924–1935, DOI 10.1126/science.267.5206.1924.

[57] D. Plazek, M O'Rourke, *J. Polym. Sci. Part A-2* **1971**, *9*, 209–243, DOI 10.1002/pol.1971.160090202.

[58] G. Urbain, Y. Bottinga, P. Richet, *Geochim. Cosmochim. Acta* **1982**, *46*, 1061–1072, DOI 10.1016/0016-7037(82)90059-X.

[59] J. C. Dyre, *Rev. Mod. Phys.* **2006**, *78*, 953–972, DOI 10.1103/RevModPhys.78.953.

[60] M. L. Williams, R. F. Landel, J. D. Ferry, *J. Am. Chem. Soc.* **1955**, *77*, 3701–3707, DOI 10.1021/ja01619a008.

[61] Y. Nishimura, J. Chung, H. Muradyan, Z. Guan, *J. Am. Chem. Soc.* **2017**, *139*, 14881–14884, DOI 10.1021/jacs.7b08826.

[62] L. Zhou, G. Zhang, Y. Feng, H. Zhang, J. Li, X. Shi, *J. Mater. Sci.* **2018**, *53*, 7030–7047, DOI 10.1007/s10853-018-2015-z.

[63] P. Taynton, K. Yu, R. K. Shoemaker, Y. Jin, H. J. Qi, W. Zhang, *Adv. Mater.* **2014**, *26*, 3938–3942, DOI 10.1002/adma.201400317.

[64] F. Du Prez, J. Winne, W. Denissen, L. Leibler, R. Nicolaÿ, COMPOSITIONS COMPRISING A POLYMERIC NETWORK (WO2016097169), **2016**.

[65] W. Denissen, I. De Baere, W. Van Paepegem, L. Leibler, J. Winne, F. E. Du Prez, *Macromolecules* **2018**, *51*, 2054–2064, DOI 10.1021/acs.macromol.7b02407.

[66] T. Stukenbroeker, W. Wang, J. M. Winne, F. E. Du Prez, R. Nicolaÿ, L. Leibler, *Polym. Chem.* **2017**, *8*, 6590–6593, DOI 10.1039/c7py01488k.

[67] W. Denissen, M. Droesbeke, R. Nicola, L. Leibler, J. M. Winne, F. E. Du Prez, *Nat. Commun.* **2017**, *8*, 14857, DOI 10.1038/ncomms14857.

[68] Y. X. Lu, F. Tournilhac, L. Leibler, Z. Guan, *J. Am. Chem. Soc.* **2012**, *134*, 8424–8427, DOI 10.1021/ja303356z.

[69] Y. X. Lu, Z. Guan, *J. Am. Chem. Soc.* **2012**, *134*, 14226–14231, DOI 10.1021/ja306287s.

[70] M. M. Obadia, B. P. Mudraboyina, A. Serghei, D. Montarnal, E. Drockenmuller, *J. Am. Chem. Soc.* **2015**, *137*, 6078–6083, DOI 10.1021/jacs.5b02653.

[71] B. Hendriks, J. Waelkens, J. M. Winne, F. E. Du Prez, *ACS Macro Lett.* **2017**, *6*, 930–934, DOI 10.1021/acsmacrolett.7b00494.

[72] M. Röttger, T. Domenech, R. Van Der Weegen, A. Breuillac, R. Nicolaÿ, L. Leibler, *Science* **2017**, *356*, 62–65, DOI 10.1126/science.aah5281.

[73] O. R. Cromwell, J. Chung, Z. Guan, *J. Am. Chem. Soc.* **2015**, *137*, 6492–6495, DOI 10.1021/jacs.5b03551.

[74] A. Demongeot, R. Groote, H. Goossens, T. Hoeks, F. Tournilhac, L. Leibler, *Macromolecules* **2017**, *50*, 6117–6127, DOI 10.1021/acs.macromol.7b01141.

[75] W. Zou, J. Dong, Y. Luo, Q. Zhao, T. Xie, *Adv. Mater.* **2017**, *29*, 1606100, DOI 10.1002/adma.201606100.

[76] L. Imbernon, S. Norvez, *Eur. Polym. J.* **2016**, *82*, 347–376, DOI 10.1016/j.eurpolymj.2016.03.016.

[77] C. J. Kloxin, C. N. Bowman, *Chem. Soc. Rev.* **2013**, *42*, 7161–7173, DOI 10.1039/C3CS60046G.

[78] K. P. Menard, N. R. Menard in *Encycl. Polym. Sci. Technol.* (Ed.: F. M. Herman), John Wiley & Sons, Inc., Hoboken, NJ, USA, **2015**, pp. 1–33, DOI 10.1002/0471440264.pst102.pub2.

[79] J Foreman, S Sauerbrunn, C Marcozzi, *Kyoritsu Chem. & Co. Ltd Kisarazu Japan* **2013**.

Chapter 2

ODIN, a Novel Sextuple Hydrogen Bonding Motif

Abstract: Multiple hydrogen bonding motifs are promising tools for polymer functionalization with the goal to obtain adaptable networks. Here, a new type of multiple hydrogen bonding motif was envisioned and synthesized. This motif (ODIN), is comprised of two regular and two bifurcated hydrogen bonds, elucidated *via* x-ray crystallography. A K_a of $4{\cdot}10^4$ M^{-1} (in $CHCl_3$) was estimated from fluorescence measurements. To demonstrate the concept, ODIN was used for the formation of a supramolecular polymer by cross-linking the liquid tri-functional Jeffamine T3000 bearing pendant amines with an isocyanate bearing ODIN derivative, resulting in a moldable suprapolymer. The reversible nature of this cross-linking was elucidated *via* VTIR measurements. The TOC-graphic depicts the structure of the sextuple hydrogen bonding motif ODIN and the arrangements of D and A moieties.

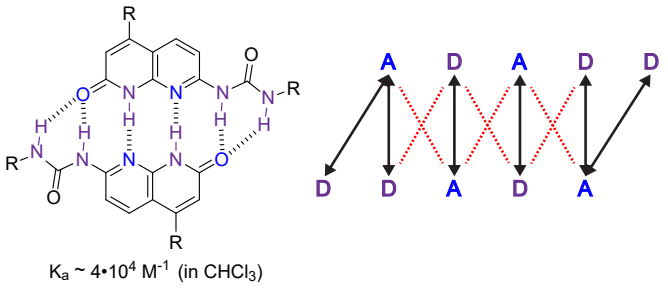

The contents of this chapter were partially adapted from: J. Tellers, S. Canossa, R. Pinalli, M. Soliman, J. Vachon, E. Dalcanale *Macromolecules* **2018**, *51*, 7680–7691, DOI 10.1021/acs.macromol.8b01715.

Recently, arrays of multiply hydrogen bonds have been explored to improve polymer properties. These are molecules inspired by DNA base pairs with a favorable arrangement of hydrogen bonding D and A groups, allowing for organized self-assembly.[1] Following this concept, molecules with a plethora of different structures were developed with the ability to homo-, or heterodimerize.[1–3] by employing these multiple hydrogen bonding moieties, properties such as controlled degradation,[4] optical responsiveness,[5] high strength and stiffness,[6] increased peel strength,,[7] reversible chain extension[8,9] miscibility between immiscible polymers,[10] and self-healing[11] can be introduced into polymers. The increased strength of these hydrogen bonding arrays can lead to their assembly even in water,[12,13] thus making them an excellent tool for the preparation of humidity and moisture resistant materials.

Among the different types of multiple hydrogen bonding array molecules, the most prominent is the ureidopyrimidone (UPy) motif,[8] a self-dimerizing quadruple hydrogen bonding motif known for its high association constant (K_a),[14] its ease of synthesis,[15] and its readily available derivatives for functionalization of polymers.[16] To date, UPy has been the most important studied synthetic multiple hydrogen bonding motif.[17] Research on polymers functionalized with UPy has largely been focused on telomers at lab scale, while functionalization of long chain polyolefins remains largely unexplored. Coates *et al.* polymerized 1-hexene with alkene functionalized UPy, obtaining a completely amorphous, wax like polyolefin with improved tensile properties over non functionalized homopolymer.[18] Nojiri *et al.* reported a UPy functionalized PP,[19] where melt viscosity was increased after functionalization with UPy units. The reported dissociation temperature of UPy moieties is at 190 °C, which is about 40 °C higher than its degradation temperature reported by other sources in the literature.[16,20] Additionally, they described the compatibilization of isotactic polypropylene functionalized with UPy and ethylene-*co*-propylene functionalized with a naphthyridine (Napy) motif, using the ability of these moieties to form heterodimers.[21] Here, melt mixing of polymers was performed at 170 °C and 210 °C, exceeding the reported temperature of degradation of UPy in polymers by 20 °C and 60 °C, respectively. Together, this raises concerns

about the chemical integrity of the analyzed polymer samples.

Since typical polymer processing occurs at relatively high temperature, the development of a more temperature stable hydrogen bonding motifs is desirable. In the following Sections we consider the design for a novel self-dimerizing multiple hydrogen bonding array and report its synthesis, characterization, and use for the preparation of a supramolecular polymer. The main objective is to improve upon thermal stability compared to UPy, targeting the preparation of functional PE.

2.1 A New Hydrogen Bonding Motif

2.1.1 Design Considerations

As the most ubiquitous self-dimerizing multiple hydrogen bonding motif to date, we first considered the quadruple hydrogen bonding motif UPy[22] (Figure 2.1 **A**) for the preparation of functional polyolefins. However, because of concerns about thermal stability due to the UPy urea bond being cleaved at elevated temperatures,[25,26] and a degradation temperature of UPy moieties in polymers given at ≈150 °C,[16] we desired an alternative.

This alternative needs to be more temperature stable, but retain the advantages of UPy such as ease of synthesis, self-dimerization, easy graftability, and high directionality of the motif provided by multiple hydrogen bonds. In addition, it should be slightly weaker than UPy because already 1 – 2 mol% of weakly hydrogen bonded dimers are sufficient to affect the mechanical behavior in thermoplastics substantially,[27,28] a feature that should allow to ease processing of thermoplastics cross-linked with multiple hydrogen bonding.

Thus, we first need to consider the causes for the thermal decomposition of UPy. Some of the UPy degradation compounds have been identified as isocyanate species,[25,29] that form as a result of the thermoreversible nature of the urea moiety.[30] It has been shown, that urea thermal stability and extend of electron delocalization in aryl substituted urea can be correlated.[31] Thereby, extending the conjugation of the aryl substituent (in case of UPy the substituent can be viewed as isocytosine) should result in a more temperature stable urea.

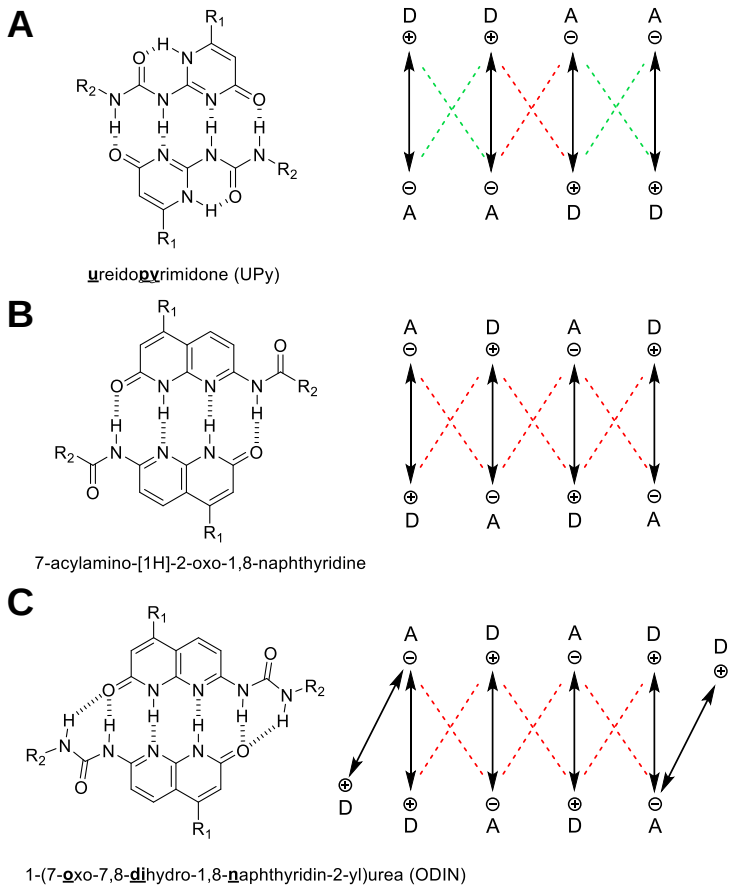

Figure 2.1: Structures of A: Ureidopyrimidinone (UPy) motif,[22] B: 7-acylamino-[1H]-2-oxo-1,8-naphthyridine[23] and C: The naphtyridine based motif ODIN. On the right, the respective arrangement of donor (D) and acceptor (A) moieties, as well as attractive (green dotted) and repulsive (red dotted) secondary electrostatic interactions (according to Jorgensen[24]), are illustrated.

One way to extend the conjugated system is by employing fused aromatic species.[32] Naphthyridines, a class of heterocycles made up of two fused aromatic rings,[33] could provide a suitable alternative to UPy with increased thermal stability. Additionally, the arrangement of D and A in Naphtyridines can be varied, which can be used to obtain a motif with the same or more hydrogen bonds than UPy, but an overall weaker association. This is possible by making use of the cross-interactions between D and A moieties not directly opposite from each other, arranging them in such a way that they weaken the dimer interaction (see Section 1.2.1).

So, for the DDAA arrangement of UPy there are two favorable interaction present highlighted by the green lines in Figure 2.1 **A**, and one unfavorable indicated by the red lines. In keeping with the design philosophy, the amount of hydrogen bonds should be retained or increased, but D and A arranged in such a way that no favorable cross-interaction takes place.

2.1.2 From Conceptualization to Reality - Synthesis of the New Hydrogen Bonding Motif ODIN

A known quadruple hydrogen bonding motif can be obtained by acylation of naphthyridine **1** (Figure 2.2).[23,34] This molecule self assembles driven by an alternating DADA arrangement of D and A moieties with an K_a of $\approx$750 – 1900 M^{-1} (in $CHCl_3$), dependent on the side chain.[34] In order to facilitate the introduction of these hydrogen bonding arrays into functional polymers with little synthetic effort, an excess of di-isocyanate was employed to react with the free amino group of naphtyridine **1**, forming **4** with an urea link and free aliphatic isocyanate available for functionalization. The introduction of the urea group provides an additional hydrogen bonding donor that can interact with one of the oxygen lone pairs of the lactam, resulting in a self-assembly mode involving six hydrogen bonds (1-(7-oxo-7,8-dihydro-1,8-naphtiridin-2-yl)urea (ODIN), Figure 2.1 **C**).

The assembly mode of ODIN was elucidated by synthesizing derivative **3** with an increased solubility in organic solvents, which allowed the growth of single crystals. Compound **3** maintains the same DDADA arrangement of D and A groups as **4**, specifically an urea group with two N-H as D, an aromatic N as A and a lactam N-H D, C=O A moiety. The crystal structure

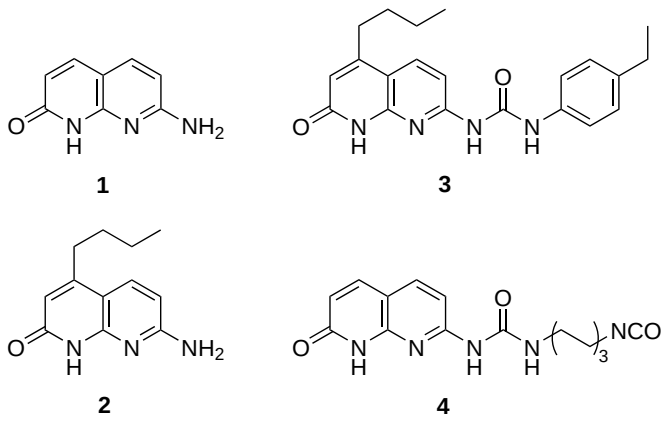

Figure 2.2: Overview of employed naphthyridine derivatives.

of **3** reveals the formation of dimers that stack head to tail driven by the self-complementary DDADA arrangement (Figure 2.3 **A**). As consequence the molecules are coplanar, and their mutual disposition allows for the formation of two bifurcated hydrogen bonds between both urea N-H donor moieties and the oxygen of the lactam, while the aromatic nitrogens are involved with the aromatic N-H groups of the respective molecular counterparts of the dimer. The only heteroatoms not involved in the intra dimer interactions are the oxygen atoms of the urea group, which accept weak hydrogen bonds from the aliphatic C-H groups belonging to adjacent dimers (Figure 2.3 **B**).

The most common way to estimate the hydrogen bonding strength is to determine the K_a in solution *via* nuclear magnetic resonance (NMR). This proved unsuccessful because the low concentration of the samples hampered acquisition of NMR spectra well defined enough to obtain K_a. For strongly bonding dimers, fluorescence spectroscopy is the more sensitive method. Solutions of **3** in $CHCl_3$ with concentrations ranging from $5.33{\cdot}10^{-7}$ mol·L^{-1} to $4{\cdot}10^{-3}$ mol·L^{-1} were prepared and their fluorescence emission measured, exciting at 325 nm. The absorbance and selected emission spectra are shown in Figure 2.4 **A**. At higher concentrations, the fluorescence emission undergoes a bathochromic shift, and a second peak appears. Based on previous observations that derivatives of 1,8-naphthyridines can form excimers,[35,36] the band dominating at lower concentrations with a peak maximum at around 375 nm was assigned to the monomer, and the band at higher concentrations

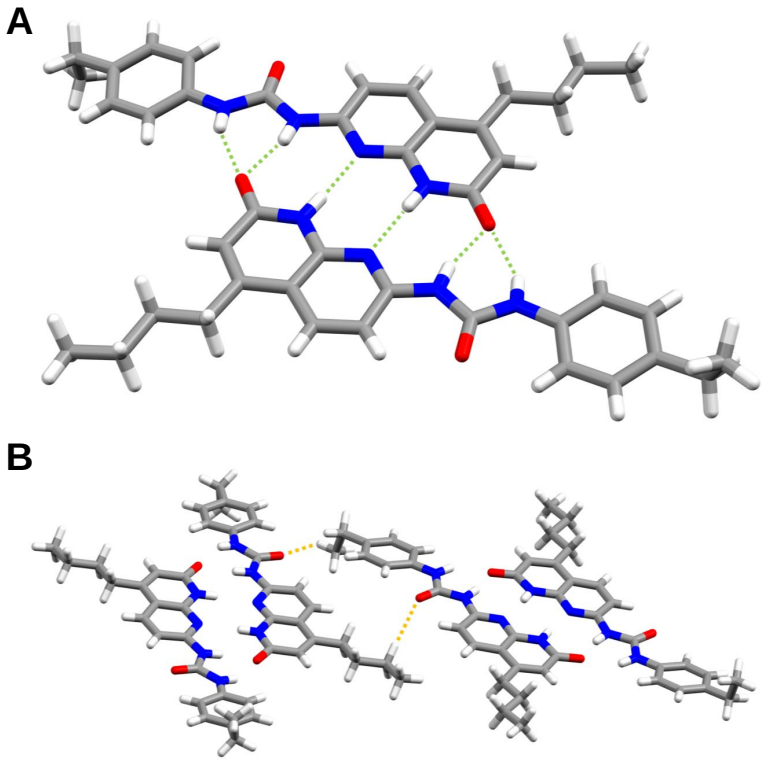

Figure 2.3: Dimeric structure of **3** (**A**) and its interactions with adjacent dimers (**B**), as observed in the crystalline phase. The intra-dimer and inter-dimer hydrogen bonds are highlighted in light green and orange respectively.

with a maximum at 395 nm to a naphytirdine excimer, which we propose forms due to the association of dimers facilitated by the complimentary hydrogen bonding. Increasing the concentration further causes quenching of the fluorescence intensity due to collisional self-quenching between the fluorophore itself,[37] which makes the estimation of the K_a by following the excimer emission difficult. Therefore, the intensity of the disappearing monomer band was followed. To avoid integrating the dimer band, integration was performed between 350 nm and 375 nm and divided by the concentration of ODIN, assuming that the intensity is linearly dependent on ODIN concentration at high dilutions. The resulting normalized intensity was plotted against the respective concentration. To determine the K_a, the intercept of zero and the linearly decreasing intensity was taken as estimate

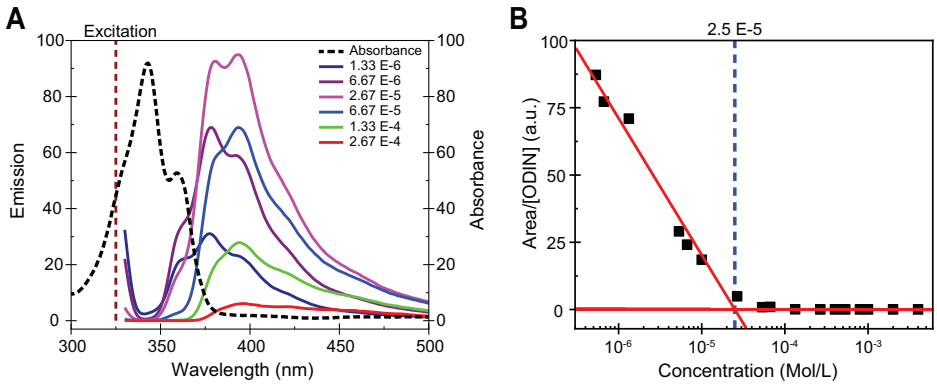

Figure 2.4: **A**: Absorbance, and fluorescence emission spectra of **3** at selected concentrations. For fluorescence measurements an excitation wavelength of 325 nm was chosen. **B**: Normalized intensity (integration performed between 350 nm and 375 nm) plotted versus respective concentration. The left red line was fitted using the areas obtained for concentrations $2.5 \cdot 10^{-2}$ mol·L^{-1} or lower, the right one is aligned with zero.

for K_a (Figure 2.4 **B**). Thereby, a K_a of $4 \cdot 10^4$ M^{-1} was determined, placing its strength between UPy and the DADA Naphtyridine (Figure 2.1 **B**).

The strength of the hydrogen bonding motif can also be determined from calculating the intermolecular interaction energy of the dimer in the solid state. Such calculations were carried out for the dimer of **3** using the program *Crystal Explorer*.[38] According to the adopted methods (see Appendix A.1), the total energy of the dimeric unit amounts to 166.8 kJ·mol^{-1}. Analogue calculations were carried out considering the two different dimeric forms **A** and **B** in Figure 2.1 discussed previously, showing 116.3 kJ·mol^{-1} for the DADA, and 203.5 kJ·mol^{-1} for the DDAA type. As a matter of fact, the most stabilizing interaction can only be achieved avoiding alternation of D and A groups. Indeed, although for the dimer of **3** the greater number of interactions could potentially lead to a better stabilization, both studies in the solid state and in solution reveal that the DDADA sequence results into a less effective association than the DDAA. This aspect has already been addressed by Jorgensen *et al.* on the basis of ab initio computational studies,[24] experimentally confirmed by Zimmerman *et al.*,[39] and the present evidence further confirms the applicability of this rule to the cited systems.

2.2 Supramolecular Polymer Network Using Sextuple Hydrogen Bonding

One of the most promising features of hydrogen bonding arrays is their potential use for the formation of supramolecular polymers, using the reversible interaction to bridge oligomeric species together to form an easy to process polymer, the concept of which is described in more detail in Section 1.3.1. To showcase whether the ODIN-dimer can be used for the preparation of a supramolecular polymer, oligomeric JEFFAMINES T3000 with pendant amines were reacted with ODIN derivative **4**, bearing a reactive isocyanate moiety that reacts easily with the amines (reaction scheme in Section 2.4). The oligomeric JEFFAMINE with an M_n of approximately 3000 g·mol^{-1} is a highly viscous liquid, but was plasticized after cross-linking with ODIN, forming a supramolecular polymer (T_g = -58 °C), hitherto referred to as JEFFODIN (see Figure A.1). It was possible to produce either solution cast or compression molded films, demonstrating the concept. However, mechanical properties of the films were poor and breaking occurred easily. This is likely a result of the weaker K_a of ODIN compared to UPy, since for efficient assembly of supramolecular polymers with high virtual weight average molecular weight (M_w), dimers with an K_a greater than 10^5 M^{-1} are recommended.[40] This is slightly above the estimated K_a of ODIN of $4{\cdot}10^4$ M^{-1} (see Section 2.1.2).

To study the enhanced association of ODIN functional JEFFAMINE oligomers, viscosity measurements of the JEFFODIN suprapolymer dissolved in $CHCl_3$ were performed at different concentrations and then compared to the viscosity of solutions of the non-cross linked oligomers. The η_{sp} was given in reference to the viscosity of $CHCl_3$, and the data is plotted in Figure 2.5. The effect of the reversible cross-linking is evident as the η_{sp} of the suprapolymer is growing significantly faster with increasing concentration than that of the JEFFAMINE solutions, indicating the assembly of larger polymeric structures in solution.[41]

Characteristic for these dimers is their temperature triggered reversibility, making it possible to depolymerize the suprapolymer assembly at elevated temperatures. This can be studied using variable temperature infrared

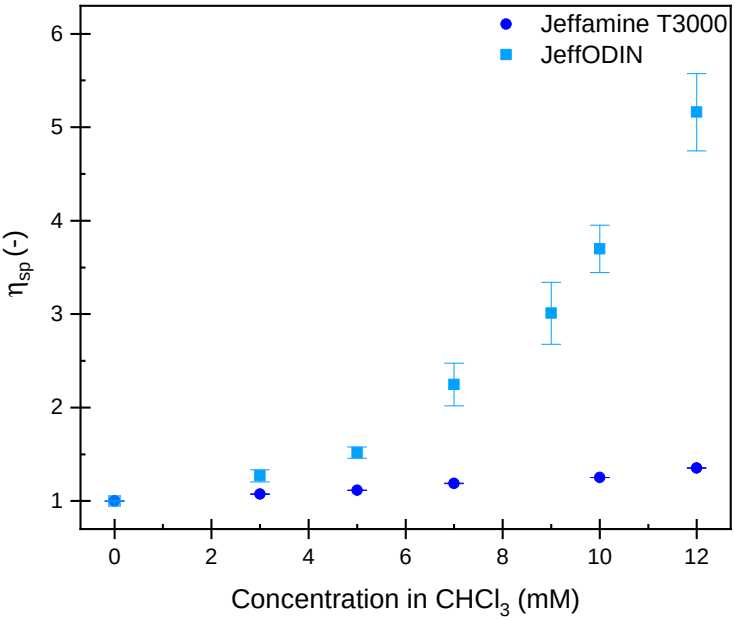

Figure 2.5: Plot of the η_{sp} as function of concentration for solutions of JEFFAMINE T3000 and suprapolymer JEFFODIN in $CHCl_3$.

spectroscopy (VTIR), by investigating a small film of the suprapolymer (spectra in Figure 2.6). During the measurement, the bands of amino and carbonyl groups involved in hydrogen bonding are monitored, which are known to shift as they dissociate.[16,42–44] When looking at the temperature influence on the absorption peaks of JEFFODIN, clear shifts are apparent in the C=O stretching and N-H bending region. Specifically, with increasing temperature the band at 1610 cm^{-1} loses intensity and the absorption band observed at 1570 cm^{-1} shifts significantly towards lower wavenumbers. Together, these shifts indicate the progressive dissociation of hydrogen bonds at elevated temperatures.[44] This is in line with visual observations, where viscous flow can be observed for JEFFODIN starting at around 140 °C.

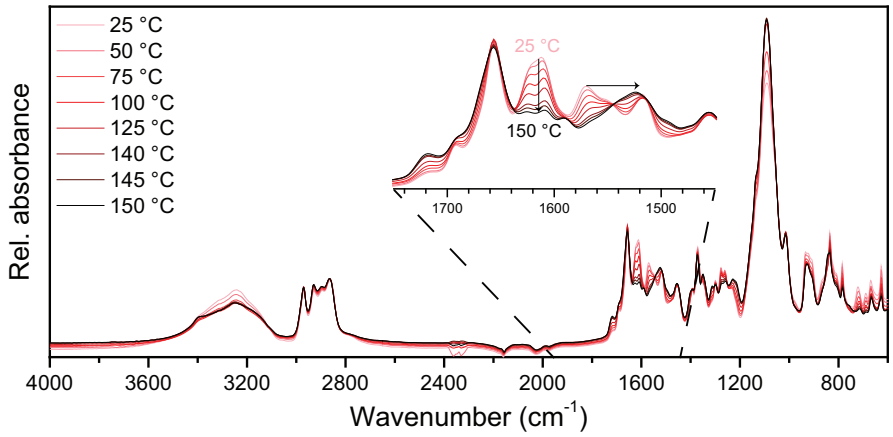

Figure 2.6: VTIR spectra of trifunctional supramolecular polymer JEFFODIN. Samples were heated step-wise starting from 25 °C up to 150 °C. The shifting absorption bands are indicated with arrows. Spectra are normalized for the C-H stretch region around 2830 cm^{-1}.

2.3 Conclusions

The main objective of this part of the work was to obtain an easy to synthesize hydrogen bonding array, which is more temperature stable and has a lower K_a than the established UPy motif. By alternating the arrangement of D and A moieties a motif (ODIN) with a greater number of hydrogen bonds than UPy, but lower K_a, was obtained. The extended electron delocalization should increase the stability of the connecting urea. The structure of the new motif ODIN was elucidated *via* single crystal X-ray diffraction (SCXRD), revealing the formation of dimers in the solid state involving two regular and two bifurcated hydrogen bonds, resulting in a total of six hydrogen bonds.

The reversible interaction of ODIN can be used to form a supramolecular polymer by connecting oligomeric JEFFAMINES end-capped with ODIN motifs. Even if, due to the weak K_a of ODIN ($4{\cdot}10^4$ M^{-1}), the resulting suprapolymer was brittle and broke easily, the motif can be useful in applications where a high number of hydrogen bonds are required for directionality, but a low K_a is necessary for ease of processing. One such example would be the extension or cross-linking of strongly apolar oligomers/polymers, which are known to

strengthen the K_a of such multiple hydrogen bonding motifs.[9,17] While the temperature stability of ODIN was not analyzed here, it will be tackled in Section 3.1.2, after incorporation into main chain polymers.

2.4 Experimental Section

2.4.1 Methods

Nuclear magnetic resonance (NMR). NMR-spectra were recorded on a Bruker Avance 400 (400 MHz) spectrometer and a Bruker Avance 300 (300 MHz) at room temperature. Chemical shifts are reported in parts per million (ppm). ^{1}H NMR chemical shifts are given in reference to the residual solvent peak at 7.26 ppm in $CDCl_3$ and at 2.50 ppm in dimethyl sulfoxide-d_6 (DMSO-d_6).

Infrared spectroscopy (IR). IR-spectra were recorded on a Perkin Elmer *Spectrum One* equipped with a Golden Gate accessory (diamond ATR). VTIR spectra were recorded on a Bruker Vertex 70 spectrometer which is equipped with a heatable diamond ATR accessory (*GladiATR* 300 by PIKE *Technologies*). First, spectra were recorded of the empty crystal at all employed temperatures. These spectra were subsequently used as background spectra for the actual measurements to compensate for the change in transmission of diamond at elevated temperatures.

Single crystal X-ray diffraction (SCXRD). SCXRD analysis was perfomed at the Elettra Synchrotron facility (XRD1 beamline).[45] Diffraction data were collected using a monochromatic 0.7 Å wavelength at 100 K, using an Oxford *Cryostream* 700[46] cooling device. Diffraction datasets were processed using *CrysAlisPro* software ver. 1.171.38.43.[47] Structure solution and refinement were conducted using Olex2 software ver. 1.2.9.[48] CCDC 1825490 contains crystallographic data relative to the described phases. This data can be obtained free of charge from the Cambridge *Crystallographic Data Centre via* https://www.ccdc.cam.ac.uk/structures.

Viscosimetry. Viscosimetry was performed on a Ubbelohde OC (K = 0.003180) at 25 °C. Polymer solutions with varying concentrations in dry

$CHCl_3$ were obtained by diluting a stock solution to the appropriate amounts. The specific viscosity (η_{sp}) of the polymer solutions was given in reference to $CHCl_3$. The HAGENBACH correction was used to calculate the viscosity.

Fluorescence measurements. Samples for fluorescence characterization were prepared by diluting a stock solution to get the desired sample concentrations. Spectra were recorded on a PERKINELMER *LS 55 Fluorescence spectrometer* using *FL WinLab.*[49]

2.4.2 Synthesis

Unless otherwise specified, chemicals and solvents were purchased from SIGMA-ALDRICH and used as received. JEFFAMINE T3000 was procured from HUNTSMAN and used as received. All solvents employed were laboratory grade and used as received.

7-Amino-1,8-naphthyridin-2(1H)-one (**1**).

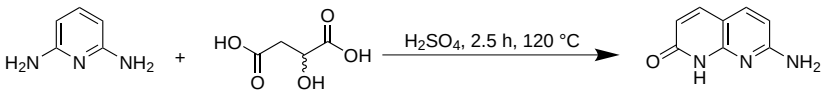

Naphthyridine **1** was synthesized according to literature.[50] Ground diaminopyridine (109.13 g, 0.98 mol, 1 eq) and malic acid (145 g, 1.08 mol, 1.1 eq) were placed in a 3-neck flask and cooled in an ice bath. Sulfuric acid (500 mL) was slowly added while maintaining an internal temperature below 45 °C. The obtained mixture was slowly heated to 110 °C and reacted for 2.5 h. Subsequently after cooling down the temperature, the lukewarm solution was poured over ice and concentrated ammonia (≈1.5 L) was slowly added while stirring until a pH of ≈7 – 8 was reached. The precipitate was filtered and first washed with ≈9 L of water, then with a mixture of H_2O and MeOH (9 : 1) until the wash was colorless. The solid residue was dried in vacuum at 100 °C to obtain the product as deep brown solid (133.2 g, 84 % yield). The characterization gave values consistent with the literature.[50] ^{1}H NMR (300 MHz, DMSO-d_6) δ: 11.85 (s, 1H), 7.65 (d, J = 9.3 Hz, 2H), 7.64 (d, J = 8.6 Hz, 1H), 6.34 (d, J = 8.5 Hz, 1H), 6.11 (d, J = 9.2 Hz, 1H).

7-Amino-4-butyl-1,8-naphthyridin-2(1H)-one (**2**).

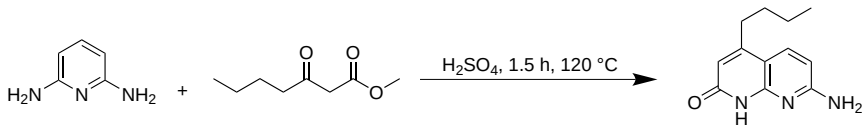

The synthesis for **2** was adapted from literature.[51] A three neck flask equipped with thermometer, mechanical stirrer, and dropping funnel was charged with diamino-pyridine (12.67 g, 1 eq), methyl 3-oxoheptanoate (20.20 g, 1.1 eq) and stirred for 1 h. The mixture was then cooled to 0 °C and sulfuric acid (65 mL) was slowly added while maintaining a temperature below 45 °C. After full addition the dropping funnel was replaced with a reflux condenser and the mixture was heated for 1.5 h at 120 °C. The solution was then cooled to room temperature, poured over 100 g ice and brought to pH ≈7 – 8 by slow addition of a 30 % ammonia solution (≈125 mL). The formed precipitate was filtered, washed with water, then triturated with a 1 : 9 methanol/water mixture, filtered again, and washed with methanol/acetone until the wash was colorless. The product was dried at high vacuum and obtained as yellow solid (10 g, 40 % yield), which was used immediately without further purification. MS (ESI) m/z: $[M + H]^+$ calcd for $C_{12}H_{15}N_3O$, 218.13; found, 218.09.

1-(5-butyl-7-oxo-7,8-dihydro-1,8-naphthyridin-2-yl)-3-(4-ethylphenyl)urea (**3**).

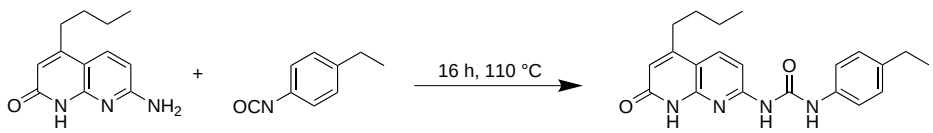

Compound **2** (0.1 g, 0.46 mmol, 1 eq) and 4-ethylphenylisocyanate (0.3 mL, 2.1 mmol, 4.6 eq) were combined in a 10 mL vial and stirred overnight at 110 °C. A 1 : 1 hexane/acetone mixture (5 mL) was added and the precipitate filtered off and washed with acetone until the wash was colorless. The compound was dried at high vacuum and obtained as a tan colored powder. (0.106 g, 63 % yield). Crystals shaped like needles suitable for x-ray crystallography were obtained from **3** dissolved in chloroform and layered with acetone. ^{1}H NMR (300 MHz, DMSO-d_6) δ: 12.26 (s, 1H), 10.56 (s, 1H), 9.87 (s, 1H), 8.11 (d, J = 8.7 Hz, 1H), 7.62 (d, J = 8.5 Hz, 2H), 7.16 (d, J = 8.4 Hz, 2H), 7.07 (d, J = 8.7 Hz, 1H), 6.24 (s, 1H), 2.74 (t, J = 7.6 Hz,

2H), 2.58 (q, J = 7.6 Hz, 2H), 1.64 – 1.51 (m, 2H), 1.38 (m, 2H), 1.18 (t, J = 7.6 Hz, 3H), 0.92 (t, J = 7.3 Hz, 3H). MS (ESI) m/z: $[M + H]^+$ calcd for $C_{21}H_{24}N_4O_2$, 365.20; found, 365.23.

1-(6-isocyanatohexyl)-3-(7-oxo-7,8-dihydro-1,8-naphthyridin-2-yl)urea (**4**).

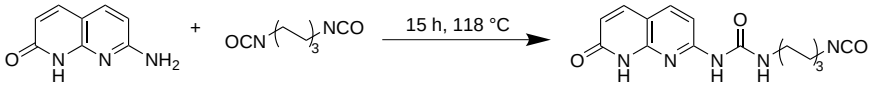

Compound **1** (50 g, 0.31 mol, 1 eq) and hexamethylene diisocyanate (HDI) (500 ml, 3.1 mol, 10 eq) were combined and stirred. The resulting slurry was heated for 15 h at a temperature of 118 °C (temperature of oil bath). After cooling to room temperature, the solid was filtered over a Buchner funnel and washed with hexane and acetone until the wash was colorless. The solid residue was dried under vacuum at 60 °C, yielding the product as a tan powder with minor impurities (72.7 g, 71 % yield). ^{1}H NMR (400 MHz, DMSO-d_6) δ: 12.18 (s, 1H, Ar-N*H*), 9.65 (s, 1H, Ar-N*H*-CO-NH), 8.99 (s, 1H, N*H*-CO-NH-Ar), 7.91 (d, J = 8.4 Hz, 1H), 7.78 (d, J = 9.4 Hz, 1H), 6.84 (d, J = 8.5 Hz, 1H), 6.34 (d, J = 9.4, 1.8 Hz, 1H), 3.39 – 3.31 (m, 2H), 3.20 (dd, J = 6.7 Hz, 2H), 1.62 – 1.48 (m, 4H), 1.43 – 1.19 (m, 4H). MS (ESI) m/z: $[M + H]^+$ calcd for $C_{17}H_{23}N_5O_4$ (methanol adduct), 362.18; found, 362.26.

Supramolecular Jeffamine *T3000*

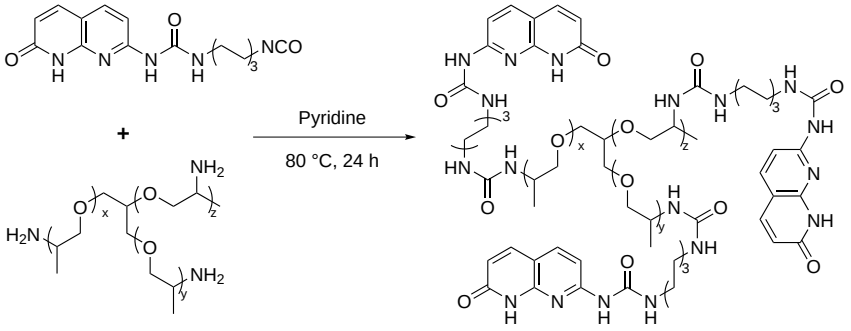

Jeffamine T3000 (100 g, 33.33 mmol, 1 eq) was added to a dry three neck flask equipped with mechanical stirrer. Pyridine (300 mL) was added followed by ground **4** (39.5 g, 120 mmol, 3.6 eq). The mixture was then heated to 80 °C and stirred for 24 h. After bringing the mixture to room

temperature, $CHCl_3$ (300 mL) and MeOH (50 mL) are added and the solution filtered through a pad of celite. The solution was evaporated, dissolved in a mixture of MeOH and $CHCl_3$ (1 : 1, 300 mL), and precipitated into a hexane/acetone mixture (1 : 1, 600 mL). The material was filtered off and dried. The product was obtained as yellow polymeric chunks (61.2 g, 46 % yield). ^{1}H NMR (300 MHz, DMSO-d_6) δ: 11.99 (s, 1H), 9.66 (s, 1H), 9.00 (s, 1H), 7.91 (d, J = 8.5 Hz, 1H), 7.78 (d, J = 9.4 Hz, 1H), 6.87 (d, J = 8.5 Hz, 1H), 6.34 (d, J = 9.4 Hz, 1H), 5.80 (s, 1H), 5.56 (d, J = 7.9 Hz, 1H), 3.71 – 3.14 (m, backbone), 3.03 – 2.88 (m, 2H), 1.59 – 1.15 (m, JEFFAMINE methylene), 1.04 (d, J = 5.7 Hz, JEFFAMINE methyl group).

References

[1] S. C. Zimmerman, P. S. Corbin, *Struct. Bond.* **2000**, *96*, 63–94, DOI 10.1007/3-540-46591-X_3.

[2] T. Park, S. C. Zimmerman, S. Nakashima, *J. Am. Chem. Soc.* **2005**, *127*, 6520–6521, DOI 10.1021/ja050996j.

[3] P. S. Corbin, S. C. Zimmerman, P. A. Thiessen, N. A. Hawryluk, T. J. Murray, *J. Am. Chem. Soc.* **2001**, *123*, 10475–10488, DOI 10.1021/ja010638q.

[4] C. C. Cheng, J. J. Huang, Z. S. Liao, S. Y. Huang, D. J. Lee, Z. Xin, *Polym. Chem.* **2017**, *8*, 1454–1459, DOI 10.1039/c7py00182g.

[5] D. W. R. Balkenende, C. A. Monnier, G. L. Fiore, C. Weder, *Nat. Commun.* **2016**, *7*, 1–9, DOI 10.1038/ncomms10995.

[6] B. Zhu, N. Jasinski, A. Benitez, M. Noack, D. Park, A. S. Goldmann, C. Barner-Kowollik, A. Walther, *Angew. Chemie - Int. Ed.* **2015**, *54*, 8653–8657, DOI 10.1002/anie.201502323.

[7] K. Yamauchi, J. R. Lizotte, T. E. Long, *Macromolecules* **2003**, *36*, 1083–1088, DOI 10.1021/ma0212801.

[8] R. P. Sijbesma, F. H. Beijer, L Brunsveld, B. J. Folmer, J. H. Hirschberg, R. F. Lange, J. K. Lowe, E. W. Meijer, *Science* **1997**, *278*, 1601–1604, DOI 10.1126/science.278.5343.1601.

[9] B. J. B. Folmer, R. P. Sijbesma, R. M. Versteegen, J. A. J. Van Der Rijt, E. W. Meijer, *Adv. Mater.* **2000**, *12*, 874–878, DOI 10.1002/1521-4095(200006)12:12<874::AID-ADMA874>3.0.CO;2-C.

[10] T. Park, S. C. Zimmerman, *J. Am. Chem. Soc.* **2006**, *128*, 11582–11590, DOI 10.1021/ja0631854.

[11] A. Faghihnejad, K. E. Feldman, J. Yu, M. V. Tirrell, J. N. Israelachvili, C. J. Hawker, E. J. Kramer, H. Zeng, *Adv. Funct. Mater.* **2014**, *24*, 2322–2333, DOI 10.1002/adfm.201303013.

[12] P. Y. Dankers, T. M. Hermans, T. W. Baughman, Y. Kamikawa, R. E. Kieltyka, M. M. Bastings, H. M. Janssen, N. A. Sommerdijk, A. Larsen, M. J. Van Luyn, A. W. Bosman, E. R. Popa, G. Fytas, E. W. Meijer, *Adv. Mater.* **2012**, *24*, 2703–2709, DOI 10.1002/adma.201104072.

[13] R. E. Kieltyka, A. C. H. Pape, L. Albertazzi, Y. Nakano, M. M. C. Bastings, I. K. Voets, P. Y. W. Dankers, E. W. Meijer, *J. Am. Chem. Soc.* **2013**, *135*, 11159–11164, DOI 10.1021/ja403745w.

[14] S. H. M. Söntjens, R. P. Sijbesma, M. H. P. Van Genderen, E. W. Meijer, *J. Am. Chem. Soc.* **2000**, *122*, 7487–7493, DOI 10.1021/ja000435m.

[15] H. M. Keizer, R. van Kessel, R. P. Sijbesma, E. Meijer, *Polymer* **2003**, *44*, 5505–5511, DOI 10.1016/S0032-3861(03)00631-1.

[16] D. J. Van Beek, A. J. Spiering, G. W. Peters, K. Te Nijenhuis, R. P. Sijbesma, *Macromolecules* **2007**, *40*, 8464–8475, DOI 10.1021/ma071 2394.

[17] S. Seiffert, *Supramolecular Polymer Networks and Gels*, *Vol. 268*, Springer, **2015**, p. 288, DOI 10.1007/978-3-319-15404-6.

[18] L. R. Rieth, R. F. Eaton, G. W. Coates, *Angew. Chemie Int. Ed.* **2001**, *40*, 2211–2214, DOI 10.1002/1521-3757(20010601)113:11<2211:: AID-ANGE2211>3.0.CO;2-L.

[19] S. Nojiri, H. Yamada, S. Kimata, K. Ikeda, T. Senda, A. W. Bosman, *Polymer* **2016**, *87*, 308–315, DOI 10.1016/j.polymer.2016.02.010.

[20] G. M.L. H. van Gemert, H. M. Janssen, E. W. Meijer, A. W. Bosman, Supramolecular polymers from low-melting, easily processable building blocks (WO2008063057A3), **2014**.

[21] S. Nojiri, S. Kimata, K. Ikeda, T. Senda, A. W. Bosman, J. W. Peeters, H. M. Janssen, *Macromolecules* **2017**, *50*, 5687–5694, DOI 10.1021 /acs.macromol.7b00550.

[22] F. H. Beijer, R. P. Sijbesma, H. Kooijman, A. L. Spek, E. W. Meijer, *J. Am. Chem. Soc.* **1998**, *120*, 6761–6769, DOI 10.1021/ja974112a.

[23] B. Ośmialowski, E. Kolehmainen, E. Kalenius, B. Behera, R. Kauppinen, E. Sievänen, *Struct. Chem.* **2011**, *22*, 1143–1151, DOI 10.1007 /s11224-011-9808-x.

[24] W. L. Jorgensen, J. Pranata, *J. Am. Chem. Soc.* **1990**, *112*, 2008–2010, DOI 10.1021/ja00161a061.

[25] G. Armstrong, M. Buggy, *Mater. Sci. Eng. C* **2001**, *18*, 45–49, DOI 10.1016/S0928-4931(01)00359-9.

[26] G. Armstrong, M. Buggy, *Polym. Int.* **2002**, *51*, 1219–1224, DOI 10.1002/pi.949.

[27] R Stadler, L. de Lucca Freitas, *Colloid Polym. Sci.* **1986**, *264*, 773–778, DOI 10.1007/BF01500752.

[28] L. L. de Lucca Freitas, R. Stadler, *Macromolecules* **1987**, *20*, 2478–2485, DOI 10.1021/ma00176a027.

[29] R. F. M. Lange, M. Van Gurp, E. W. Meijer, *J. Polym. Sci. Part A Polym. Chem.* **1999**, *37*, 3657–3670, DOI 10.1002/(SICI)1099-0518(19991001)37:19<3657::AID-POLA1>3.0.CO;2-6.

[30] E. Delebecq, J. P. Pascault, B. Boutevin, F. Ganachaud, *Chem. Rev.* **2013**, *113*, 80–118, DOI 10.1021/cr300195n.

[31] G. S. Skuches, P. S. Carleton, *J. Appl. Polym. Sci.* **1984**, *29*, 3431–3443, DOI 10.1002/app.1984.070291120.

[32] W. Wu, Y. Liu, D. Zhu, *Chem. Soc. Rev.* **2010**, *39*, 1489–1502, DOI 10.1039/B813123F.

[33] C. F. H. Allen, *Chem. Rev.* **1950**, *47*, 275–305, DOI 10.1021/cr60147a004.

[34] S. Goswami, S. Dey, J. F. Gallagher, A. J. Lough, S. García-Granda, L. Torre-Fernández, I. Alkorta, J. Elguero, *J. Mol. Struct.* **2007**, *846*, 97–107, DOI 10.1016/j.molstruc.2007.01.024.

[35] H. M. Zhang, W. F. Fu, X. Gan, Y. Q. Xu, J. Wang, Q. Q. Xu, S. M. Chi, *J. Chem. Soc. Dalt. Trans.* **2008**, *0*, 6817–6824, DOI 10.1039/b809701a.

[36] K. Nakatani, N. Natsuhara, Y. Mori, S. Mukherjee, B. Das, A. Murata, *Chem. - An Asian J.* **2017**, *12*, 3077–3087, DOI 10.1002/asia.201701293.

[37] A. Andersson, J. Danielsson, A. Gräslund, L. Mäler, *Eur. Biophys. J.* **2007**, *36*, 621–635, DOI 10.1007/s00249-007-0131-9.

[38] S. Wolff, D. Grimwood, J. McKinnon, M. Turner, D. Javatilaka, M. Spackman, CrystalExplorer, **2012**.

[39] J. R. Quinn, S. C. Zimmerman, J. E. Del Bene, I. Shavitt, *J. Am. Chem. Soc.* **2007**, *129*, 934–941, DOI 10.1021/ja066341f.

[40] L Brunsveld, B. J. B. Folmer, E. W. Meijer, R. P. Sijbesma, *Chem. Rev.* **2001**, *101*, 4071–4098, DOI 10.1021/cr990125q.

[41] R. Houwink, *J. für Prakt. Chemie* **1940**, *157*, 15–18, DOI 10.1002/prac.19401570102.

[42] S. Cheng, M. Zhang, N. Dixit, R. B. Moore, T. E. Long, *Macromolecules* **2012**, *45*, 805–812, DOI 10.1021/ma202122r.

[43] S. H. Gellman, G. P. Dado, G. B. Liang, B. R. Adams, *J. Am. Chem. Soc.* **1991**, *113*, 1164–1173, DOI 10.1021/ja00004a016.

[44] K. Zhang, M. Aiba, G. B. Fahs, A. G. Hudson, W. D. Chiang, R. B. Moore, M. Ueda, T. E. Long, *Polym. Chem.* **2015**, *6*, 2434–2444, DOI 10.1039/C4PY01798F.

[45] D. R. Allan, S. P. Collins, G. Evans, D. Hall, K. McAuley, R. L. Owen, T. Sorensen, C. C. Tang, F. von Delft, A. Wagner, H. Wilhelm, *Eur. Phys. J. Plus* **2015**, *130*, 1–20, DOI 10.1140/epjp/i2015-15056-x.

[46] Contact Oxford Cryosystems, **1999**, http://www.oxcryo.com/contact-us/ (visited on 02/15/2018).

[47] Rigaku Oxford Diffraction, CrysAlisPro Software System, Oxford, UK, **2017**.

[48] O. V. Dolomanov, L. J. Bourhis, R. J. Gildea, J. A. K. Howard, H. Puschmann, *J. Appl. Crystallogr.* **2009**, *42*, 339–341, DOI 10.1107/S0021889808042726.

[49] PerkinElmer, FL WinLab, **2001**.

[50] C. A. Anderson, P. G. Taylor, M. A. Zeller, S. C. Zimmerman, *J. Org. Chem.* **2010**, *75*, 4848–4851, DOI 10.1021/jo100476x.

[51] M. F. Mayer, S. Nakashima, S. C. Zimmerman, *Org. Lett.* **2005**, *7*, 3005–3008, DOI 10.1021/ol050987f.

Appendix A

A.1 Calculations of total Energy of Dimers

Energy calculations for the considered dimers were carried out by adopting the B3LYP functional and 6-31G(d,p) basis set. For the three systems the outcome of the simulations is reported below. The names are given according to Figure 2.1, the values are in kJ·mol^{-1}.

Compound A: E(electrostatic): -235.4; E(polarisation): -73.3; E(dispersion): -36.5; E(repulsion): 212.8; E(total): -203.5

Compound B: E(electrostatic): -143.0; E(polarisation): -35.2; E(dispersion): -45.0; E(repulsion): 162.1; E(total): -116.3

Compound C: E(electrostatic): -223.1; E(polarisation): -53.8; E(dispersion): -43.3; E(repulsion): 237.5; E(total): -166.8

A.2 Supramolecular polymer JeffODIN

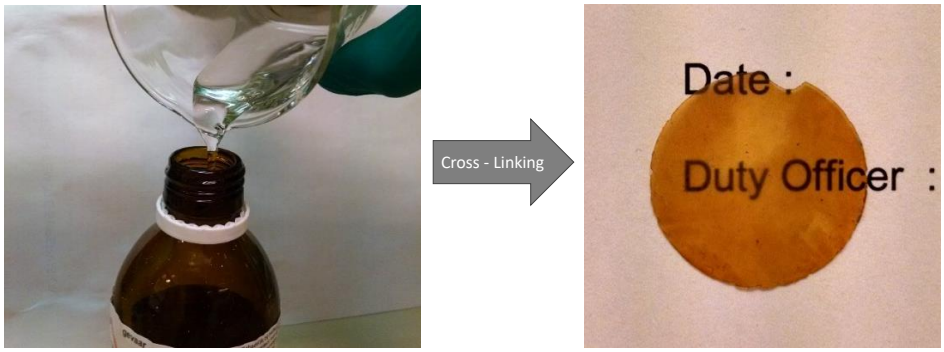

Figure A.1: Pictures of JEFFAMINE T3000 solution before cross-linking (left side) and of a film of supramolecular polymer JEFFODIN (right side) formed after reaction with a reactive ODIN motif (**4**).

A.3 NMR-spectra

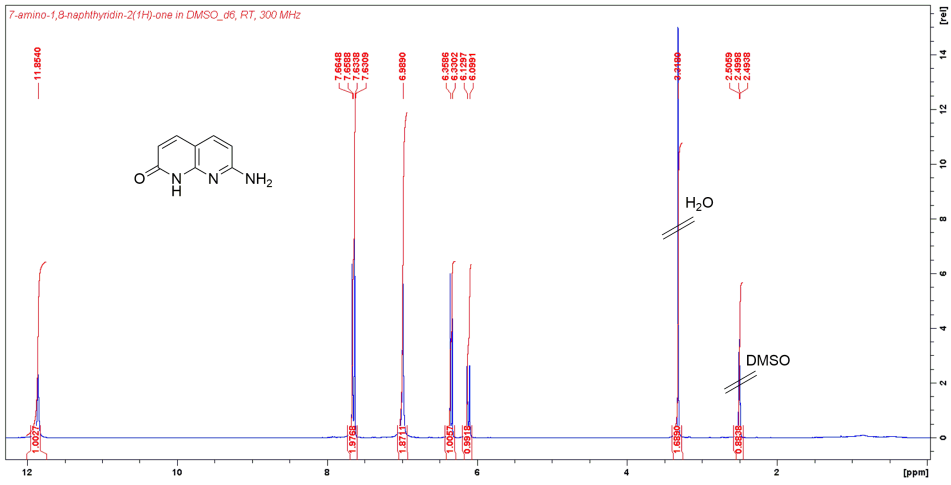

Figure A.2: ^{1}H NMR spectra of compound **1** in DMSO-d_6.

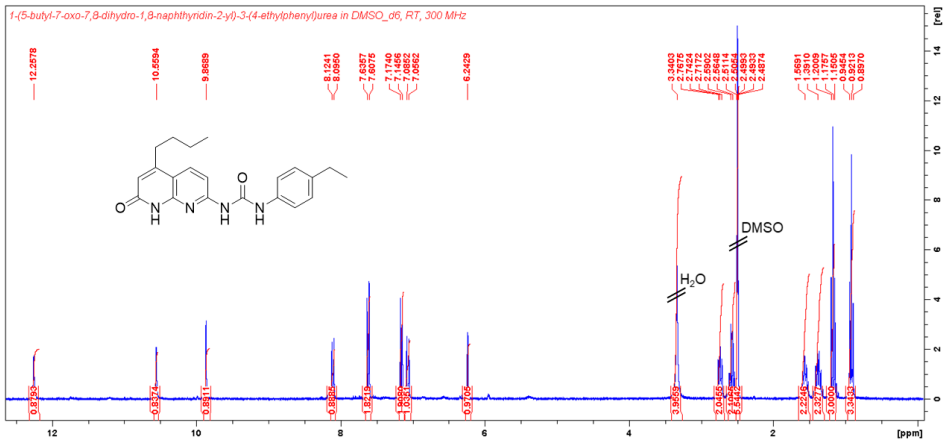

Figure A.3: ^{1}H NMR spectra of compound **3** in DMSO-d_6.

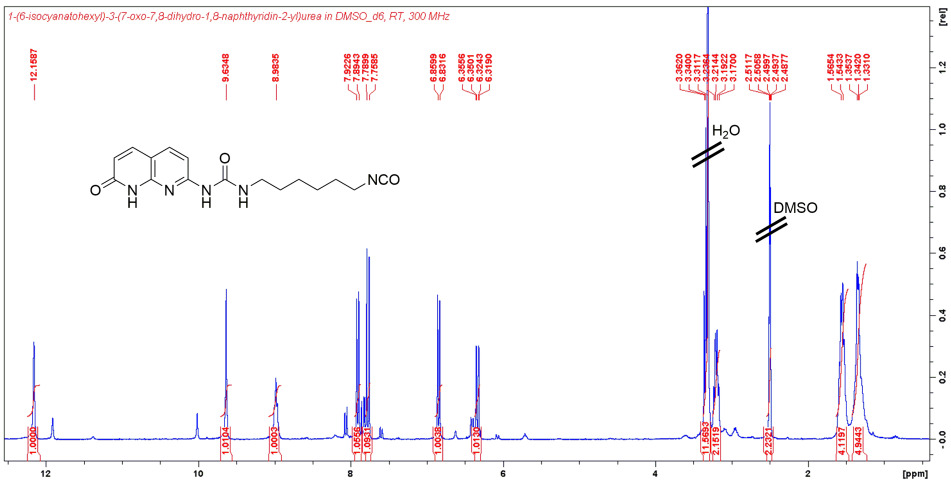

Figure A.4: ^{1}H NMR spectra of compound **4** in DMSO-d_6.

Chapter 3

Dynamic Cross-Linking of Polyolefins *via* Hydrogen Bonding

Abstract: Multiple hydrogen bonding motifs are promising tools to obtain adaptable networks combining advantages of permanently cross-linked systems with processability of thermoplastics. Here we describe the use of a new multiple hydrogen bonding motif (ODIN) to create adaptable polyolefins networks with increased tensile strength, stiffness, barrier properties, and a plateau modulus after melting. The cross-linked nature of these polymers was elucidated by thermal and mechanical analysis. The apolar polymer matrix was found to stabilize the new hydrogen bonding motif at elevated temperatures. The resulting polymer showed thermal resistance superior to UPy motif functionalized materials, the most commonly employed synthetic multiple hydrogen bonding motif to date. TOC-graphic: Cross-linking of polyolefins with mutliple hydrogen-bonding and resulting enhanced shape stability above T_m.

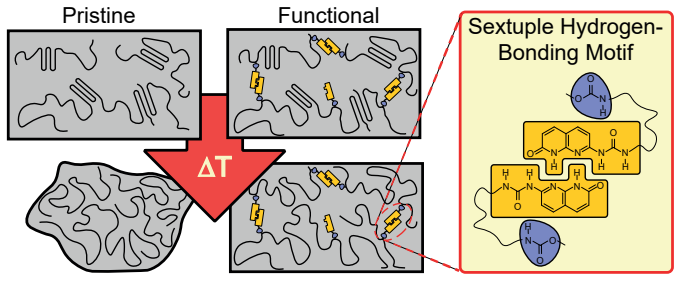

The contents of this chapter were partially adapted from: J. Tellers, S. Canossa, R. Pinalli, M. Soliman, J. Vachon, E. Dalcanale *Macromolecules* **2018**, *51*, 7680–7691, DOI 10.1021/acs.macromol.8b01715 and from **PCT/EP2018/072316.**

3.1 Dynamic Cross-Linking of Polyethylene *via* Sextuple Hydrogen Bonding Array

The most widely employed polymer in the world is polyethylene (PE),[1,2] owing to its low cost and excellent properties such as chemical resistance, processability, moisture resistance and low conductivity.[3] However, there is an ongoing interest to overcome the flaws of PE such as wear,[4,5] poor oxygen barrier properties,[6,7] low strength[8,9] and creep,[8,10] relying mostly on fillers as property enhancing tool.

The introduction of hydrogen bonding in polymers can lead to extraordinary properties. For example NYLON, possibly described as a PE backbone chain with equally spaced di-functional hydrogen bonding moieties (amides), has superior tensile, barrier, fatigue and heat resistance properties.[11–13] The same is true for ethylene vinyl alcohol (EVOH), which shows superior barrier properties ascribed to a high crystallinity resulting from the considerable cohesive energy between chains provided by the large amount of hydrogen bonds present.[14] Other notable examples of polymers that own some of their remarkable properties to hydrogen bonding are polyurea and polyurethanes.[15] The properties of these polymers are however profoundly dependent on moisture, as it can interfere with the hydrogen bonds.[16–19]

More recently, arrays of multiply hydrogen bonds have been explored to improve polymer properties. These are molecules inspired by DNA base pairs with a favorable arrangement of hydrogen bonding donor (D) and acceptor (A) groups, allowing for organized self-assembly.[19] Following this concept, molecules with a plethora of different structures were developed with the ability to homo-, or heterodimerize.[19–21] Using multiple hydrogen bonding moieties, polymers can be augmented with properties such as controlled degradation,[22] optical responsiveness,[23] high strength and increased stiffness,[24] improved peel strength,[25] self-healing,[26] miscibility between immiscible polymers,[27] and reversible chain extension.[28,29] The increased strength of these hydrogen bonding arrays can lead to their assembly even in water,[30,31] thus making them an excellent tool for the preparation of humidity and moisture resistant materials.

As was previously discussed in Chapter 2, the most studied multiple

hydrogen bonding motif is the ureidopyrimidone (UPy) motif.[31,32] Due to the established concerns about temperature stability a new motif, the 1-(7-oxo-7,8-dihydro-1,8-naphtiridin-2-yl)urea (ODIN) motif, was developed. Introduction of ODIN into a functional PE is expected to give rise to improved mechanical and barrier properties, an increased melt strength, and should show improved thermal stability compared to UPy functionalized polymers, all of which will be demonstrated in the following sections.

3.1.1 Dynamic Cross-Linking of Polyethylene *via* Sextuple Hydrogen Bonding Array: Synthesis

A suitable Polymeric Precursor for Grafting: PE-HEMA

For the preparation of multiple hydrogen bonding cross-linked polyolefins, polymers bearing moieties suitable for grafting of the hydrogen bonding motifs are required. Since ODIN motif **4** bears an aliphatic isocyanate (see Chapter 2), polymers with pendant hydroxy or amino groups were considered. A suitable polymer, namely poly (ethylene-*co*-(2-hydroxethyl methacrylate)) (PE-HEMA), a *co*-polymer of ethylene and 2-hydroxyethyl methacrylate (HEMA), was selected and is available within SABIC with HEMA contents ranging from 1.6 mol% to 12.4 mol% (Table 3.1).

The pendant hydroxy groups of HEMA allow for easy grafting of the isocyanate bearing ODIN motif **4**.[33–35] A homo-polymeric PE sample, prepared employing the same reaction conditions that were employed to synthesize PE-HEMA, was used as a reference material. The provided *co*-polymers used in this study, their HEMA content in mol% determined *via* high temperature nuclear magnetic resonance (HTNMR), their M_w determined by gel permeation chromatography (GPC) (traces in Figure B.1, Appendix **B**), T_m determined *via* DSC (graphs in Figure B.2), and T_β obtained from DMTA are reported in Table 3.1. In addition to the molecular weight, GPC was used to investigate the short chain branching (SCB) of the PE-HEMA polymers and their homogeneity. An indication for homogeneous incorporation of branches is that all molecular weight fractions of polymers should have the same amount of SCB. In Figure B.1, the distribution of SCB as a function of the molecular weight is plotted, which is found to be near linear for all polymers but **PE-HEMA 4**. This shows that the

Table 3.1: HEMA content, GPC data and thermal data for PE-HEMA *co*-polymers.

Entry	HEMA[a] (mol%)	M_w[b,c] (Kg·mol^{-1})	Đ[b]	T_m[d] (°C)	X_c[d,e] (°C)	T_β[f] (°C)
(LD)PE	0	200	7.7	119.5	29.2	n.d.
PE-HEMA 1	1.6	270	9.2	108.3	25.6	10.0
PE-HEMA 2	5.15	85	6.3	97.9	14.8	-0.3
PE-HEMA 3	6.8	37	3.8	91.5	7.9	-3.5
PE-HEMA 4	12.4	35	3.6	80.5	5.0	-10.8

[a] det. *via* NMR; [b] det. *via* GPC; [c] decreasing molecular weight due to HEMA acting as a chain transfer agent;[36] [d] det. *via* DSC; [e] X_c calc. with heat of fusion of PE = 286.2 J·g^{-1};[37]
[f] det. *via* DMTA.

introduction of HEMA is reasonably homogeneous and blocks of HEMA are unlikely. Unsurprisingly, with higher HEMA content the amount of SCB increases, as the number of SCB is obtained from the methyl signal of the acrylate.

In PE and related *co*-polymers such as PE-HEMA, usually three main relaxations α, β, and γ are observed during DMTA measurements. Specifically, α, the melting temperature, β close to room temperature and γ below 100 °C, respectively.[38,39] The obtained DMTA data for all PE-HEMA polymers is shown in Figure 3.1. The γ relaxation was not observed within the available measurement regime between 100 °C and 200 °C. A non-PE related relaxation is observed for at -70 °C, which increases in intensity with increasing HEMA content. We thus supposed that this relaxation is the result of motion induced by breaking and reforming hydrogen-bonds of the HEMA side chain.[40]

Associated with main chain movements in the amorphous region,[41] recent evidence denotes the β relaxation as the T_g of PE and its copolymers.[42] This relaxation has been found to change in intensity and location with the degree of crystallinity because of hindered amorphous chain segments as a result of the physical cross-links provided by the polymer crystallites.[43,44] The T_β is found to decrease with HEMA content, even though the hydrogen

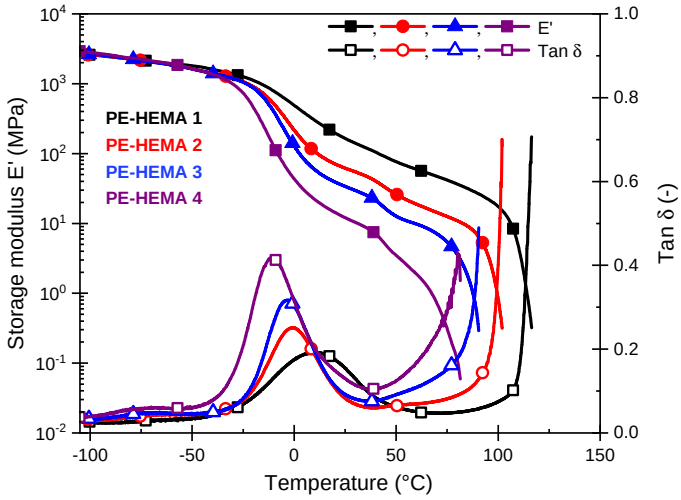

Figure 3.1: DMTA data of PE-HEMA polymers **1** – **4**. E' is represented by closed, Tan δ by open symbols.

bonding provided by HEMA has the possibility to increase T_β. A better correlation of T_β and polymer properties is found by the reduction of degree of crystallinity (X_c). Figure 3.2 shows the content of HEMA and X_c as a function of the obtained T_β for PE-HEMA polymers **1** – **4**. A clear correlation between the reduction of X_c and decrease of T_β is found, and the reduction of X_c is a result of the increasing HEMA content which cannot *co*-crystallize.

Synthesis of Multiple Hydrogen-Bonding Functionalized PE Polymers.

The synthesis pathway for the formation of multiple hydrogen-bonded semi-crystalline low density polyethylene ((LD)PE) is depicted in Figure 3.3. The reaction was carried out for 4 h at 100 °C in toluene with dibutyltin dilaurate (DBTDL) acting as a catalyst. An overview of the prepared functional polymers **P1** – **P4**, the content of introduced ODIN determined *via* either NMR or elemental analysis (EA) and some characteristic thermal data are given in Table 3.2.

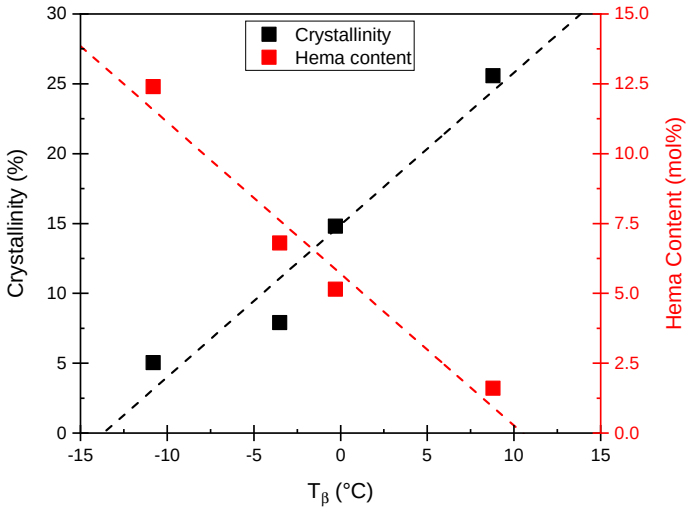

Figure 3.2: Relationship of T_β observed in PE-HEMA *co*-polymers with their crystallinity and HEMA content.

The M_w was not determined after functionalization due to solubility issues in *o*-dichlorobenzene. Because of the nature of cross-linking *via* multiple hydrogen bonding moieties, the virtual M_w should increase, reflected by the decreased solubility.[45] ^{1}H NMR of **P1** – **P4** in tetrachloroethane-d_2 (TCE-d_2) at 120 °C revealed the characteristic, strongly downfield shifted signals corresponding to amine protons participating in multiple hydrogen bonding (Figure 3.4 **A**).[46] The degree of functionalization could be investigated *via* ^{1}H NMR by following the intensity of the HEMA methylene signals (δ = 3.85 ppm and 4.25 ppm).

A selected portion of the ^{1}H NMR spectrum for **P1**, detailing the hydroxyethylene methylene signals, is shown in Figure 3.4 **B**. The two distinct methylene signals of non-functional HEMA combine to a single peak after formation of the carbamate (δ = 4.3 ppm). From the ratio of these two signals (non-functionalized and ODIN functionalized HEMA) the degree of functionalization can be determined. About 40 – 60 % of hydroxy groups were grafted with the ODIN motif, with increasing reaction time having no considerable effect on grafting percentage.

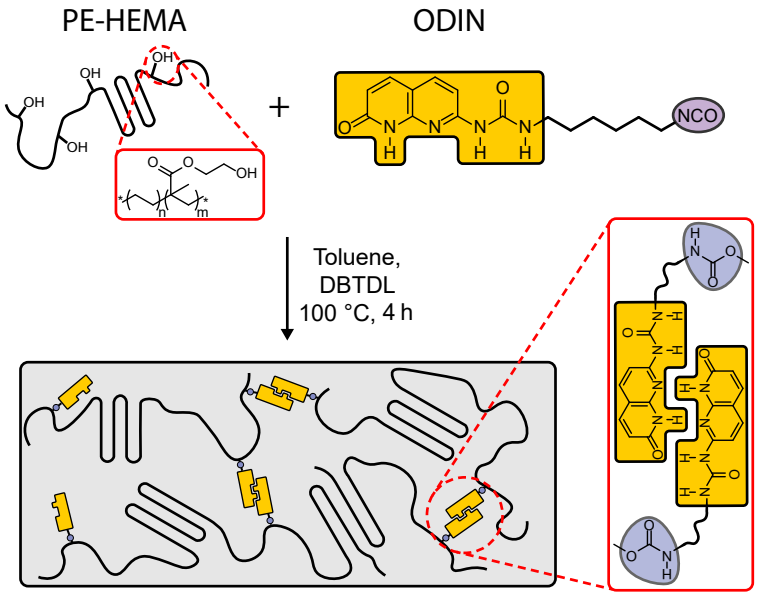

Figure 3.3: Synthesis of hydrogen bonding functionalized PE-HEMA; Cartoon depicts semi-crystalline nature of resulting polymer cross-linked *via* multiple hydrogen bonding moieties.

Table 3.2: HEMA content, GPC data and thermal data for PE-HEMA *co*-polymers.

Entry	Parent-Polymer	ODIN[a] (mol%)	ODIN[b] (mol%)	T_m[d] (°C)	X_c[d,e] (%)	T_β[f] (°C)
P1	PE-HEMA 1	0.96	0.98	107.3	25.0	17.2
P2	PE-HEMA 2	2.16	2.25	95.5	8.2	20.0
P3	PE-HEMA 3	3.06[c]	3.45	86.5	3.1	33.0
P4	PE-HEMA 4	2.98[c]	6.05	79.4	1.3	48.2

[a] det. *via* NMR; [b] det. *via* EA; [c] barely dissolved (TCE-d_2, 120 °C); [d] det. *via* DSC; [e] X_c calc. with heat of fusion of PE = 286.2 J·g^{-1};[37] [f] det. *via* DMTA.

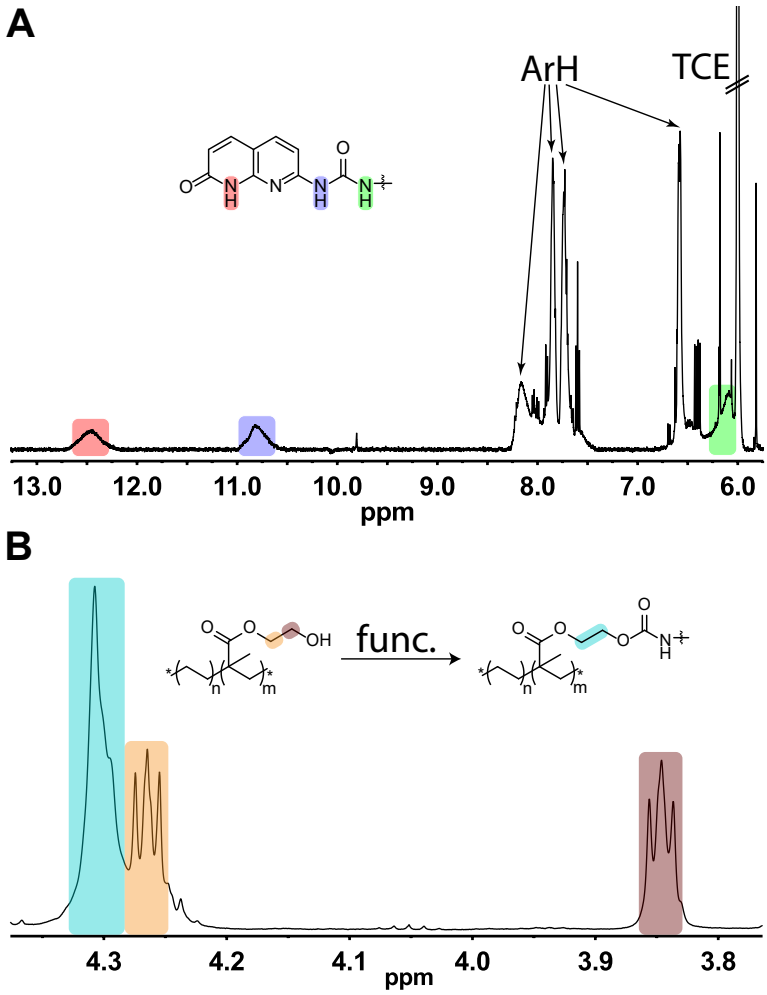

Figure 3.4: **A**: Selected portion of **P1** ^{1}H NMR (120 °C, in TCE-d_2) highlighting the hydrogen bonding region; signal of CH_2-NH is superimposed by the residual solvent TCE signal. **B**: Selected portion of **P1** ^{1}H NMR (120 °C, TCE-d_2), highlighting the HEMA hydroxyethyl signal region; the methylene groups of functionalized HEMA give rise to only a single signal.

However, for functional polymers **P3** and **P4**, ^{1}H NMR was not successful in determining the ODIN content, due to only partial solubility in TCE-d_2 at 120 °C. Therefore, elemental analysis (EA) was performed to determine the amount of incorporated ODIN. Empiric calculations were performed in order to match the observed hydrogen, carbon, and nitrogen content with the theoretical amount of ODIN that would have to be present in the polymer to match these values. The EA determined ODIN content was in good agreement with the ^{1}H NMR determined content for soluble polymers **P1** and **P2**. For **P3** and **P4**, a higher amount of grafting percentage was determiend by EA. Due to the low solubility, the NMR determined content underestimated the actual one, and the EA determined content will be used for subsequent comparison of these materials. Thereby, polymers with ODIN content ranging from 1 mol% – 6 mol% could be obtained (Table 3.2). If we assume that the number of repeating units per chain does not change with functionalization, the average number of hydrogen bonding motifs per chains n_{HB} can be calculated according to equation 3.1:[47]

$$n_{HB} = \frac{M_n \cdot x_{HB}}{M_{HEMA} \cdot x_{HEMA} + M_{Et} \cdot (1 - x_{HEMA})} \tag{3.1}$$

with M_n as the number average molecular weight of parent PE-HEMA, x_{HB} and x_{HEMA} as the molar fraction of ODIN (HB) and HEMA and M_{HEMA}, and M_{Et} as the molecular weight of HEMA and ethylene. According to eq 3.1, n_{HB} was determined to be 9.9, 9.5, 9.5, and 14.3 for polymers **P1**, **P2**, **P3**, and **P4**, respectively. Given that there are many more than two moieties per chain, a supramolecular network should be formed as long as the association of dimers is thermodynamically favored.

3.1.2 Dynamic Cross-Linking of Polyethylene *via* Sextuple Hydrogen Bonding Array: Material Properties

Hydrogen Bonding in ODIN-PE-HEMA Polymers

The influence of the introduction of the multiple hydrogen bonding moieties was investigated *via* DSC measurements on functional polymers (graphs in Figure B.3). Compared to the pristine polymers, T_m and X_c of functionalized materials decreases. The bulky motif grafted onto the polymer backbone

hinders crystallization of the polymer main chain, reducing crystallinity and T_m.[48–51]

To showcase the adaptable nature of the hydrogen bonding functionalized system, stress relaxation was performed on **P2** at 140 °C in tensile mode. A strain of 0.5 % was applied to **P2** and the resulting stress, normalized for the initial stress, was monitored over time (see Figure B.4). A slow decline of the normalized stress to 20 % of the initial value is observed within 1,000 s, with full relaxation expected to be reached within 10,000 s. Even though relaxation is slow, stress of the physically cross-linked material can relax over time. In addition, it was possible to prepare defect free samples suitable for mechanical analysis *via* compression molding at 150 °C (see Figure B.5), revealing indeed adaptability of our hydrogen bonding network. Compression molded samples of functionalized polymers and their respective PE-HEMA counterparts were analyzed *via* DMTA. The data, obtained for **P2** and corresponding PE-HEMA **2**, is presented in Figure 3.5 **A** (DMTA Graphs for **P1**, **P3**, and **P4** in Figure B.6). Because not all HEMA groups of the pristine polymers were functionalized, the relaxation related to the motion induced by breaking and reforming hydrogen-bonds of the HEMA side chain[40] is still observable in the polymers **P2** – **P4**.

The β relaxation is related to any type of branching and cross links inside the polymer,[44] and any type of additional branching points or cross-links should raise T_β. Indeed, T_β is found to shift to higher temperatures for all functionalized polymers. This is a result of the multiple hydrogen bonding facilitated formation of physical cross-links between chains. A similar influence for the T_g of multiple hydrogen bonding functionalized polymers was previously observed, attributed to a restricted chain movement.[47,52,53] Since the β relaxation has been denoted as T_g of PE and its copolymers,[42] we anticipated the same effect for our functional materials. In fact, despite large molecular weight differences between pristine PE-HEMA polymers, DMTA determined ΔT_g increases linearly with ODIN content between pristine and functional polymers (Figure B.7). This reflects a behavior previously observed for UPy functionalized methacrylate, where the T_g increased linearly with UPy content for polymers of equal molecular weight.[47,54] The same relationship was not apparent for DSC determined T_g, which we attribute

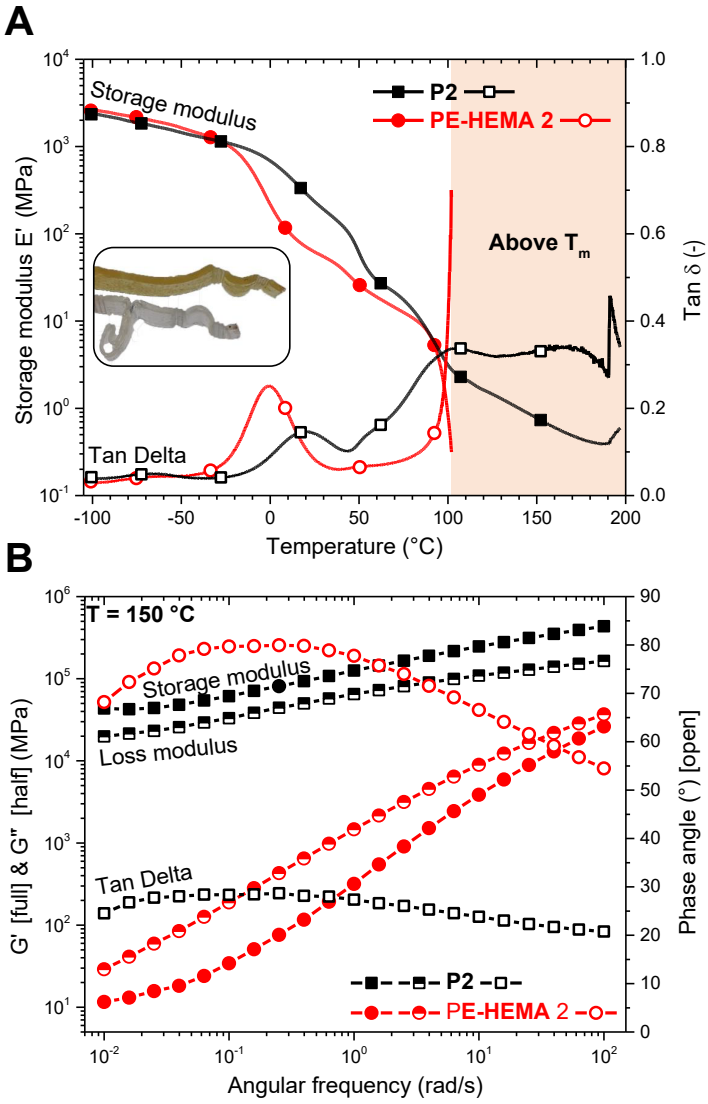

Figure 3.5: **A**: DMTA sweep of **P2** (black) and PE-HEMA **2** (red); E' is represented by closed, Tan δ by open symbols; The light red square highlights the temperature range above melting of the crystalline region; Inset shows DMTA strips after measurements: **P2** top, PE-HEMA **2** bottom. **B**: Rheology frequency sweep from 0.01 rad·s^{-1} to 100 rad·s^{-1} of **P2** (black) and PE-HEMA **2** (red) at 150 °C. G' is represented by closed, G" by half, and phase angle by open symbols.

to the low signals to noise ratio, making exact determination of T_g difficult.

The cross-links were still in effect within the region between T_β and T_α ($T > 50$ °C), where a greater E' was measured for **P2** and **P3**, with a less pronounced difference observed for **P1**.[55] The α transition, usually related to main chain movements that become possible at the onset of melting of the crystalline phase,[38,44,56] is observed as a rapid increase of the Tan δ for all of the pristine polymers until melting of the sample specimen leads to measurement stop. For functionalized samples, a more gradual increase of Tan δ is observed leading into a peak for **P2**, **P3**, and **P4** with Tan δ of **P1** forming a shoulder around the melting temperature.

Remarkably, heating above T_m did not lead to measurement stop for functionalized samples and the elastic character was retained, revealing a rubbery plateau after melting, which is characteristic for cross-linked polymers.[57–59] We attribute the formation of this plateau modulus to the cross-linking *via* multiple hydrogen bonding arrays, that is still effective above T_m. This was unexpected, because these arrays of hydrogen bonds are expected to progressively dissociate at elevated temperatures,[29,60] and adaptability of our network was apparent from stress relaxation measurements and from the possibility to obtain defect free samples *via* compression molding. In contrast to cross-linked rubber, where E' usually remains constant above T_g,[61–63] E' decreases gradually after T_m up until 190 °C for the functional polymers. At 190 °C, the polymer structure changes involving the formation of permanent cross-links causing an increase in E', which will be discussed at a later stage. Because the hydrogen bonding moieties are in equilibrium between dissociated and associated states, we conclude that the increasing temperature causes a shift from the dimeric to monomeric state, thus decreasing the cross-link density.[53,54,64] The conformational stability of functional samples at elevated temperatures is easily visualized by looking at the DMTA sample strips after measurement displayed in the inset picture of Figure 3.5 **A**. Melting compromised the shape of pristine- (bottom), but not of functional sample (top).

To investigate the properties of ODIN functional polymers in the melt state, **P2** was subjected to a frequency sweep at 150 °C using parallel plate rheology, which is the temperature of compression molding, and compared

to the pristine PE-HEMA **2**. The data for both polymers are shown in Figure 3.5 **B**. At 150 °C, the pristine sample (red line) was completely molten and displayed typical behavior of entangled polymer melts.[65] The loss modulus (shear) (G") is above the storage modulus (shear) (G') over the entire frequency range, typical for non-cross-linked thermoplastics in the melt. No crossover point is observed for the pristine polymer within the measured frequency range, likely because it would occur outside of the measurement range. Both, G" and G' are strongly dependent on the observed time scale, displaying NEWTONIAN like flow behavior at long timescales (low frequencies) and more elastic behavior at short timescales (higher frequencies). However, the frequency sweep of the functional polymer reveals a completely different behavior. G' is above G" over the entire frequency range, displaying solid, not melt like behavior. Additionally, the moduli are largely unaffected by frequency. Both are characteristic properties of cross-linked polymer systems, revealing the effective cross linking *via* multiple hydrogen bonding in the melt.[65]

To confirm our theory that the multiple hydrogen bonding motifs are largely associated at elevated temperatures, VTIR was performed on **P3** and compared to the VTIR data of the supramolecular polymer JEFFODIN described in Section 2.2. For JEFFODIN (Spectra in Figure 2.6) clear shifts were observed in the C=O stretching and N-H bending region, which indicate the dissociation of hydrogen bonds.[66] On the contrary, for the spectra of **P3** depicted in Figure 3.6, only one peak can be observed to clearly change around 720 cm^{-1}, corresponding to the melting of PE crystallites.[67] No clear influence of temperature on peaks involved in hydrogen bonding is apparent for ODIN functionalized polymers. This can be attributed either to the influence of the apolar polymer matrix known to increase the strength of hydrogen bonds,[29,32] or by the cooperative associative effect due to the increased amount of moieties per chain. This effect was previously elucidated by LONG *et al.*, showing that more thermal energy was required to disrupt association of species with increasing numbers of UPy moieties.[68] Based on these results, multiple hydrogen bonding is clearly still in effect for ODIN functional polyolefins after melting of the crystalline regions and responsible for the observed plateau moduli after melting.

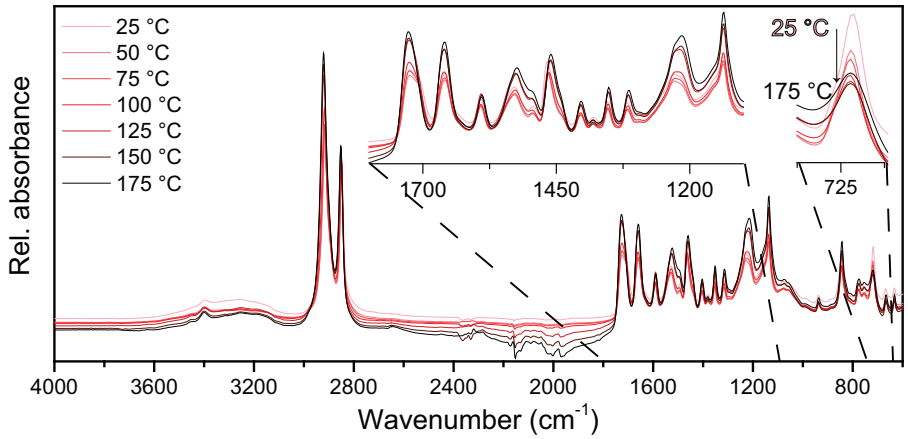

Figure 3.6: VTIR spectra of ODIN functional polymer **P3**. Samples were heated step-wise starting from 25 °C to 175 °C. The shifting absorption bands are indicated with arrows. Spectra are normalized for the C-H stretch region around 2830 cm^{-1}.

Thermal Stability of ODIN-PE-HEMA Polymers

One of the main motivations for developing the ODIN motif was the desired improved thermal stability over UPy functionalized polymers. To investigate the temperature of degradation, heat cycling DSC measurements were performed, repeatedly heating in steps of 10 °C/cycle from 160 °C to 250 °C using a heating rate of 10 $K \cdot min^{-1}$ (Figure B.8). The evolution of T_m was followed, and its shift interpreted as degradation of the polymer structure. Indeed, for ODIN functionalized PE-HEMA, a T_m shift occurs at about 190 °C, placing the degradation temperature around 40 °C higher than the degradation temperature of UPy.[69,70] For some UPy functionalized polymer systems, thermal stability above 200 °C is claimed in literature, based on thermogravimetric analysis (TGA) results alone.[71,72] Given the contradicting nature of these claims with other reported thermal stabilities of UPy functionalized polymers,[69] we suspected that TGA would give a false sense about the thermal stability of ODIN functional polymers, as it relates to the formation of volatiles.

To investigate whether TGA would report thermal stability higher than 190 °C for ODIN functionalized polymers, polymers **P3** and corresponding

PE-HEMA **3** were subjected to TGA and TGA-DSC measurements. Two major weight loss steps were observed for the functionalized polymer at 300 °C and 440 °C (Figure B.9). During the first step, a mass loss of 24.76 % was observed, in line with the theoretical weight loss of 24.58 % for full abstraction of ODIN-motif in **P3**, cleaved at the carbamate linkage. Consequently, we surmise that during the first weight loss step ODIN and the linker chain degrade into volatiles, whereas the second weight loss step is caused by the polymer main chain degradation. This is coherent with the measurement of parent PE-HEMA 3, where only one weight loss step, in line with the second weight loss step of the functional polymer, was observed (Figure B.10). No weight loss or peak in DSC-TGA was observed at 190 °C, the temperature of degradation determined *via* DSC.

As previously mentioned, the urea group in UPy is thermoreversible, and raising the temperature to a certain point break the urea bond and initiates the formation of amine and isocyanate species. Likewise, we assumed that the urea moiety of ODIN motif is thermoreversible. Therefore, thermal treatment of functional polymer species between 190 °C and 300 °C would not lead to degradation as such, but to formation of permanent cross-links facilitated by isocyanate-amine reactions according to the concept illustrated in Figure 3.7. To investigate this theory, DMA was performed on **P4** at 190 °C, the degradation temperature determined *via* DSC, while monitoring the E', the E", and the Tan δ as a function of time. **P4** was chosen because it has the highest amount of ODIN and changes should be seen easily. The obtained data are shown in Figure 3.8. After 2 min at 190 °C, an increase in E' accompanied by a decrease of Tan δ is observed. It is known that the formation of permanent cross-links can be result in an increase of the E'.[73,74] The propose, that permanent cross-linking takes place in the polymer sample and theorize, that this is the result of reformation of isocyanates and amines followed by immediate cross-linking of these species. Based on these results, together with the results obtained from DSC and TGA, we believe that TGA alone cannot be the sole technique on which to claim thermal stability and structural integrity on for these aryl urea type multiple hydrogen bonding species attached to polymers.

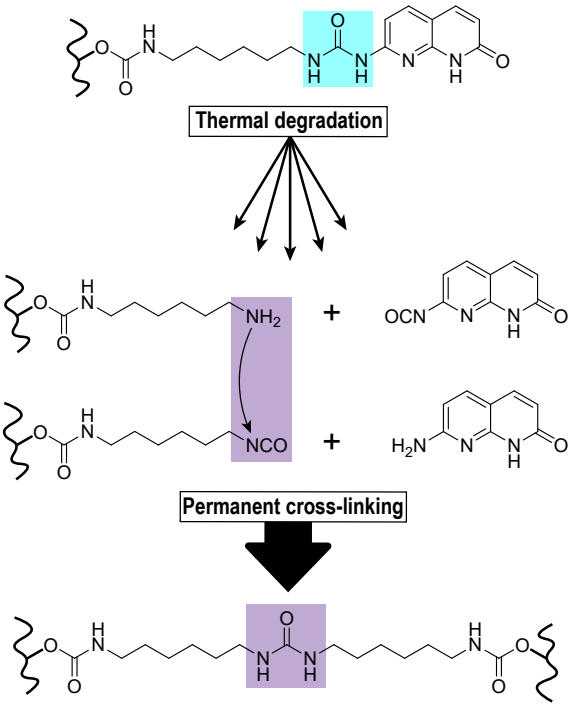

Figure 3.7: Illustration of proposed pathway leading to permanent cross-links. Temperature triggered thermal reversion of the isocyanate groups results in formation of amines and isocyanates on the aryl and alkyl parts of the motif. Then, permanent cross-links are introduced when amine and isocyanate chains attached to the polymer backbone react with each other, forming a more stable urea.

Tensile Properties of Functionalized Polymers

To assess the influence of cross-linking with ODIN on tensile properties, functionalized polymers **P1** – **P4** were subjected to tensile tests and compared to their respective pristine counterparts, as well as the reference PE sample. The tensile strength and Young's modulus data for the measured polymers are given in Figure 3.9. Not shown are the data for strain at break, which generally decreases for functionalized polymers due to the formed cross-links.[75,76] The tensile strength of our reference (LD)PE material was within commonly obtained values.[77]

For **P1**, no improved strength or increased stiffness was observed after functionalization, likely because of the reduced crystallinity of functionalized

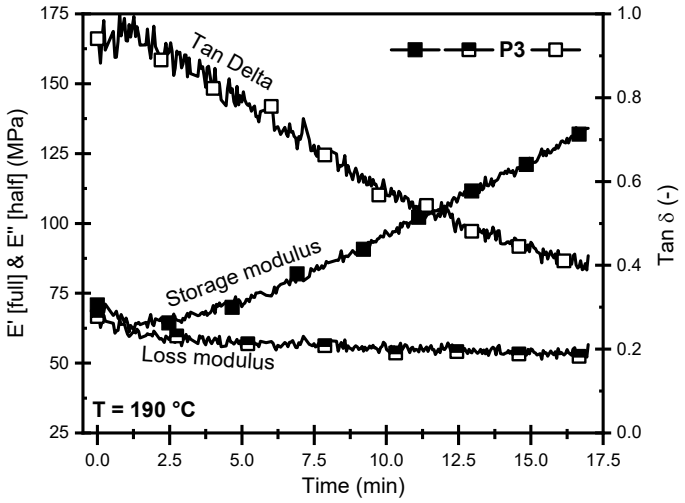

Figure 3.8: Graph of E', E", and Tan δ of **P3** measured in DMA tensile mode over 16 min at a constant temperature of 190 °C.

sample without yet forming a strong enough multiple hydrogen bonding network. For PE-HEMA **2**, **3**, and **4** however, the functionalization with ODIN tends to increase tensile strength and significantly increases stiffness of the soft polymers. The tensile strength of PE-HEMA **4** was improved threefold, displaying the potential of the ODIN motif to improve mechanical properties of polymeric species.[78] Interestingly, no improvement of tensile strength and only slightly increased stiffness was observed between **P3** and **P4**, despite the latter being functionalized with almost twice the amount of ODIN, revealing diminishing returns of extensive ODIN functionalization. Compared to the PE reference, tensile properties seem to be on par or slightly increased. This is due to the significantly reduced crystallinity of functionalized samples compared to the semi-crystalline PE reference.[79]

Multiple Hydrogen Bonding Cross-Linked Polyethylene as Oxygen Barrier Material

To reduce gas permeability through semi crystalline polymers, the free volume available for permeation may be reduced.[80] Reduction of the polymer free

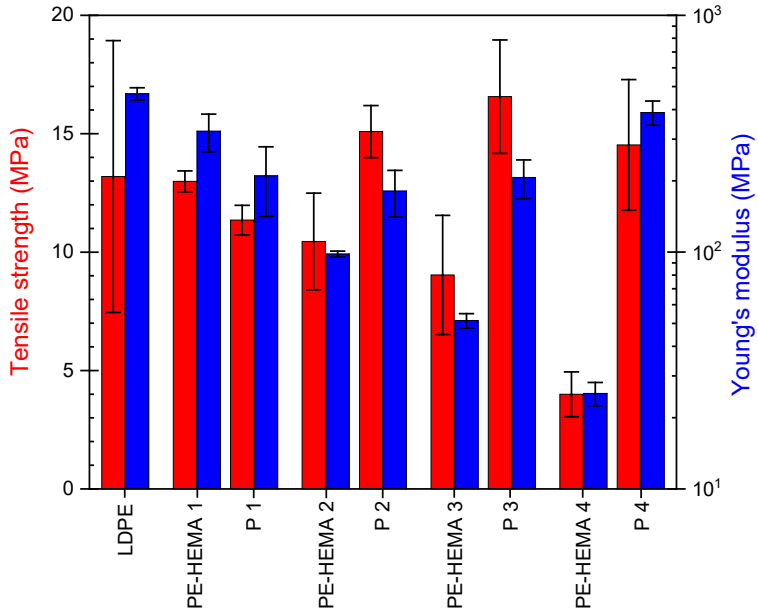

Figure 3.9: Measured average Tensile strength and Young's modulus for reference LDPE, **P1** – **4** and related parent PE-HEMA polymers determined from at least three test specimens.

volume can be achieved by affecting either size or shape of polymer crystals, or by reducing the chain mobility in the amorphous regions.[14] By introducing cross-links in the amorphous phase, the cohesive energy density between chains can be increased, which in turn reduces the oxygen permeability.[81] The formation of an efficient hydrogen bonding network should provide such cross-links resulting in increased barrier properties.

To investigate the effect of HEMA content and ODIN functionalization on the water and oxygen barrier properties, standard measurements[82] were performed to determine oxygen transmission rates (OTRs) and water vapor transmission rates (WVTRs) of selected polymers. The thickness corrected values for OTR obtained at 38 °C, 50 % r.h. and WVTR measured at 23 °C, 85 % r.h., are illustrated in Figure 3.10 (tabulated data and graph for OTR measured at 23 °C, 0 % r.h. are reported in Table B.1 and Figure B.11, respectively). For PE-HEMA copolymers, a HEMA content dependent increase in both WVTR and OTR is observed during the 50 % r.h. measurement. This is due to the water penetrating the polymer matrix,

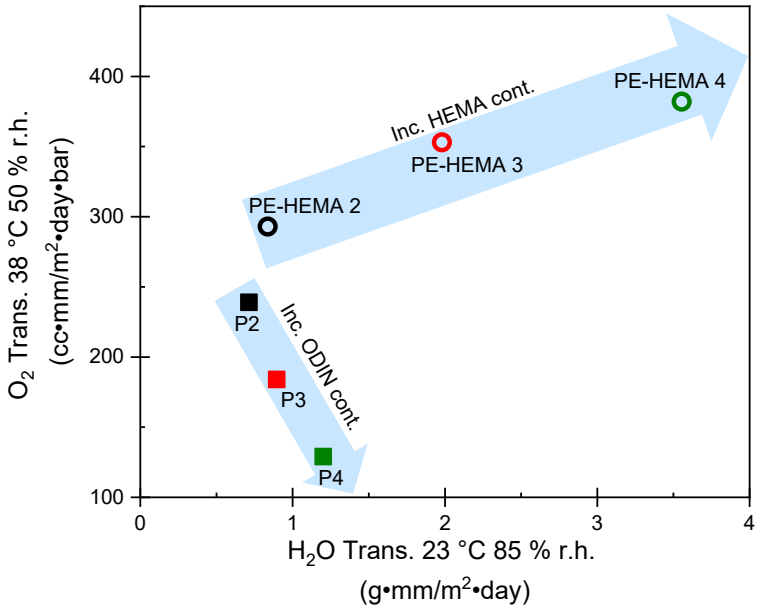

Figure 3.10: OTR and WVTR of pristine and ODIN functional polymers. OTR was measured at 38 °C, 50 % r.h. and WVTR at 23 °C, 85 % r.h.. Corresponding pristine (open circles) and ODIN functional (closed squares) polymers share the same color. The arrows highlight the trend in transmission rates with respect to increasing HEMA and ODIN content for pristine and ODIN functional polymers.

revoking the interchain hydrogen bonds, therefore progressively affecting polymers with greater HEMA content.[14] By contrast, the measurements at near zero humidity reveal an almost constant OTR between different PE-HEMA polymers, because the hydrogen bonding remains intact (Figure B.11). The increased HEMA content should decrease the OTR due to network formation, but the advantageous effects are likely off set by the loss in crystallinity caused by the introduction of HEMA (see Figure B.2 and Figure 3.2). Upon functionalization of PE-HEMA polymers with ODIN, a gradual decrease in OTR is observed between pristine and functional polymers measured at 38 °C, 50 % r.h.. Also, with increasing ODIN content a lower OTR rate is observed, not being adversely affected by humidity in the same manner as pristine polymers with higher HEMA content were. In addition, an almost equal WVTR can be observed for all functional samples,

showcasing the increased stability of these hydrogen bonding arrays towards humidity compared to single hydroxy hydrogen bonds. Regardless, in order to match the performance of current multilayer solutions employing layers of EVOH and polyolefins a 10- or 100 fold decrease of the OTR would be required, revealing the current limit of the presented solution.

3.2 Dynamic Cross-Linking of Polypropylene *via* Sextuple Hydrogen Bonding Array

The increased thermal stability of ODIN described in Section 3.1.2 allows its use in polymers with higher melting points. Thus, the functionalization of PP was targeted, a polymer with a melting point usually found above 160 °C,[83] which is above the degradation temperature of UPy. The initial challenge here is to design or find a PP with suitable functionalities for the incorporation of ODIN.

3.2.1 Synthesis of ODIN Functional Polypropylene

One of the most common and thus easily accessible grades of functional PP is polypropylene-*graft*-(maleic anhydride) (PP-MA). PP-MA is usually obtained by in reactor grafting of MA onto grades of PP using small amounts of peroxides as initiator, an easy to upscale process.[84,85] We decided to use a commercially available PP-MA grade from EXXELOR, PO 1020. This grade is listed with a MA content of 0.64 wt% to 0.8 wt% by the manufacturer. The MA content can be determined using ^{1}H NMR,[84] and we found a MA content of 0.77 wt% (0.325 mol%) (see Figure B.12). The MA moiety can readily react with nucleophiles such as amines to form an imide,[86] making it possible to introduce further functionality. Therefore, in order to introduce ODIN in an easy manner, either an ODIN derivative with amine functionality is required, or a PP-MA with a hydroxy or amine moiety suitable to react with the isocyanate of **4**.

We decided to use **4** and employ an established method to introduce free hydroxy groups to PP-MA, which is readily achieved by reacting the MA moiety with a slight excess of aminoalcohols.[48,86] The thereby obtained free hydroxy groups can then react with the isocyanate of **4**, forming a

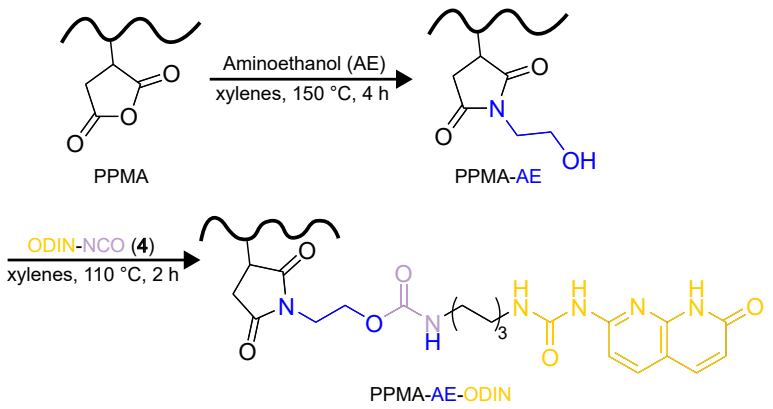

Figure 3.11: Synthesis scheme for ODIN functional PP (PP-MA-AE-ODIN).

multiple hydrogen bonding cross-linked PP. The general strategy is illustrated in Figure 3.11. To ensure full functionalization with aminoethanol, a twofold excess was used for the functionalization of PP-MA. The successful reaction was confirmed by FTIR and NMR. Specifically, the symmetric and asymmetric C=O stretching band of the anhydride at 1790 cm^{-1} and 1840 cm^{-1} (see Figure 3.12 **A**)[84] are found to disappear after reaction with aminoethanol. No clear new band appears, but from the overlay of the PP-MA and PP-MA-AE spectra the band located at 1714 cm^{-1}, corresponding to the open diacid form of the MA moiety,[85] shifts to 1705 cm^{-1} after formation of the maleimide. This absorption is caused by the C=O groups of the closed imide ring, confirming the successful reaction.[48]

The NMR signals of the MA and aminoethanol moieties are not well resolved due to the relatively low amount of functional group content and the complex correlation times associated with proton NMR of polymers,[87] but the disappearance of the MA peaks at 2.86 ppm and 2.91 ppm, and appearance of the aminoethanol peaks in the range of 3.2 ppm – 4.0 ppm in combination with the shifted MA signals is associated with the success of the reaction in literature (NMR in Figure 3.12 **B**).[48]

The grafting of the ODIN motif onto PP-MA-AE was done in xylenes, using a small excess of ODIN and DBTDL as a catalyst to ensure full grafting. The overlay of the FTIR spectra of PP-MA-AE and PP-MA-AE-ODIN seen in Figure 3.12 **A** reveals the appearance of multiple new

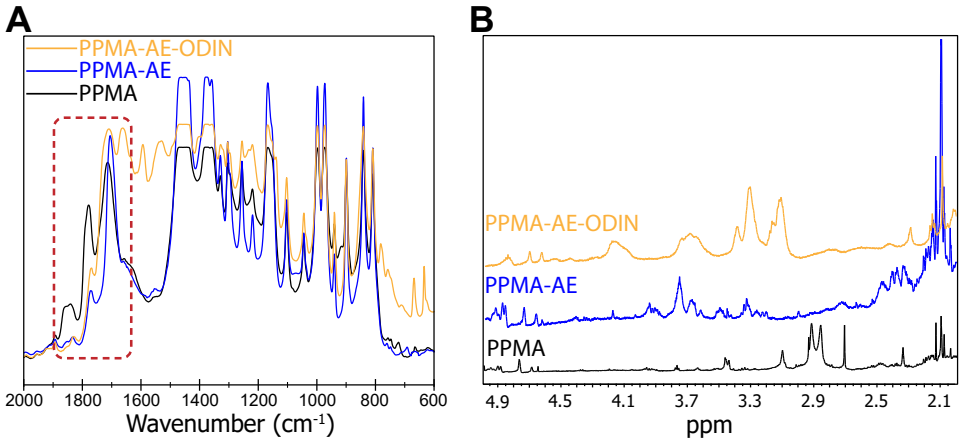

Figure 3.12: Analysis of functional PP-MA. **A**: FTIR-spectra from 600 cm^{-1} to 2000 cm^{-1} of PP-MA, PP-MA-AE, and PP-MA-AE-ODIN. The dashed red colored triangle highlights the C=O absorption region. **B**: Part of the ^{1}H NMR spectrum (in TCE-d_2, at 120 °C) of PP-MA, PP-MA-AE, and PP-MA-AE-ODIN, focusing on the signals in the vicinity of the MA moieties.

absorption bands in the carbonyl absorption region in the range between 1500 cm^{-1} and 1750 cm^{-1}, which correspond to the C=O stretching bands of the naphthyridine C=O, urea C=O, as well as the newly formed carbamate linkage. The cutout of the ^{1}H NMR spectrum of PP-MA-AE-ODIN in Figure 3.12 **B** reveals the appearance of multiple new signals. The signals at 3.2 ppm and 3.4 ppm belong to the methylene protons directly adjacent to the urea and carbamate group of the HDI linker chain, revealing the successful attachment of the ODIN motif. The aminoethanol methylene groups form two broad peaks at 3.8 ppm and 4.3 ppm. The MA signals of the ring are superimposed by the methylene signals of the linker chain and aminoethanol. An overview of the two synthesized and the commercial polymer with functional group content and thermal data are given in Table 3.3.

3.2.2 Hydrogen Bonding in Polypropylene

The T_g determined by DSC increases for the ODIN functional sample, which is in line with the observations made for the supramolecular PE described in 3.1.2, a result from the cross-linking with ODIN motif.[47,52,53]

For PP-MA and PP-MA-AE the X_c is close enough to be considered within the experimental error (Table 3.3. The bulky ODIN motif decreases X_c, but T_m is not affected, indicating that only the degree of crystallinity, not the lamellar thickness were affected.[89]

As the main point of interest, the dynamic properties of hydrogen bonding cross-linked PP were analyzed to see if similar observations can be made as for the supramolecular PE. Therefore, suitable samples, that were obtained by compression molding of the polymer powder obtained after synthesis, were analyzed using DMTA and parallel plate rheology. The obtained DMTA data for PP-MA-AE and PP-MA-AE-ODIN is depicted in Figure 3.13 **A**. With dynamic measurements such as DMTA, the T_g of PP can be found around 0 °C.[90] For PP-MA-AE, a T_g at 9 °C is observed. Unsurprisingly, the hydrogen bonding cross-linked PP-MA-AE-ODIN displays a slightly increased T_g at 15 °C due to the introduced cross-links that hamper chain movement.[47,54] Apart from the slight shift in T_g, the DMTA data of both polymers is near identical and upon melting of sample strips the measurement stopped, which stays in contrast to the functionalized PE samples described above. Most likely, the significantly lower amount of the ODIN motif does not give enough strength to the polymer after melting, and a higher melt strength could be achieved by using a PP with a higher MA content, allowing for the grafting of additional motif.

A more substantial difference can be observed from the frequency sweeps. These were performed at 180 °C, in order to be above the T_m of the used materials, but below the degradation temperature of ODIN at 190 °C. The

Table 3.3: Overview of prepared functional PP-MA polymers starting from PP-MA and their characteristic thermal data.

Entry	MA content[a] (mol%)	T_m[b] (°C)	X_c[b] (%)	T_g[c] (°C)
PP-MA	0.325	158.94	31.8	-2.50
PP-MA-AE	-	156.02	32.6	-2.09
PP-MA-AE-ODIN	-	159.05	26.8	3.44

[a] det. *via* NMR; [b] X_c calc. with heat of fusion of PP = 238.5 J·g^{-1};[88] [c] det. *via* DSC .

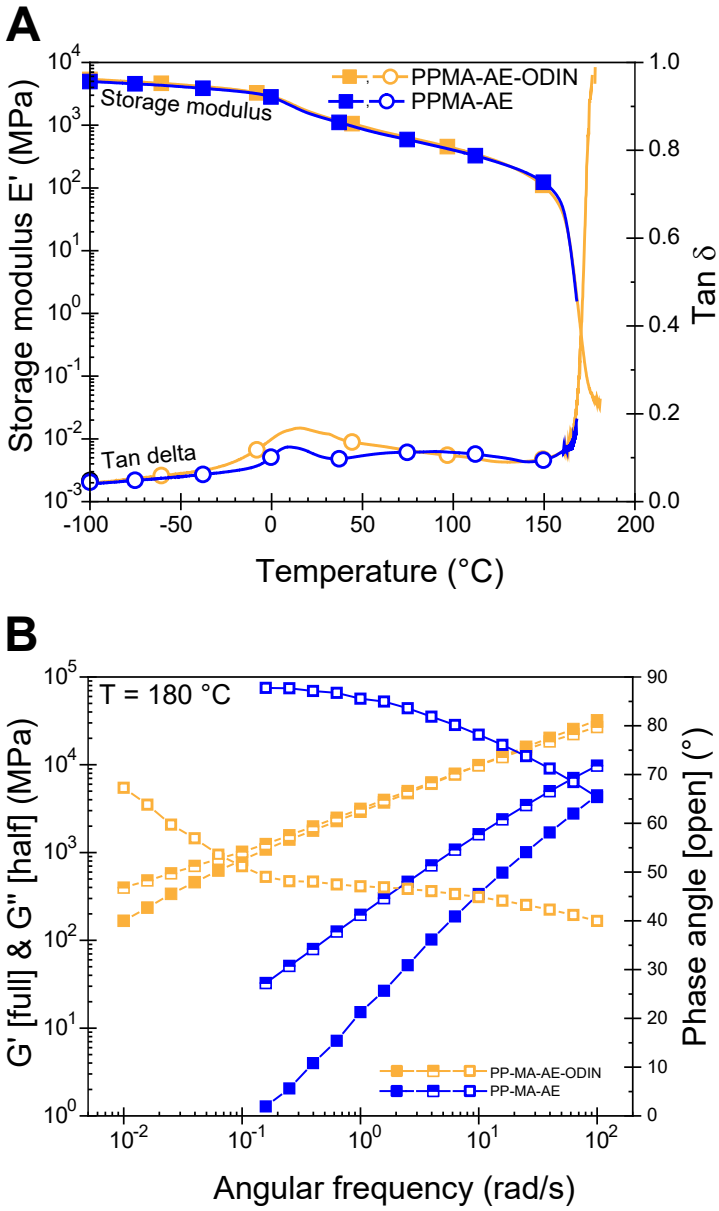

Figure 3.13: **A**: DMTA sweep of PP-MA-AE-ODIN (orange) and PP-MA-AE-ODIN (blue); E' is represented by closed, δ by open symbols. **B**: Rheology frequency sweep from 0.01 rad·s^{-1} to 100 rad·s^{-1} of PP-MA-AE-ODIN (orange) and PP-MA-AE (blue) at 180 °C. G' is represented by closed, G" by half, and phase angle by open symbols.

obtained data for PP-MA-AE and PP-MA-AE-ODIN is shown in Figure 3.13 **B**. Over the entire frequency range, PP-MA-AE without ODIN functionalities behaves like an non-entangled polymer melt with G" staying above G', and no crossover frequency was observed.[65] The ODIN functionalized material displays significantly higher moduli and the rheology behavior changed to the point that a crossover frequency occurs at about 10 Hz. This also explains why no plateau modulus was found during DMTA, since the sample was stressed at a frequency of 1 Hz.

Evidently, using the ODIN motif presents a viable option to change the flow properties of PP and is superior to UPy due to the increased thermal stability needed for polymers with a T_m point such as PP.

3.3 Conclusions

Using the UPy motif, a plethora of multiple hydrogen bonding functionalized materials have been developed in the past twenty years. However, functionalization of polyolefins has been largely unexplored, with few examples including a fully amorphous (LD)PE material[78] and functionalized PP tested way above the degradation temperature of the UPy motif.[48,69] To overcome the thermal stability issues, the novel self-complementary multiple hydrogen bonding motif ODIN was developed. By reacting ODIN bearing pendant aliphatic isocyanate functionality with PE-HEMA, multiple hydrogen bonding array functionalized polyolefins with an ODIN content ranging from 1 mol% to 6 mol% were obtained. The adaptable nature of the hydrogen bonding system was revealed *via* stress relaxation measurements and compression molding of thin films and sample strips. The formation of a cross-linked network was apparent from (i) the increased T_g determined *via* DMTA, (ii) the increased storage modulus of functionalized polymers above T_g and (iii) the near frequency independent loss and storage moduli determined by parallel plate rheology. Remarkably, cross-linking *via* multiple hydrogen bonding was still relevant after melting of the crystalline lattice, as revealed by parallel plate rheology and DMTA, where a rubbery plateau modulus was observed after melting. The apparent increased strength of hydrogen bonds is attributed to the apolar polymer matrix, elucidated by

VTIR measurements. In comparison to UPy functionalized polymers, degradation involving permanent cross-linking of ODIN functional polyolefins occurs about 40 °C later. Moreover, compared to single hydrogen bonds, an increased resilience of the sextuple hydrogen bonding motif towards humidity was revealed during measurements of the OTRs and the WVTRs. The concept of changing the flow properties of polymers could be extended to MA functionalized PP, a polymer that usually melts above the degradation temperature of the UPy motif. For subsequent research, the influence of the polymer matrix must be considered in the design of multiple hydrogen bonding functionalized polymers. An appropriate polymer matrix could be used to tune the strength of hydrogen bonding moieties, making dimers with weaker association constants attractive choices. The increased thermal stability of ODIN should provide a useful tool for functionalization of polyolefins, but a key aspect will be to introduce moieties without adversely affecting the crystallinity of these polymers.

3.4 Experimental Section

3.4.1 Methods

High temperature nuclear magnetic resonance (HTNMR). HTNMR spectra were recorded on a Bruker AVANCE III (500 MHz) equipped with a cryogenically cooled probe head at 120 °C in TCE-d_2. ^{1}H NMR chemical shifts are reported in ppm and given in reference to the residual solvent peak of TCE-d_2 at 6.00 ppm.

Fourier *transformed infrared spectroscopy* (FTIR). FTIR-spectra were recorded on a Perkin Elmer *Spectrum One* equipped with a Golden Gate accessory (diamond ATR). the VTIR spectra were recorded on a Bruker Vertex 70 spectrometer equipped with a temperature controlled diamond ATR accessory (*GladiATR* 300 by PIKE *Technologies*). First, spectra were recorded of the empty crystal at all employed temperatures. These spectra were subsequently used as background spectra for the actual measurements to compensate for the change in transmission of diamond at elevated temperatures.

Elemental analysis (EA). A small amount of sample is burned in the presence of oxygen. The nitrogen content was determined by means of thermal conductivity (TC) and volumetric. The hydrogen and carbon content were determined by near FTIR.

Gel permeation chromatography (GPC). The GPC measurements were performed on a Polymer Char GPC-IR system using a Polymer Char IR 5 infrared detector and a Wyatt MALLS detector Helios II. As column set of two Polymer laboratories 20 µm m PLgel MIXED ALS (300 x 7.5 mm) were used. Samples were dissolved in *o*-dichlorobenzene and the runs were performed at 160 °C.

Differential scanning calorimetry (DSC). The DSC measurements were performed on a TA Instruments *Q20* equipped with a *RCS 90* cooling system. About 3 – 5 mg of polymeric sample was weighed inside an aluminum pan and subjected to DSC measurements under nitrogen atmosphere. Unless otherwise noted, polymers were screened twice from -90 °C to 200 °C at a constant heating/cooling rate of 10 K·min^{-1}. The T_m, T_g, and the X_c were determined from the second heating, crystallization temperature (T_c) from the second cooling cycle. For calculation of X_c a heat of fusion of 286.2 J·g^{-1} for PE and of 238.5 J·g^{-1} for PP was taken from literature.[37,88]

Tensile tests. Tensile tests were performed on a Zwick type *Z100* tensile tester equipped with a 100 N load cell. Specimens were obtained by cutting strips of 8 cm length and 1 cm width from square films (10 x 10 cm) with an average thickness of 150 µm. Sample strips were clamped and a pre-load of 0.3 MPa was applied, before stretching at a speed of 200 mm·min^{-1} until sample failure occurred.

Compression molding. Polymer films and samples for DMTA and rheology were obtained by following the following protocol: Appropriate molds were filled with the polymer powder, followed by treating the material in a pre-heating step for 5 min at 150 °C, then for 10 min at 150 °C with an applied force of 50 kN and finally cooling at a rate of 15 K·min^{-1} until a temperature of 40 °C was reached while maintaining the applied force.

Dynamic mechanical analysis (DMTA). Rectangular samples suitable for

DMTA were cut to dimension of 3 x 5 x 0.5 mm (length x width x thickness). Samples were measured on a TA Instruments *Q800* in tensile mode. The E' and E" were monitored while screening the samples during a temperature sweep from 100 °C to 200 °C at 3 K·min^{-1}. An oscillation frequency of 1 Hz with an oscillation amplitude of 10 µm were applied.

Rheology. Samples for rheology were prepared *via* compression molding to obtain disk shaped specimens (diameter 25 mm, thickness 1 mm). Samples were measured using a TA Instruments *DHR 2*, equipped with a parallel plate geometry. Samples were measured with a frequency sweep from 100 rad·s^{-1} – 0.01 rad·s^{-1} using a strain amplitude of 0.4 % at a temperature of 150 °C.

Oxygen and water vapor transmission rates. At least two films were measured for each polymer sample and obtained transmissions are reported as the average of both measurements. The OTRs were determined according to ISO 15105 2 at 23 °C, 0 % relative humidity (r.h.) and at 38 °C, 50 % r.h.. The WVTRs were determined at 23 °C, 85 % r.h. adhering to the ISO 15106-3 standard. The thickness of films, ranging from 100 µm to 160 µm was measured at varying locations and the average was used to report thickness corrected OTRs.

3.4.2 Synthesis

Unless otherwise specified, chemicals and solvents were purchased from Sigma-Aldrich and used as received. The poly (ethylene-*co*-(2-hydroxethyl methacrylate)) *co*-polymers were provided by Sabic.

1-(6-isocyanatohexyl)-3-(7-oxo-7,8-dihydro-1,8-naphthyridin-2-yl)urea (**4**).

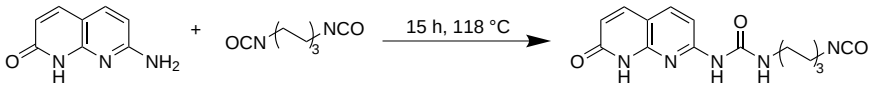

Synthesis described in 4.4.2 (72.7 g, 71 % yield).

Synthesis of ODIN-PE-HEMA polymers (**P1** – **P4**).

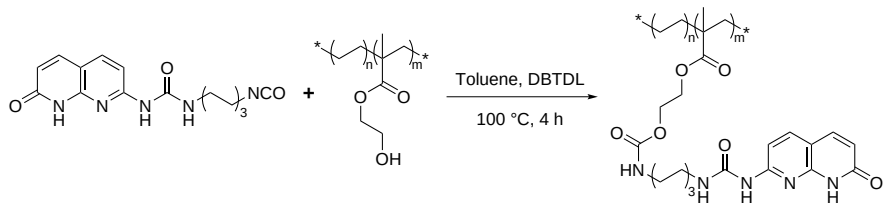

The PE-HEMA *co*-polymers were functionalized according the following general procedure: PE-HEMA (4 g) was dissolved under nitrogen atmosphere in toluene (200 mL) at 80 °C for 1 h inside a custom-made glass reactor equipped with mechanical stirring, cooling and gas inlet. The apparatus was flushed with nitrogen and **4** (1.3 eq with respect to hydroxy groups) was added as a solid, followed by addition of four drops of DBTDL as catalyst. The temperature of the mixture was raised to 100 °C and stirred for 4 h. The hot suspension was filtered through a pre-heated (140 °C) Buchner funnel to filter off residual unreacted **4** and immediately precipitated into isopropanol. The precipitate was dried under vacuum to obtain polymers **P1** – **P4** as off white to yellow solids.

Supramolecular Jeffamine *T3000*

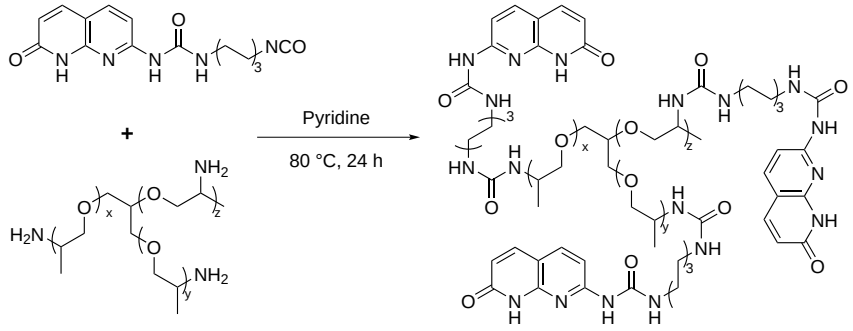

Synthesis described in 4.4.2 (61.2 g, 46 % yield).

Synthesis of PP-MA-AE polymer.

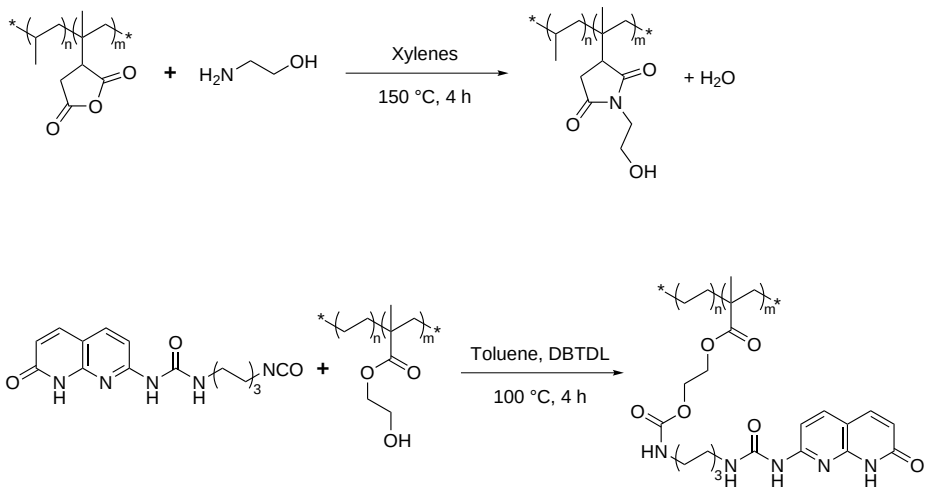

First, 50 g of the PP-MA polymer (Exxelor *PO1020*) with a MA content of 0.8 wt% were dissolved in xylenes (1 L) at 150 °C inside a 2 L round bottom flask equipped with mechanical stirrer and reflux condenser. Then, ethanolamine (0.5 mL, 2 eq with respect to MA units) was added *via* syringe and the mixture stirred for 4 h. The polymer was precipitated from the hot solution into acetone (3 L), filtered off, and dried under high vacuum overnight. 48.3 g of the polymer were recovered.

Synthesis of PP-MA-AE-ODIN polymer.

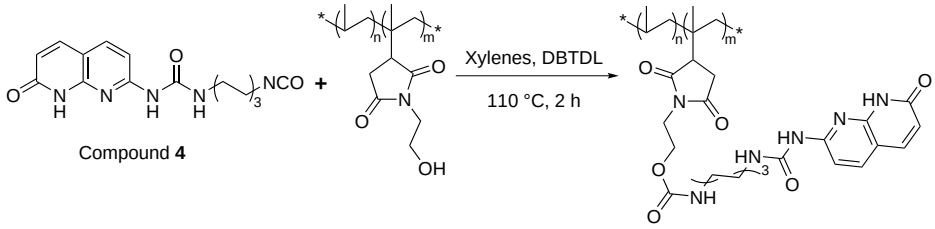

Reaction was performed under nitrogen atmosphere. First, PP-MA-AE (30 g) was dissolved in xylenes (200 mL) at 110 °C inside a custom-made glass reactor equipped with mechanical stirring, cooling and gas inlet. The apparatus was flushed with nitrogen and **4** (1.5 eq with respect to hydroxy groups) was added as a solid, followed by addition of four drops of DBTDL as catalyst. The mixture was stirred for 2 h and subsequently precipitated into acetone. The precipitate was filtered, washed with isopropanol and dried under vacuum to obtain PP-MA-AE-ODIN as light-yellow solids.

References

[1] G. B. Kauffman, *J. Chem. Educ.* **1986**, *63*, A181, DOI 10.1021/ed063pA181.1.

[2] R. Geyer, J. R. Jambeck, K. L. Law, *Sci. Adv.* **2017**, *3*, 1–5, DOI 10.1126/sciadv.1700782.

[3] P. N. Khanam, M. A. A. AlMaadeed, *Adv. Manuf. Polym. Compos. Sci.* **2015**, *1*, 63–79, DOI 10.1179/2055035915Y.0000000002.

[4] L. A. Pruitt, *Biomaterials* **2005**, *26*, 905–915, DOI 10.1016/j.biomaterials.2004.03.022.

[5] S. Wannasri, S. V. Panin, L. R. Ivanova, L. A. Kornienko, S. Piriyayon, *Procedia Eng.* **2009**, *1*, 67–70, DOI 10.1016/j.proeng.2009.06.018.

[6] Y. Zhong, D. Janes, Y. Zheng, M. Hetzer, D. De Kee, *Polym. Eng. Sci.* **2007**, *47*, 1101–1107, DOI 10.1002/pen.20792.

[7] A. M. Walker, Y. Tao, J. M. Torkelson, *Polymer* **2007**, *48*, 1066–1074, DOI 10.1016/j.polymer.2006.12.038.

[8] A Bhattacharyya, S Chen, M Zhu, *Express Polym. Lett.* **2014**, *8*, 74–84, DOI 10.3144/expresspolymlett.2014.10.

[9] Y. Pietrasanta, J. J. Robin, N. Torres, B. Boutevin, *Mech. Time-Dependent Mater.* **1998**, *2*, 85–95, DOI 10.1023/a:1009756818443.

[10] B. Xu, J. Simonsen, W. E. Rochefort, *J. Appl. Polym. Sci.* **2000**, *76*, 1100–1108, DOI 10.1002/(SICI)1097-4628(20000516)76:7<1100::AID-APP14>3.0.CO;2-B.

[11] D. Garcia, H. W. Starkweather, *J. Polym. Sci. Polym. Phys. Ed.* **1985**, *23*, 537–555, DOI 10.1002/pol.1985.180230310.

[12] G. Fairley, R. E. Prud'Homme, *Polym. Eng. Sci.* **1987**, *27*, 1495–1503, DOI 10.1002/pen.760272004.

[13] P. Kollross, A. J. Owen, *Polymer* **1982**, *23*, 829–833, DOI 10.1016/0032-3861(82)90141-0.

[14] K. K. Mokwena, J. Tang, *Crit. Rev. Food Sci. Nutr.* **2012**, *52*, 640–650, DOI 10.1080/10408398.2010.504903.

[15] J. P. Sheth, D. B. Klinedinst, G. L. Wilkes, I. Yilgor, E. Yilgor, *Polymer* **2005**, *46*, 7317–7322, DOI 10.1016/j.polymer.2005.04.041.

[16] B. C. Tsai, J. A. Wachtel in *Barrier Polym. Struct.* American Chemical Society, Washington, DC, **1990**, pp. 192–202, DOI 10.1021/bk-1990-0423.ch009.

[17] Z. Zhang, I. J. Britt, M. A. Tung, *J. Appl. Polym. Sci.* **2001**, *82*, 1866–1872, DOI 10.1002/app.2030.

[18] N. Jia, H. A. Fraenkel, V. A. Kagan, *J. Reinf. Plast. Compos.* **2004**, *23*, 729–737, DOI 10.1177/0731684404030730.

[19] B. Yang, W. M. Huang, C. Li, L. Li, *Polymer* **2006**, *47*, 1348–1356, DOI 10.1016/j.polymer.2005.12.051.

[20] T. Park, S. C. Zimmerman, S. Nakashima, *J. Am. Chem. Soc.* **2005**, *127*, 6520–6521, DOI 10.1021/ja050996j.

[21] P. S. Corbin, S. C. Zimmerman, P. A. Thiessen, N. A. Hawryluk, T. J. Murray, *J. Am. Chem. Soc.* **2001**, *123*, 10475–10488, DOI 10.1021/ja010638q.

[22] C. C. Cheng, J. J. Huang, Z. S. Liao, S. Y. Huang, D. J. Lee, Z. Xin, *Polym. Chem.* **2017**, *8*, 1454–1459, DOI 10.1039/c7py00182g.

[23] D. W. R. Balkenende, C. A. Monnier, G. L. Fiore, C. Weder, *Nat. Commun.* **2016**, *7*, 1–9, DOI 10.1038/ncomms10995.

[24] B. Zhu, N. Jasinski, A. Benitez, M. Noack, D. Park, A. S. Goldmann, C. Barner-Kowollik, A. Walther, *Angew. Chemie - Int. Ed.* **2015**, *54*, 8653–8657, DOI 10.1002/anie.201502323.

[25] K. Yamauchi, J. R. Lizotte, T. E. Long, *Macromolecules* **2003**, *36*, 1083–1088, DOI 10.1021/ma0212801.

[26] A. Faghihnejad, K. E. Feldman, J. Yu, M. V. Tirrell, J. N. Israelachvili, C. J. Hawker, E. J. Kramer, H. Zeng, *Adv. Funct. Mater.* **2014**, *24*, 2322–2333, DOI 10.1002/adfm.201303013.

[27] T. Park, S. C. Zimmerman, *J. Am. Chem. Soc.* **2006**, *128*, 11582–11590, DOI 10.1021/ja0631854.

[28] R. P. Sijbesma, F. H. Beijer, L Brunsveld, B. J. Folmer, J. H. Hirschberg, R. F. Lange, J. K. Lowe, E. W. Meijer, *Science* **1997**, *278*, 1601–1604, DOI 10.1126/science.278.5343.1601.

[29] B. J. B. Folmer, R. P. Sijbesma, R. M. Versteegen, J. A. J. Van Der Rijt, E. W. Meijer, *Adv. Mater.* **2000**, *12*, 874–878, DOI 10.1002/1521-4095(200006)12:12<874::AID-ADMA874>3.0.CO;2-C.

[30] P. Y. Dankers, T. M. Hermans, T. W. Baughman, Y. Kamikawa, R. E. Kieltyka, M. M. Bastings, H. M. Janssen, N. A. Sommerdijk, A. Larsen, M. J. Van Luyn, A. W. Bosman, E. R. Popa, G. Fytas, E. W. Meijer, *Adv. Mater.* **2012**, *24*, 2703–2709, DOI 10.1002/adma.201104072.

[31] R. E. Kieltyka, A. C. H. Pape, L. Albertazzi, Y. Nakano, M. M. C. Bastings, I. K. Voets, P. Y. W. Dankers, E. W. Meijer, *J. Am. Chem. Soc.* **2013**, *135*, 11159–11164, DOI 10.1021/ja403745w.

[32] S. Seiffert, *Supramolecular Polymer Networks and Gels*, *Vol. 268*, Springer, **2015**, p. 288, DOI 10.1007/978-3-319-15404-6.

[33] F. Biedermann, E. A. Appel, J. del Barrio, T. Gruendling, C. Barner-Kowollik, O. A. Scherman, *Macromolecules* **2011**, *44*, 4828–4835, DOI 10.1021/ma2008018.

[34] A. Farkas, P. F. Strohm, *Ind. Eng. Chem. Fundam.* **1965**, *4*, 32–38, DOI 10.1021/i160013a005.

[35] D. M. Patil, G. A. Phalak, S. T. Mhaske, *Des. Monomers Polym.* **2017**, *20*, 269–282, DOI 10.1080/15685551.2016.1231045.

[36] B. R. Bhattacharyya, U. S. Nandi, *Die Makromol. Chemie* **1968**, *116*, 8–13, DOI 10.1002/macp.1968.021160102.

[37] C. M. Cormier, B. Wunderlich, *J. Polym. Sci.* **1967**, *5*, 987–988, DOI 10.1002/pol.1967.160050514.

[38] D. E. Kline, J. A. Sauer, A. E. Woodward, *J. Polym. Sci.* **1956**, *22*, 455–462, DOI 10.1002/pol.1956.1202210211.

[39] W.-x. Fan, C.-k. Wang, C.-c. Tsai, Y. Ding, Z.-d. Tu, C.-M. Huang, K.-S. Huang, J.-t. Yeh, *RSC Adv.* **2016**, *6*, 3165–3175, DOI 10.1039/C5RA20982J.

[40] K. Pathmanathan, G. P. Johari, *J. Polym. Sci. Part B Polym. Phys.* **1990**, *28*, 675–689, DOI 10.1002/polb.1990.090280507.

[41] J. A. Sauer, A. E. Woodward, *Rev. Mod. Phys.* **1960**, *32*, 88–101, DOI 10.1103/RevModPhys.32.88.

[42] S. Martín, J. F. Vega, M. T. Expósito, A. Flores, J. Martínez-Salazar, *Colloid Polym. Sci.* **2011**, *289*, 257–268, DOI 10.1007/s00396-010-2348-x.

[43] K. H. Nitta, A Tanaka, *Polymer* **2001**, *42*, 1219–1226, DOI 10.1016/S0032-3861(00)00418-3.

[44] K. Schmieder, K. Wolf, *Kolloid-Zeitschrift* **1953**, *134*, 149–189, DOI 10.1007/BF01521621.

[45] H. Kautz, D. J. M. Van Beek, R. P. Sijbesma, E. W. Meijer, *Macromolecules* **2006**, *39*, 4265–4267, DOI 10.1021/ma060706z.

[46] X. Yan, S. Li, J. B. Pollock, T. R. Cook, J. Chen, Y. Zhang, X. Ji, Y. Yu, F. Huang, P. J. Stang, *Proc. Natl. Acad. Sci. U. S. A.* **2013**, *110*, 15585–90, DOI 10.1073/pnas.1307472110.

[47] C. L. Lewis, K. Stewart, M. Anthamatten, *Macromolecules* **2014**, *47*, 729–740, DOI 10.1021/ma402368s.

[48] S. Nojiri, H. Yamada, S. Kimata, K. Ikeda, T. Senda, A. W. Bosman, *Polymer* **2016**, *87*, 308–315, DOI 10.1016/j.polymer.2016.02.010.

[49] G. H. Edward, *Br. Polym. J.* **1986**, *18*, 88–93, DOI 10.1002/pi.4980180207.

[50] J. J. Cheng, PhD thesis, **2008**.

[51] S. Hosoda, H. Hori, K.-i. Yada, S.-y. Nakahara, M. Tsuji, *Polymer* **2002**, *43*, 7451–7460, DOI 10.1016/S0032-3861(02)00680-8.

[52] S. W. Kuo, H. T. Tsai, *Macromolecules* **2009**, *42*, 4701–4711, DOI 10.1021/ma900640a.

[53] A. Jangizehi, S. R. Ghaffarian, M. Ahmadi, *Polym. Adv. Technol.* **2017**, *29*, 726–735, DOI 10.1002/pat.4178.

[54] K. E. Feldman, M. J. Kade, E. W. Meijer, C. J. Hawker, E. J. Kramer, *Macromolecules* **2009**, *42*, 9072–9081, DOI 10.1021/ma901668w.

[55] L. E. Nielsen, *J. Macromol. Sci. Part C* **1969**, *3*, 69–103, DOI 10.1080/15583726908545897.

[56] W. G. Oakes, D. W. Robinson, *J. Polym. Sci.* **1954**, *14*, 505–507, DOI 10.1002/pol.1954.120147712.

[57] Y. Zhou, J. G. Goossens, R. P. Sijbesma, J. P. Heuts, *Macromolecules* **2017**, *50*, 6742–6751, DOI 10.1021/acs.macromol.7b01142.

[58] M. Röttger, T. Domenech, R. Van Der Weegen, A. Breuillac, R. Nicolaÿ, L. Leibler, *Science* **2017**, *356*, 62–65, DOI 10.1126/science.aah5281.

[59] M. Mauri, N. Tran, O. Prieto, T. Hjertberg, C. Müller, *Polymer* **2017**, *111*, 27–35, DOI 10.1016/j.polymer.2017.01.010.

[60] L. Li, J. Chen, B. Yan, H. Zeng in *Smart Mater. Adv. Environ. Appl.* (Ed.: P. Wang), Royal Society of Chemistry, **2016**, pp. 139 –164, DOI 10.1039/9781782622130-FP007.

[61] M. Jacob, B. Francis, S. Thomas, K. T. Varughese, *Polym. Compos.* **2006**, *27*, 671–680, DOI 10.1002/pc.20250.

[62] X. Y. Shi, W. N. Bi, S. G. Zhao, *J. Appl. Polym. Sci.* **2012**, *124*, 2234–2239, DOI 10.1002/app.35301.

[63] V. G. Geethamma, G. Kalaprasad, G. Groeninckx, S. Thomas, *Compos. Part A Appl. Sci. Manuf.* **2005**, *36*, 1499–1506, DOI 10.1016/j.compositesa.2005.03.004.

[64] R. F. M. Lange, M. Van Gurp, E. W. Meijer, *J. Polym. Sci. Part A Polym. Chem.* **1999**, *37*, 3657–3670, DOI 10.1002/(SICI)1099-0518(19991001)37:19<3657::AID-POLA1>3.0.CO;2-6.

[65] S. Goodyer, Measuring Polymers using a Rotational Rheometer in Oscillatory Mode Product Manager for Rheology, **2013**.

[66] K. Zhang, M. Aiba, G. B. Fahs, A. G. Hudson, W. D. Chiang, R. B. Moore, M. Ueda, T. E. Long, *Polym. Chem.* **2015**, *6*, 2434–2444, DOI 10.1039/C4PY01798F.

[67] H. Hagemann, R. G. Snyder, A. J. Peacock, L. Mandelkern, *Macromolecules* **1989**, *22*, 3600–3606, DOI 10.1021/ma00199a017.

[68] C. L. Elkins, K. Viswanathan, T. E. Long, *Macromolecules* **2006**, *39*, 3132–3139, DOI 10.1021/ma052754+.

[69] D. J. Van Beek, A. J. Spiering, G. W. Peters, K. Te Nijenhuis, R. P. Sijbesma, *Macromolecules* **2007**, *40*, 8464–8475, DOI 10.1021/ma071 2394.

[70] G. M.L. H. van Gemert, H. M. Janssen, E. W. Meijer, A. W. Bosman, Supramolecular polymers from low-melting, easily processable building blocks (WO2008063057A3), **2014**.

[71] G. Armstrong, M. Buggy, *Polym. Int.* **2002**, *51*, 1219–1224, DOI 10.1002/pi.949.

[72] K. Cao, G. Liu, *Macromolecules* **2017**, *50*, 2016–2023, DOI 10.1021 /acs.macromol.7b00156.

[73] A. Charlesby, N. H. Hancock, *Proc. R. Soc. London. Ser. A Mat. Phys. Sci.* **1953**, *218*, 245–255, DOI 10.1098/rspa.1953.0102.

[74] L. Imbernon, S. Norvez, L. Leibler, *Macromolecules* **2016**, *49*, 2172–2178, DOI 10.1021/acs.macromol.5b02751.

[75] J. I. Thompson, J. T. Czernuszka, *Biomed. Mater. Eng.* **1995**, *5*, 37–48, DOI 10.3233/BME-1995-5105.

[76] H. A. Khonakdar, J. Morshedian, U. Wagenknecht, S. H. Jafari, *Polymer* **2003**, *44*, 4301–4309, DOI 10.1016/S0032-3861(03)00363-X.

[77] R. Krishnaswamy, M. Lamborn, *Polym. Eng. Sci.* **2000**, *40*, 2385–2396, DOI 10.1002/pen.11370.

[78] L. R. Rieth, R. F. Eaton, G. W. Coates, *Angew. Chemie Int. Ed.* **2001**, *40*, 2211–2214, DOI 10.1002/1521-3757(20010601)113:11<2211:: AID-ANGE2211>3.0.CO;2-L.

[79] G. Sarkhel, A. Banerjee, P. Bhattacharya, *Polym. - Plast. Technol. Eng.* **2006**, *45*, 713–718, DOI 10.1080/03602550600609663.

[80] K Ganesh, R Nagarajan, J. L. Duda, *Ind. Eng. Chem. Res.* **1992**, *31*, 746–755, DOI 10.1021/ie00003a016.

[81] J. M. Lagaron, R. Catalá, R Gavara, *Mater. Sci. Technol.* **2004**, *20*, 1–7, DOI 10.1179/026708304225010442.

[82] Barrier and Permeation Properties of Polymers and Plastics.

[83] G. Farrow, *Polymer* **1963**, *4*, 191–197, DOI 10.1016/0032-3861(63)90025-9.

[84] G. R. P. Henry, X. Drooghaag, D. D. J. Rousseaux, M. Sclavons, J. Devaux, J. Marchand-Brynaert, V. Carlier, *J. Polym. Sci. Part A Polym. Chem.* **2008**, *46*, 2936–2947, DOI 10.1002/pola.22628.

[85] C. Gartner, M. Suárez, B. L. López in Polym. Eng. Sci. *Vol. 48*, Wiley-Blackwell, **2008**, pp. 1910–1916, DOI 10.1002/pen.21106.

[86] Y. Sugai, T. Aosaki, C.-L.F. I. Agent, Ceramide-Like Function Imparting Agent (WO2014142116A1), **2016**.

[87] F. A. Bovey, *Prog. Polym. Sci.* **1971**, *3*, 1–108, DOI 10.1016/0079-6700(71)90002-5.

[88] I. Kirshenbaum, Z. W. Wilchinsky, B. Groten, *J. Appl. Polym. Sci.* **1964**, *8*, 2723–2730, DOI 10.1002/app.1964.070080618.

[89] M. R. Kamal, L. Feng, T. Huang, *Can. J. Chem. Eng.* **2002**, *80*, 432–442, DOI 10.1002/cjce.5450800312.

[90] A. H. Willbourn, *Trans. Faraday Soc.* **1958**, *54*, 717, DOI 10.1039/tf9585400717.

Appendix B

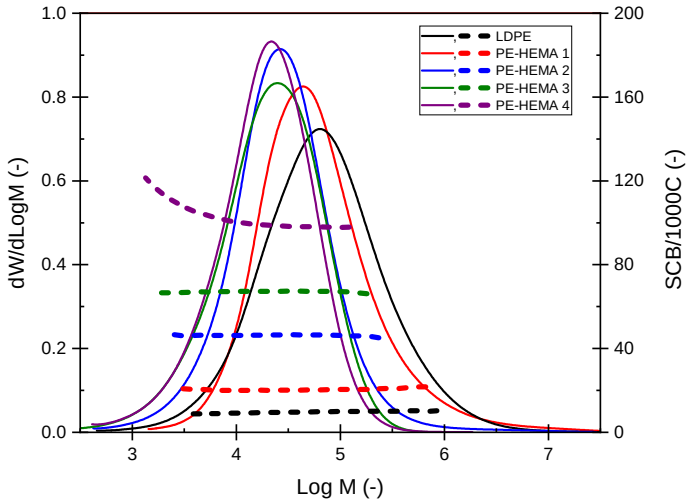

Figure B.1: Overlay of the chemical composition as function of the molar mass of (LD)PE and PE-HEMA Polymers **1** – **4**. Continues line represents the intensity data, dashed lines the amount of SCB.

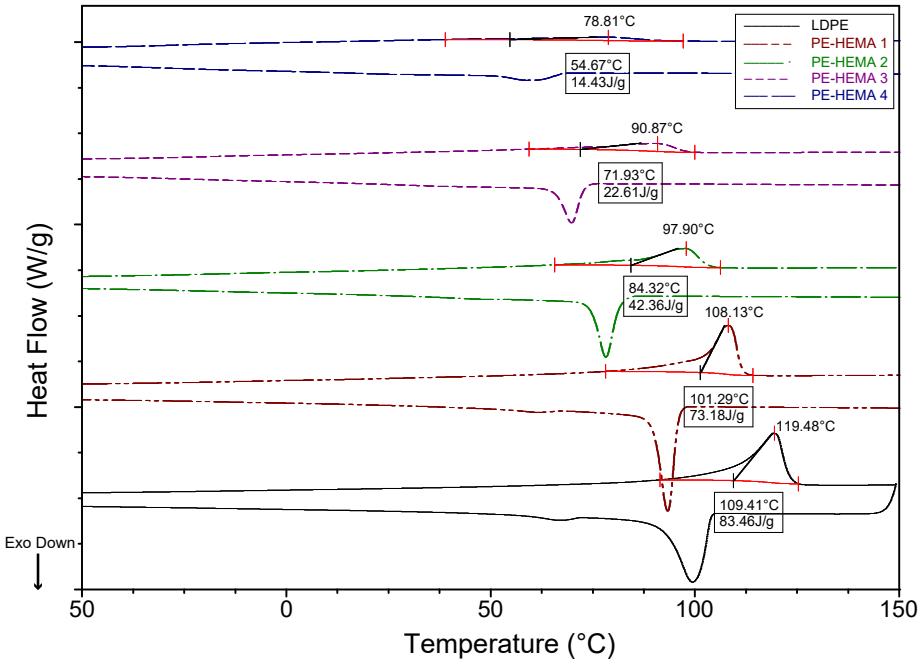

Figure B.2: DSC data for (LD)PE and PE-HEMA Polymers **1** – **4**. The annotation (black box) gives the onset of melting and melting enthalpy of the respective polymer. Exotherm down.

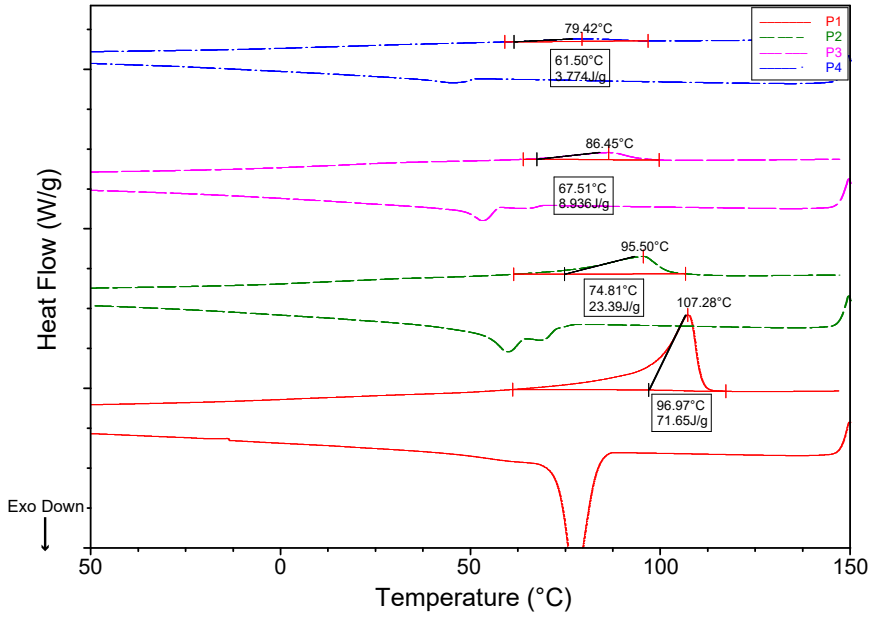

Figure B.3: DSC data for ODIN-PE-HEMA Polymers **P1** – **P4**. The annotation (black box) gives the onset of melting and melting enthalpy of the respective polymer. Exotherm down.

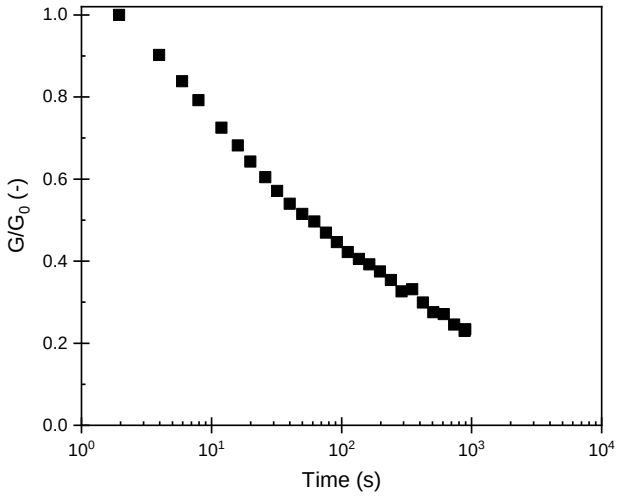

Figure B.4: Stress relaxation measurement following the development of the normalized stress (strain = 0.5 %, T = 140 °C) of **P2** as function of time.



Figure B.5: Compression molded thin film prepared of Polymer **P3**.

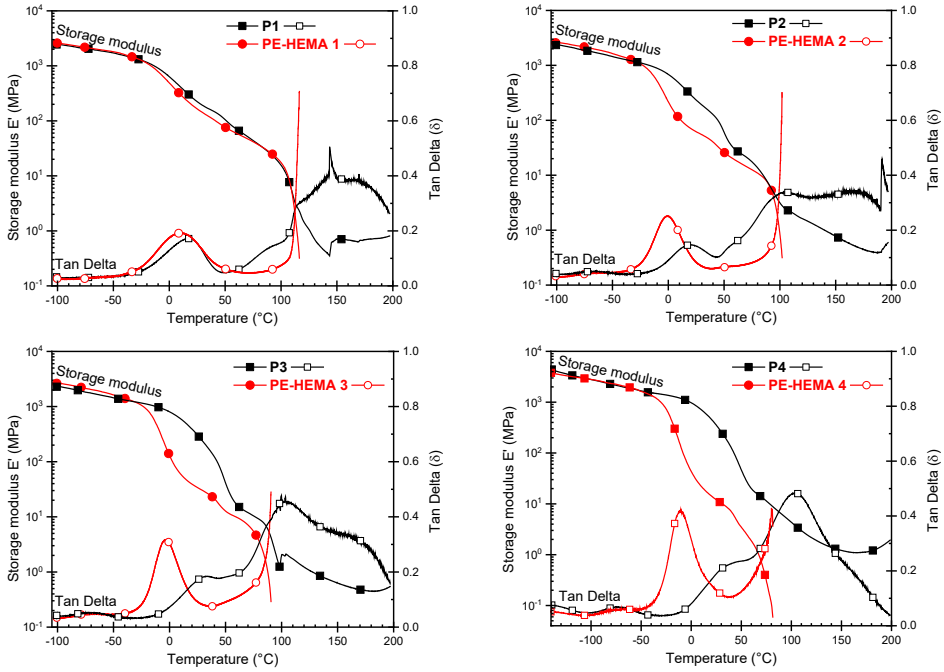

Figure B.6: DMTA data of polymers **P1** – **P4** and their pristine counterparts.

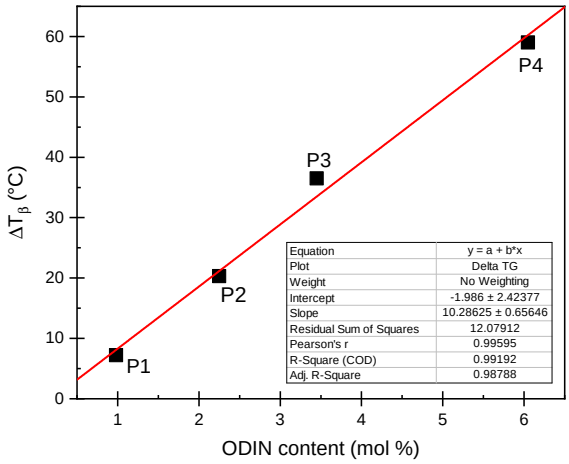

Figure B.7: Plot of ΔT_β difference determined *via* DMTA between pristine and sextuple hydrogen-bonding motif functionalized samples as a function of ODIN content. The fit reveals the linear relationship between ΔT_β and ODIN content.

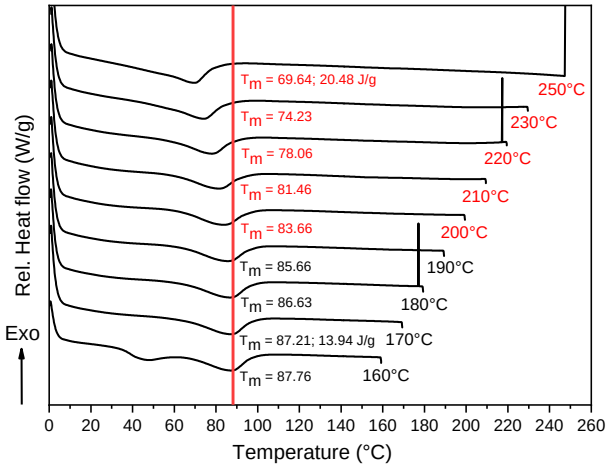

Figure B.8: Thermal stability of ODIN-PE-HEMA Polymers: A polymeric ODIN-PE-HEMA sample was monitored during DSC while heating in steps of 10 °C from 160 °C to 250 °C at a heating rate of 10 K/min for each step. The red line is meant to guide the eye to highlight the shift of melting temperature associated with the degradation of the sample. The onset of melting point change is observed at 190 °C.

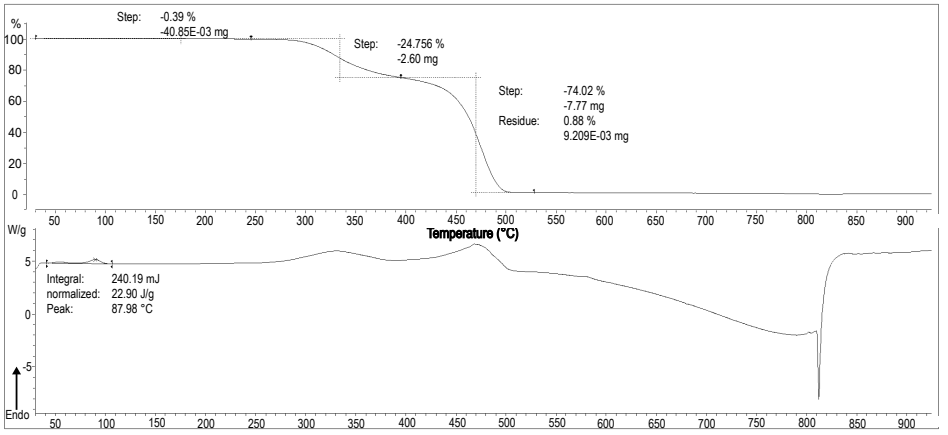

Figure B.9: DSC-TGA of ODIN-PE-HEMA **P3** with calculated weight loss.

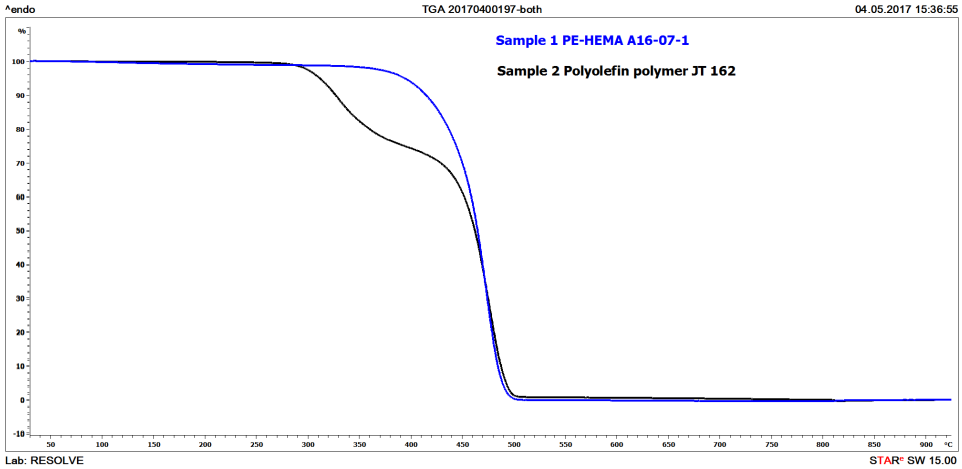

Figure B.10: TGA data for **PE-HEMA 3** and ODIN-PE-HEMA **P3**.

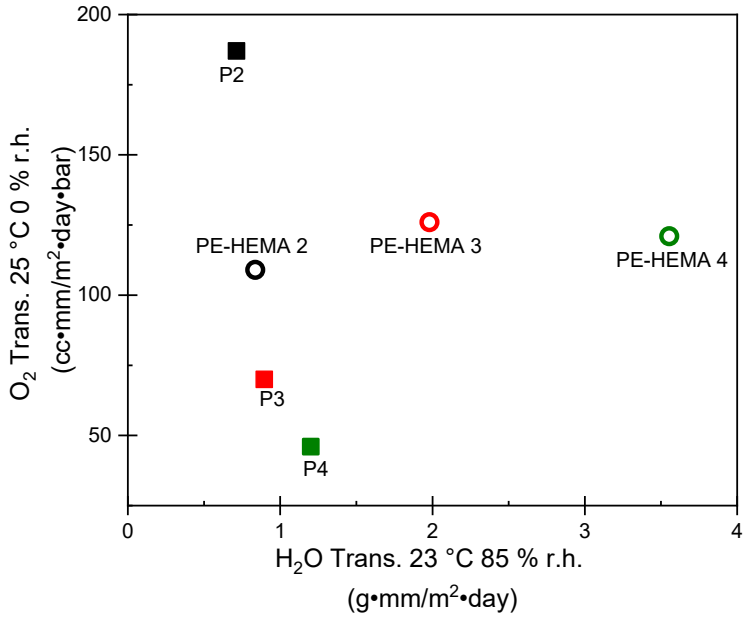

Figure B.11: OTR and WVTR of pristine and ODIN functional polymers. OTR was measured at 23 °C, 0 % r.h. and WVTR at 23 °C, 85 % r.h..

Table B.1: Thickness corrected OTR and WVTR data for pristine and ODIN functional polymers.

Entry	HEMA (mol%)	ODIN (mol%)	WVTR (cc·mm/ m^2·day·bar) (23 °C, 85 % r.h.)	OTR (cc·mm/ m^2·day·bar) (23 °C, 0 % r.h.)	OTR (cc·mm/ m^2·day·bar) (38 °C, 50 % r.h.)
PE-HEMA 2	6.8	0	1.98	126	353
P2	6.8	2.25	0.9	70	184
PE-HEMA 3	7.5	0	1.9	116	344
P3	7.5	3.45	1	66	172
PE-HEMA 4	12.4	0	3.6	121	382
P4	12.4	6.05	1.2	46	129

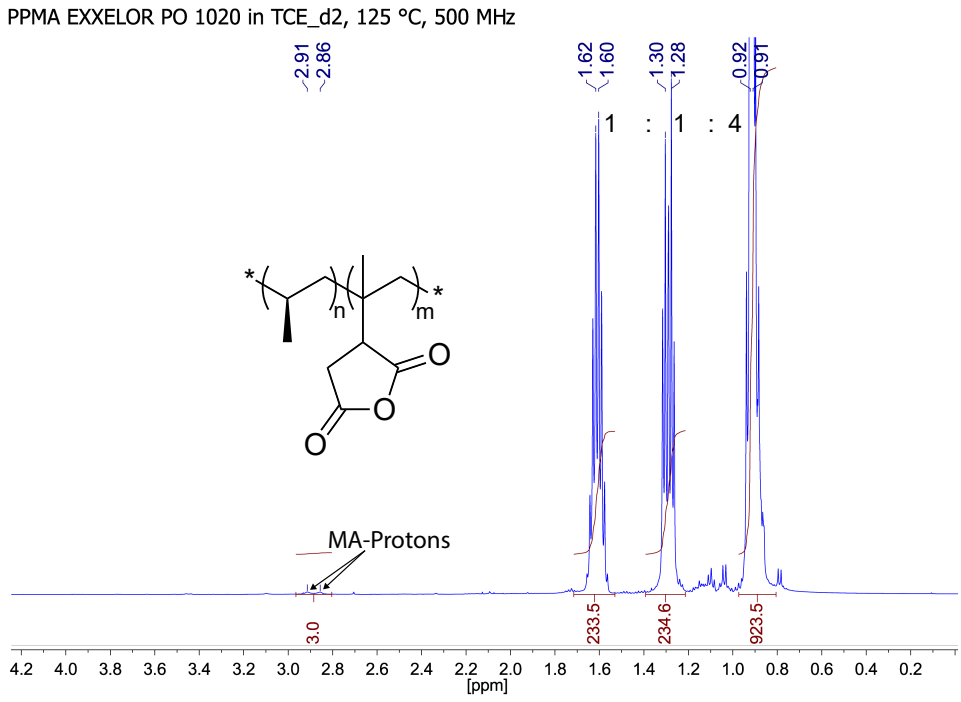

Figure B.12: NMR spectra of EXXELOR *PO 1020* MA functionalized polypropylene. Assignment of MA groups done according to literature.[84]

Chapter 4

Cavitand Functionalized Polyethylene

Abstract: A quinoxaline CAVITAND in *kite* conformation was functionalized with an isocyanate group at the lower rim so that functionalization of a hydroxy or amine containing polymer can be readily achieved. This was achieved by reacting this CAVITAND with PE-HEMA, a polymer with free hydroxy groups. The obtained polymer was characterized by NMR, DSC, and FTIR. Films with varying amounts of CAVITAND, obtained by solution casting and slow evaporation, were tested for their oxygen barrier, which was found to be negatively affected due to a severely reduced crystallinity. TOC-graphic: Introduction of VELCRANDS into PE-HEMA.

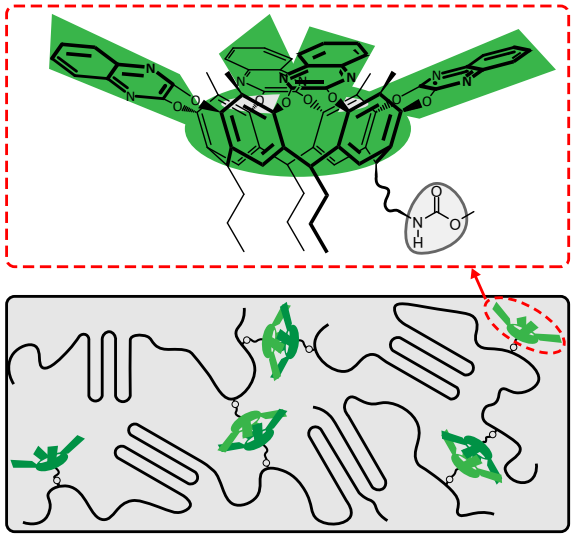

The 4Qxkite CAVITAND is capable of independent self-assembling interactions, forming a dimer named VELCRAPLEX. The driving forces for dimerization are dipole–dipole, VAN DER WAALS, and solvophobic interactions.[1] The major motivation in exploring these CAVITAND functionalized polymers is to study whether the reversible interaction can be used to cross-link the polymer matrix. A first step is to affirm that assembly of the CAVITAND will occur when embedded inside a polymer matrix. In addition, we foresaw potential benefits regarding the oxygen barrier properties of functionalized films. The idea was twofold. A major contribution to the oxygen barrier properties of polymers is the tortuous pathway that oxygen will have to travel inside the polymer matrix. Here, the considerably large CAVITAND molecules could provide an obstacle for the oxygen traveling inside the matrix, effectively increasing the barrier.[2] Furthermore, the expected increased inter-facial cohesion between chains in the amorphous phase, which is associated with increased barrier properties, should be enhanced due to the cross-linking with the CAVITAND.[3] The latter idea requires compared to the first one, that the moieties are attached to the polymer backbone. An advantage of CAVITANDS is that their association is not based on polar interactions such as hydrogen bonding, which makes them not susceptible to humidity.

4.1 Design and Synthesis of a Suitable Cavitand

In order to avoid the requirement of additional species for the association between CAVITANDS such as suitable guests or coordinating metals, we decided to employ the self-dimerizing 4Qx (short for four quinoxaline) CAVITAND with a relatively large K_a of $5 - 8.5 \cdot 10^4$ M^{-1} in chloroform at room temperature (structure in Figure 4.1).[1,4] To avoid implicating the assembly of the dimer, the upper rim with the quinoxaline moieties should not be altered. Therefore, a synthesis pathway with a single functionality at the lower rim of the 4QxCav was selected, which is illustrated in Figure 4.2.

Firstly, a resorcinarene functionalized at the lower rim with a hydroxyl group was prepared by combining 4 eq of 2-methylbenzene-1,3-diol with 1 eq of 2,3-dihydrofuran and 3 eq of butyraldehyde in methanol and concentrated hydrochloric acid. This procedure leads to a mixture with zero

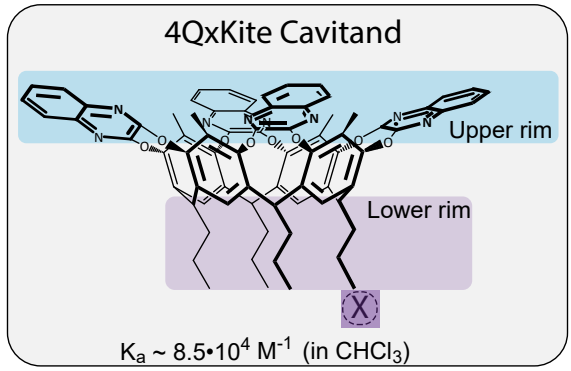

Figure 4.1: General structure of a 4QxKite CAVITAND with alkyl chains at the lower rim. The K_a is related to the dimer formation.

to two hydroxy groups at the lower rim. It was more convenient to use the crude resorcinarene without purification for the next step, eliminating an additional purification step. Therefore, the crude was directly reacted with a slight excess of dichloroquinoxaline in dimethylformamide (DMF) overnight at 80 °C in the presence of potassium carbonate needed to deprotonate the eight OH groups at the upper rim and to scavenge the HCl. The CAVITAND with a single hydroxy group on the lower rim, hitherto referred to as 4Qx-CavOH, was isolated *via* column chromatography. To obtain isocyanate functional cavitand for introduction into polymers, 4QxCavOH was reacted with an excess of HDI in the presence of DBTDL acting as a catalyst. The isocyanate functionalized CAVITAND, namely 4QxCavNCO, could be isolated by precipitation in hexane with a yield of 69 %.

4.2 Synthesis and Properties of Cavitand Functional Polymer Networks

The general strategy for the synthesis of CAVITAND functionalized polymers follows the approach for multiple hydrogen bonding functionalized PE presented in Chapter 3, that is using a polymer with free hydroxy group and reacting it with the isocyanate functional CAVITAND. A suitable polymer with around 0.91 mol% hydroxy groups, PE-HEMA, was selected. The polymers were obtained by reacting PE-HEMA with isocyanate functional CAVITAND

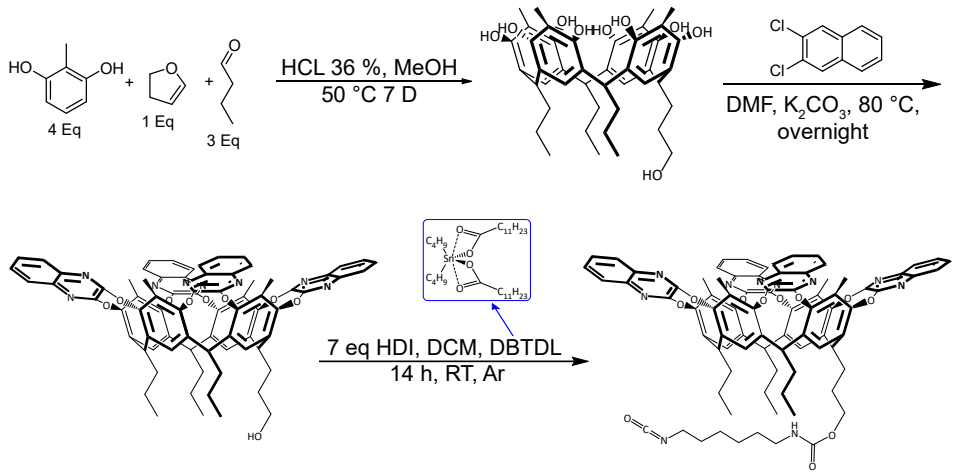

Figure 4.2: Scheme for the synthesis of mono-isocyanate functionalized 4QxKite CAVITAND.

according to the following procedure. First, PE-HEMA was dissolved in toluene at 80 °C for 1 h, then varying amounts of 4QxCavNCO in wt% were added, followed by the addition of a few drops of DBTDL as catalyst. The resulting solution was stirred for 4 h and subsequently precipitated into hexane, obtaining the polymer as white powder. An overview of the obtained polymers, the introduced amount of CAVITAND in wt%, and DSC data are given in Table 4.1.

The maximum amount of introduced CAVITAND equals the amount obtained for full functionalization of all the available PE-HEMA hydroxy groups (0.91 mol%) and amounts to 30.6 wt%. The successful synthesis was confirmed *via* FTIR and HTNMR. In Figure 4.3 the FTIR spectra of 4QxCavNCO, pristine, and functional PE-HEMA are shown. After synthesis, the disappearance of the characteristic NCO stretching band at 2269 cm^{-1}[5] of the CAVITAND was observed, indicating that all NCO groups reacted. In addition, new peaks between 1000 cm^{-1} and 1400 cm^{-1} appeared inside the spectrum of the functional polymer 4QxCav30.6, which correspond to various vibrations of the introduced CAVITAND. No clear new C=O band resulting from the carbamate linkage was observed, most likely because it is overlapping with the preexisting carbonyl C=O band of the ester of the pristine polymer.

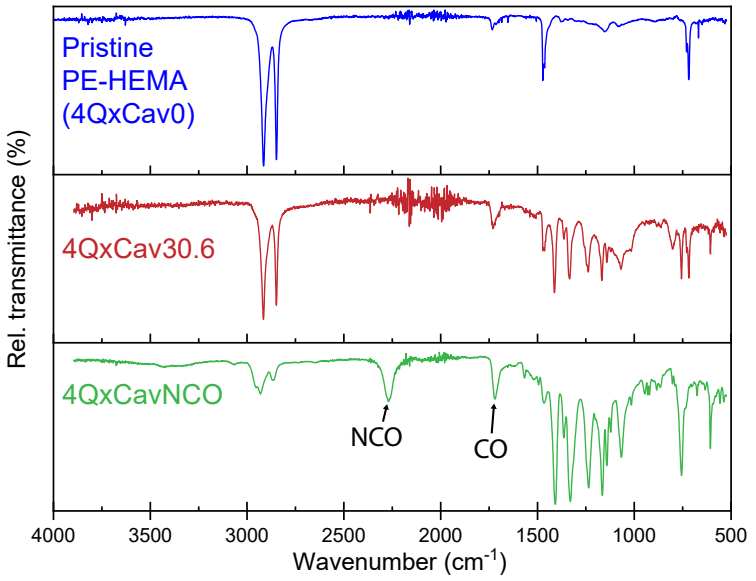

Figure 4.3: FTIR spectra of pristine PE-HEMA (4QxCav0), 4QxCav30.6, and 4QxCavNCO.

A clearer confirmation for the attachment of the CAVITAND to the polymer backbone can be found using HTNMR. The ^{1}H-NMR of pristine (blue line), 4QxCav30.6 (red line), and 4QxCavNCO (green line) are reported in Figure 4.4. After functionalization, the peaks of pristine PE-HEMA, highlighted by black and grey dots (blue spectra), combined to a single peak, marked by a dark grey circle (red spectra). The signal of methylene close to isocyanate marked by a red dot (green spectra) disappears after functionalization, indicating full functionalization. Due to overlapping of cavitand and pristine PE-HEMA signals, determination of degree of functionalization was difficult. The ^{1}H NMR spectra of 4QxCav30.6 reveals that the dimer exists in the *kite* form inside the polymer matrix as the characteristic split of the arylmethyl signals is observed (orange dots in the green colored spectrum).[1]

Introduction of the CAVITAND proved to be detrimental to the thermal properties of the polymer. The bulky motif reduced the T_m and X_c of the pristine polymers significantly. This observation was not unsuspected, as the bulky CAVITAND side chains cannot be part of the PE crystal lattice and will keep large part of the chain unavailable for crystallization. Small amounts

Table 4.1: Overview of the prepared CAVITAND functionalized polymers, theoretical amount of CAVITAND introduced in wt%, and thermal data.

Entry	HEMA[a] (mol%)	4QxCavNCO (wt%)	OH-group Func. (mol%)	T_m[b] (°C)	X_c[d] (%)
4QxCav0	0.91	-	-	112	30.0
4QxCav1	0.91	1	3	112	29.4
4QxCav5	0.91	5	16	110	25.5
4QxCav30.6	0.91	30.6[c]	100	101	11.2

[a] det. *via* NMR; [b] det. *via* DSC; [c] Calc. for full functionalization; [d] X_c calc. with heat of fusion of PE = 286.2 J·g^{-1};[6]

of CAVITAND do affect the cristallinity to a lesser extent, as is apparent from sample 4QxCav1.

Films were obtained by solution casting, which was achieved by first dissolving the polymer in tetrachloroethane (TCE) at 100 °C, then transferring the solutions into a custom made mold (drilled hole inside a polytetrafluoroethylene (PTFE) cylinder) and slowly evaporating the solvent inside a custom made oven at 120 °C (pictures of setup in Figure C.1, Appendix **C**). Thereby, thin transparent films with a thickness of around 100 µm could be obtained, which were used to determine the oxygen barrier properties of pristine and CAVITAND functionalized films.

The oxygen transmission rate for pristine and cavitand functionalized PE-HEMA as a function of CAVITAND content in wt% is given in Figure 4.5 **A**. Clearly, the introduction of CAVITAND into the polymers leads to a significant increase in oxygen transmission rate, therefore decreasing its barrier property towards oxygen. This is most likely caused by the decreased crystallinity of functionalized samples (see Table 4.1).

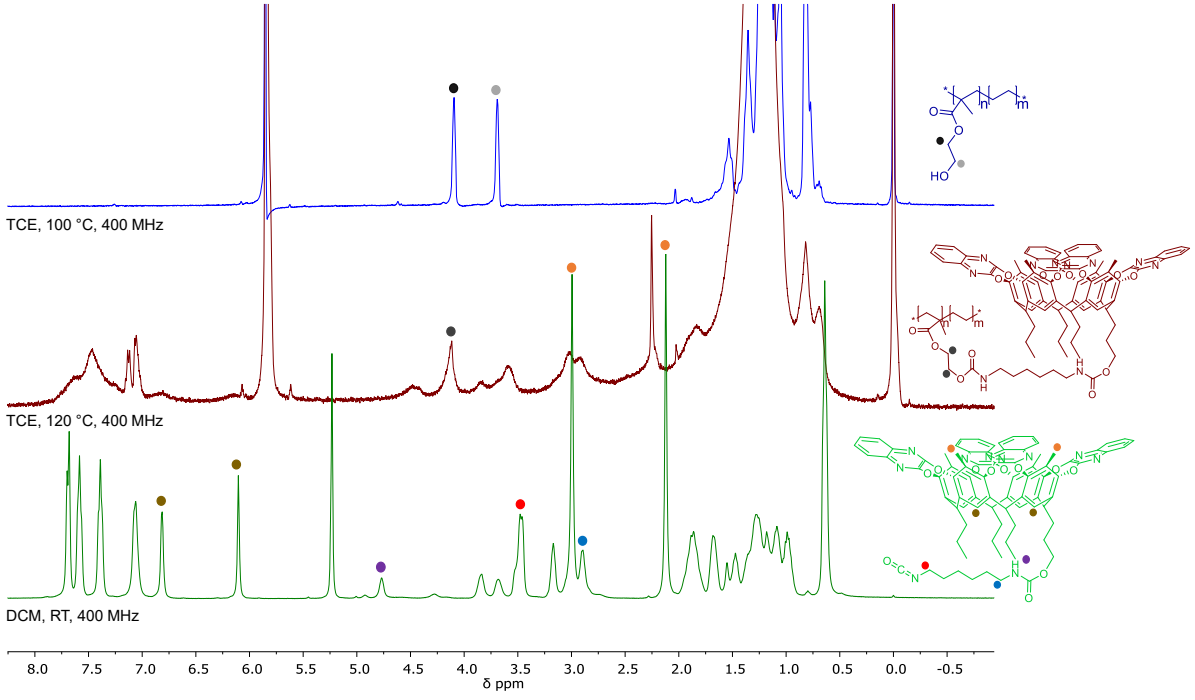

Figure 4.4: ^{1}H-NMR spectra of pristine PE-HEMA (blue line), 4QxCav30.6 (red line), and 4QxCavNCO (green line).

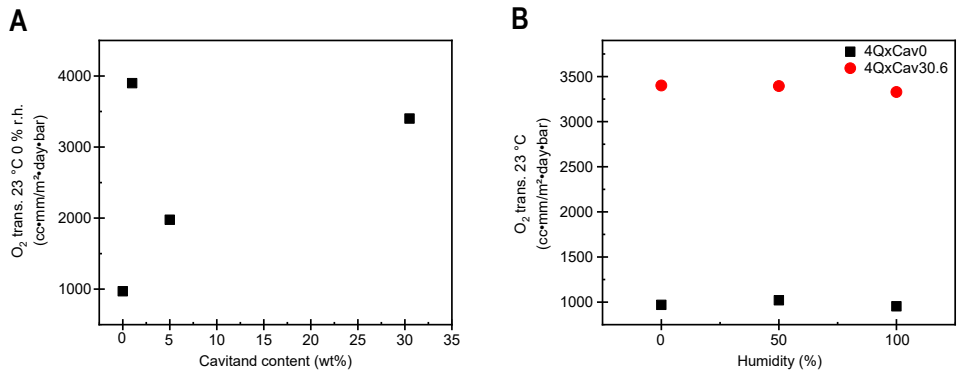

Figure 4.5: **A**: Oxygen transmission rates of pristine and CAVITAND functionalized PE-HEMA as a function of CAVITAND content in wt% (0, 1, 5, and 30.6 wt%). **B**: Influence of humidity on oxygen transmission of pristine and functional PE-HEMA.

Despite the small decrease in X_c for materials with 1 wt% and 5 wt% of CAVITAND, a significant decrease in barrier property was observed. This can likely be explained by the increase in free volume caused by the bulky CAVITAND, which also adversely affects the oxygen barrier properties of polymers.[3] Sample 4QxCav1 presents an outlier with a far greater increased transmission than the sample with higher CAVITAND content, and additional defects in the sample are likely responsible. However, due to the lackluster performance of all samples, further investigation was not conducted to explain the behavior of this outlier or to really investigate the effects of the CAVITAND introduction on the free volume.

Additionally, the effect of humidity on oxygen transmission was investigated, measuring oxygen transmission at 0 %, 50 %, and 100 % relative humidity. The result of these measurements for pristine polymer (4QxCav0) and 4QxCav30.6 are given in Figure 4.5 **B**. No influence of humidity was apparent for either pristine or functionalized materials, showing the resilience of these materials towards water. This was unexpected in the case of PE-HEMA, were hydrogen bonds of HEMA should be disturbed by increased humidity. Most likely, the apolar nature of PE backbone chains shields the hydrogen bonds of HEMA from influences of increased humidity for this polymer with low HEMA content.

4.3 Conclusions

A self-dimerizing quinoxaline CAVITAND in *kite* conformation suitable for the introduction into polymers was obtained. This CAVITAND, namely 4QxCavNCO, could be grafted onto PE-HEMA, a polymer with free hydroxy groups. The successful synthesis of these materials was confirmed *via* FTIR and ^{1}H-NMR spectroscopy. Films of functional polymers were obtained by solution casting from TCE and slow evaporation of the solvent. Thereby obtained films were tested for their oxygen transmission, which was found to sequentially increase with increasing CAVITAND concentration. This unwanted property can be a result of the severely reduced degree of crystallinity (X_c) and increased free volume due to the introduction of the bulky CAVITAND. Most significantly, 4QxCavNCO CAVITAND provides a tool to easily introduce CAVITANDS into polymers, or attach further functionality due to the isocyanate moiety.

4.4 Experimental

4.4.1 Methods

Nuclear magnetic resonance (NMR). NMR-spectra were recorded on a BRUKER AVANCE 400 (400 MHz) spectrometer and a BRUKER AVANCE 300 (300 MHz) at room temperature. Chemical shifts are reported in ppm. ^{1}H-NMR chemical shifts are given in reference to the residual solvent peak at 7.26 ppm in $CDCl_3$ and at 2.50 ppm in DMSO-d_6. High temperature nuclear magnetic resonance (HTNMR) spectra were recorded on a BRUKER AVANCE III (500 MHz) equipped with a cryogenically cooled probe head at 100 °C and 120 °C in TCE-d_2. ^{1}H-NMR chemical shifts are reported in ppm and given in reference to the residual solvent peak of TCE-d_2 at 6.00 ppm.

FOURIER *transformed infrared spectroscopy* (FTIR). FTIR-spectra were recorded on a PERKIN ELMER *Spectrum One* equipped with a Golden Gate accessory (diamond ATR).

Differential scanning calorimetry (DSC). The DSC measurements were

performed on a TA Instruments *Q20* equipped with a *RCS 90* cooling system. About 3 – 5 mg of polymeric sample was weighed inside an aluminum pan and subjected to DSC measurements under nitrogen atmosphere. Unless otherwise noted, polymers were screened twice from -40 °C to 200 °C at a constant heating/cooling rate of 10 $K \cdot min^{-1}$. The T_m, T_g, and the melting enthalpy (H_m) were determined from the second heating, crystallization temperature from the second cooling cycle.

Oxygen and water transmission. Oxygen transmission rates were determined according to ISO 15105 2 at 23 °C, and at 0 % r.h., 50 % r.h., and at 100 % r.h.. The thickness of films, which was around 100 µm, was measured at varying locations and the average was used to report thickness corrected oxygen transmission rates.

4.4.2 Synthesis

Unless otherwise specified, chemicals and solvents were purchased from Sigma-Aldrich and used as received. DMF was dried over molecular sieves prior to use. DCM was distilled and stored over molecular sieves. All other employed solvents were laboratory grade and used as received.

Mono-hydroxy methyl resorcinarene (IUPAC name in illustration).

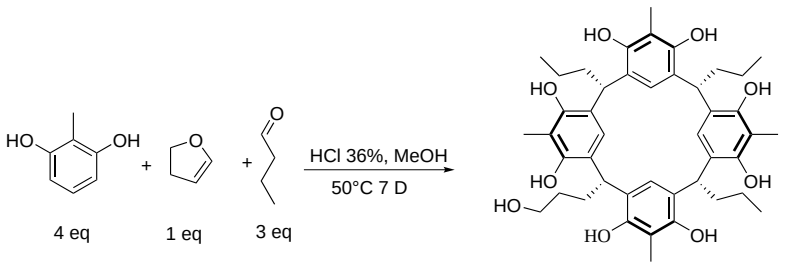

(2*s*,4*R*,6*r*,8*S*)-2-(3-hydroxypropyl)-1^5,3^5,5^5,7^5-tetramethyl-4,6,8-tripropyl-1,3,5,7(1,3)-tetrabenzenacyclooctaphan-1^4,1^6,3^4,3^6,5^4,5^6,7^4,7^6-octaol

The synthesis was adapted from literature.[7] First, 2-methylresorcinol (15 g, 120.8 mmol, 1 eq) was dissolved in methanol (90 mL) and cooled to 0 °C. Then, a solution of 2,3-dihydrofuran (2.42 mL, 30.2 mmol, 0.25 eq) and butyraldehyde (7.97 mL, 90.6 mmol, 0.75 eq) in methanol (20 mL) was

added dropwise under stirring. Subsequently, maintaining the temperature at 0 °C, hydrochloric acid (27 mL, 36 %) was added dropwise. Then, the temperature of the oil bath was increased to 50 °C and the mixture was stirred for 6 days, during which an orange precipitate was formed. The mixture was allowed to reach room temperature and poured into a beaker with water (500 mL). The precipitate was filtered using a BUCHNER funnel, washed with water, and dried at high vacuum yielding the crude product as an orange powder with 0 – 2 hydroxy groups at the lower rim. (19 g crude) A small analytic sample was obtained by column chromatography (SiO_2, CH_2Cl_2/acetone 80:20 → 60:40). ^{1}H-NMR (300 MHz, DMSO-d_6) δ: 8.66 (s, 8H), 7.30 (s, 4H), 4.35 (t, J = 5 Hz, 1H), 4.23 (m, 4H), 4.44 (m, 1H) 2.23 (m, 8H), 1.94 (s, 12H) 1.24 (m, 8H) 0.92 (m, 9H).

Synthesis of 4QxCavOH.

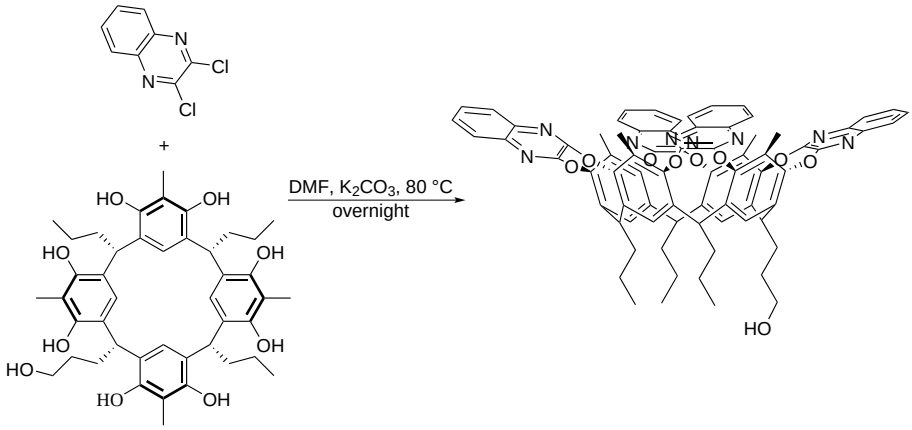

The synthesis was adapted from literature.[8] Reaction performed under dry condition. The crude mixture of hydroxy methyl resorcinarene (1.5 g, 1.93 mmol, 1 eq) was first dissolved in DMF (40 mL). Then, potassium carbonate (2.13 g, 16 mmol, 8.3 eq) and 2,3-dichloroquinoxaline (1.63 g, 9.3 mmol, 4.8 eq) are added, and the mixture is kept overnight at 55 °C. The mixture is allowed to reach room temperature, then slowly precipitated into a HCl solution (120 mL, 2 wt%). The precipitate was filtered off and dried at high vacuum. The crude was purified *via* column chromatography (SiO_2, CH_2Cl_2/EtOH 90:10 → 80:20) to give the quinoxaline bridged CAVITAND as a white powder (1.46 g). ^{1}H-NMR (300 MHz, DMSO-d_6) δ: 7.74 – 7.69 (m, 4H), 7.63 – 7.61 (m, 4H), 7.53 – 7.48 (m, 4H), 7.08 – 7.06 (m, 4H), 6.99 (s, 2H), 6.53 (s, 2H), 4.21 (t, J = 4.8 Hz, 1H), 3.46 – 3.36 (m, 4H), 3.19 – 3.11 (m, 4H) 1.92 – 1.58 (m, 4H), 1.29 – 0.81 (m, 8H) 0.65 (t, J = 7.3 Hz, 9H). MS (MALDI) m/z: $[M + H]^+$ calcd for $C_{76}H_{65}N_8O_9$, 1233.49; found, 1233.37.

Synthesis of 4QxCavNCO.

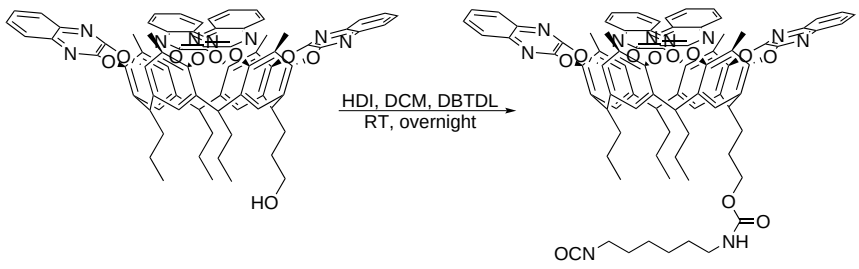

Reaction performed under dry condition. First, HDI (0.5 mL, 3.11 mmol, 8 eq) is added to the flask, degassed, followed by addition of dichloromethane (DCM) (25 mL) and the mixture cooled to 0 °C. Then, 4QxCavOH (0.5 g, 0.41 mmol, 1 eq), dissolved in DCM (50 mL), is added *via* syringe. Lastly, a drop of DBTDL is added and the reaction is stirred overnight at room temperature. The solute is precipitated in Et_2O kept at 0 °C, dried, redissolved in DCM and then precipitated into pentane. The precipitate is dried, and the product obtained as a white powder (0.39 g, 69 % yield). ^{1}H-NMR (300 MHz, CD_2Cl_2) δ: 7.78 – 7.71 (m, 4H), 7.70 – 7.63 (m, 4H), 7.52 – 7.44 (m, 4H), 7.15 (s, 4H), 6.90 (s, 2H), 6.19 (s, 2H), 4.86 (s, 1H), 4.1 – 3.74 (m, 2H), 3.71 – 3.5 (m, 4H), 3.25 (s, 2H), 3.07 (s, 6H), 3.02 – 2.84 (m, 2H), 2.20 (s, 6), 2.09 – 1.68 (m, 8H) 1.66 – 0.97 (m, 16H), 0.73 (t, J = 7.2 Hz, 9H). MS (MALDI) m/z: $[M + H]^+$ calcd for $C_{84}H_{77}N_{10}O_{11}$, 1401.58; found, 1401.41.

Synthesis of CAVITAND *functionalized polyethylene.*

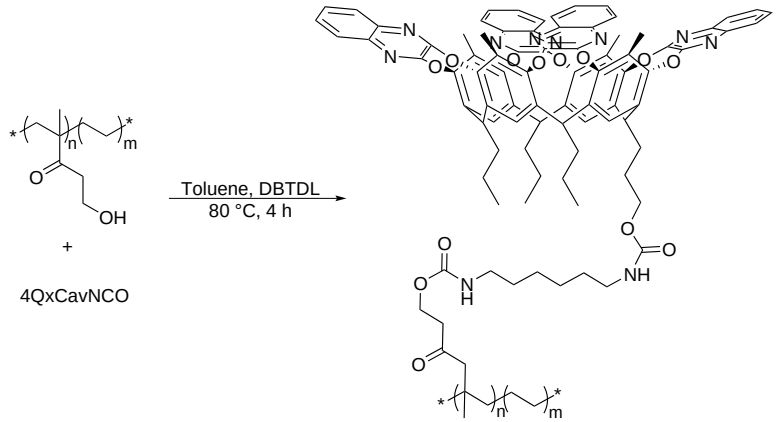

Polymer functionalization with CAVITAND was carried out according to the following general procedure, exemplified for 4QxCav30.4: The reaction was performed under dry conditions. First, PE-HEMA (0.5 g) with around 0.9 % of HEMA groups, was dissolved in toluene (50 mL) at 80 °C. Then, the 4QxCavNCO (0.28 g, 1 eq with respect to OH groups) was added as a solid. After dissolution of the CAVITAND, two drops of DBTDL were added to function as a catalyst. The mixture was stirred at 80 °C for 4 h. The hot mixture was precipitated into acetone, resulting in precipitation of a white powder. Filtration and drying of the precipitate gave the product as a white

powder.

References

[1] D. J. Cram, H. J. Choi, J. A. Bryant, C. B. Knobler, *J. Am. Chem. Soc.* **1992**, *114*, 7748–7765, DOI 10.1021/ja00046a022.

[2] H. M. de Azeredo, *Food Res. Int.* **2009**, *42*, 1240–1253, DOI 10.1016/j.foodres.2009.03.019.

[3] J. M. Lagaron, R. Catalá, R Gavara, *Mater. Sci. Technol.* **2004**, *20*, 1–7, DOI 10.1179/026708304225010442.

[4] J. R. Moran, J. L. Ericson, E. Dalcanale, J. A. Bryant, C. B. Knobler, D. J. Cram, *J. Am. Chem. Soc.* **1991**, *113*, 5707–5714, DOI 10.1021/ja00015a026.

[5] R. P. Hirschmann, R. N. Kniseley, V. A. Fassel, *Spectrochim. Acta* **1965**, *21*, 2125–2133, DOI 10.1016/0371-1951(65)80228-4.

[6] C. M. Cormier, B. Wunderlich, *J. Polym. Sci.* **1967**, *5*, 987–988, DOI 10.1002/pol.1967.160050514.

[7] F. Hauke, A. J. Myles, J. Rebek, *Chem. Commun.* **2005**, *0*, 4164–4166, DOI 10.1039/b506048f.

[8] L. Pirondini, A. G. Stendardo, S. Geremia, M. Campagnolo, P. Samorì, J. P. Rabe, R. Fokkens, E. Dalcanale, *Angew. Chemie - Int. Ed.* **2003**, *42*, 1384–1387, DOI 10.1002/anie.200390355.

Appendix C



Figure C.1: Picture of the self-made oven, an embodiment of the principles of JUGAAD, used for the slow evaporation of TCE. The circular PTFE mold is shown inside the oven with the open lid (left picture).

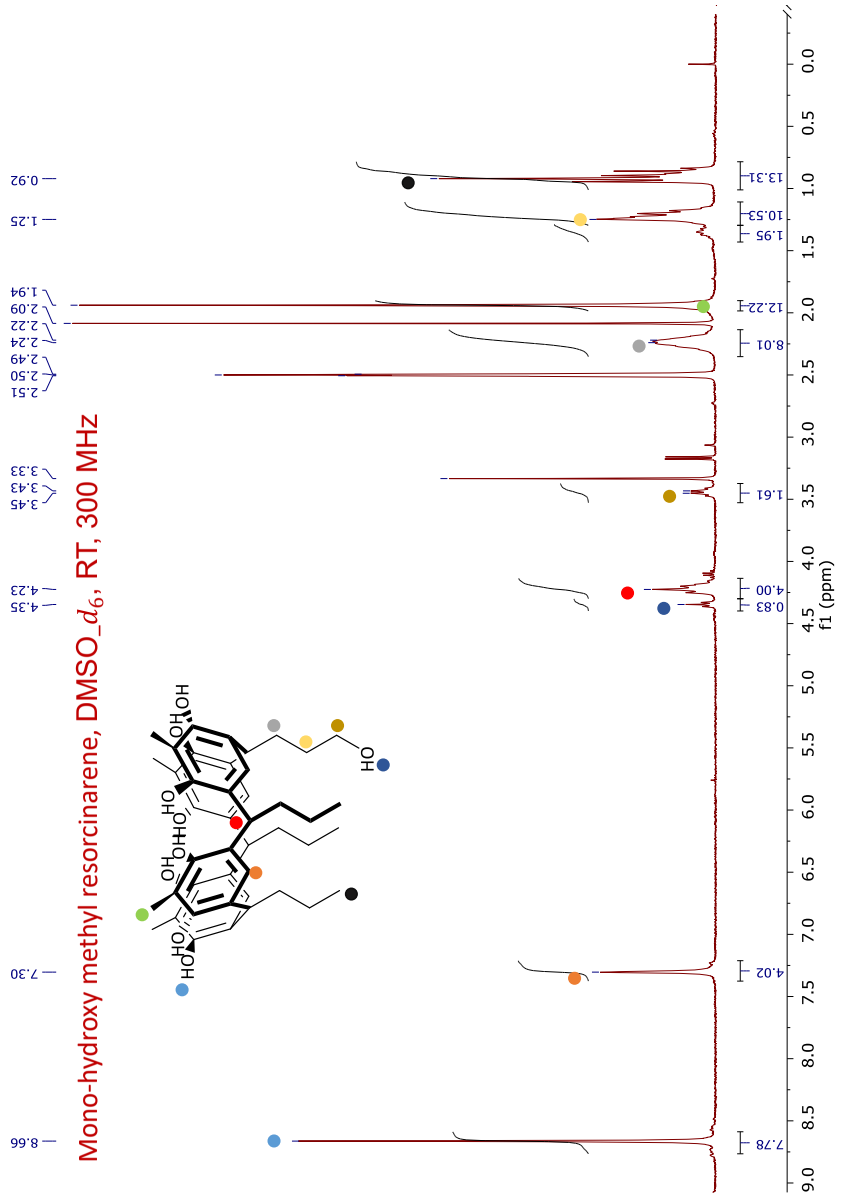

Figure C.2: ^{1}H-NMR spectrum of Mono-hydroxy methyl resorcinarene in DMSO-d_6.

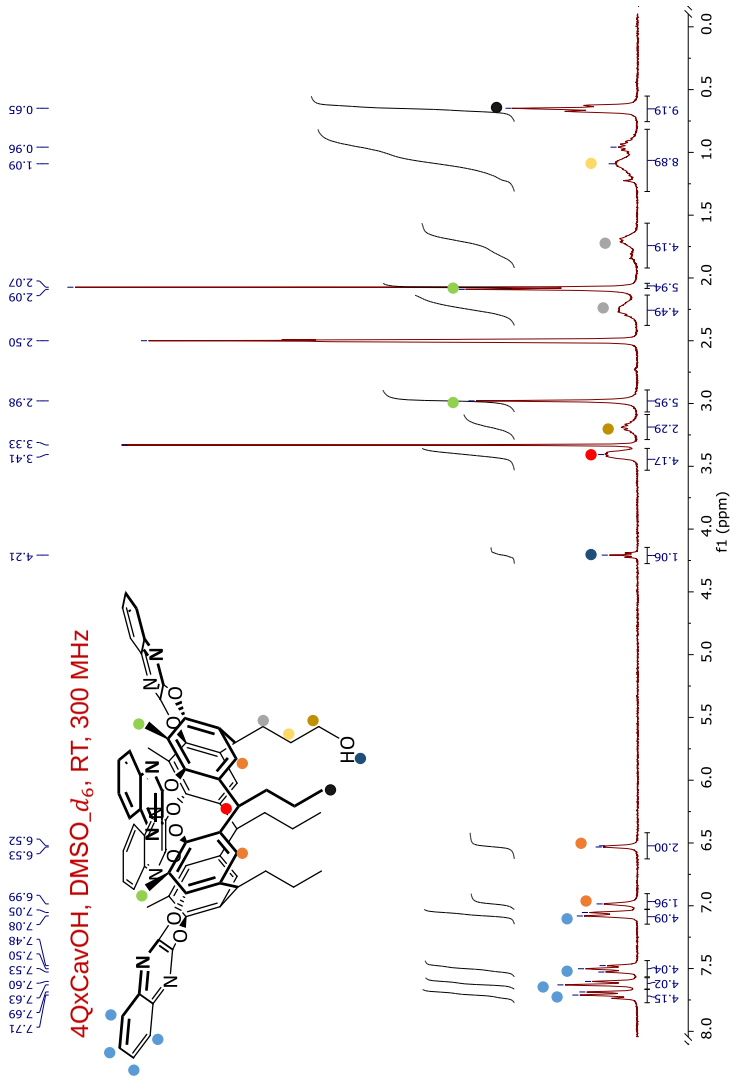

Figure C.3: ^{1}H-NMR spectrum of 4QxCavOH in DMSO-d_6.

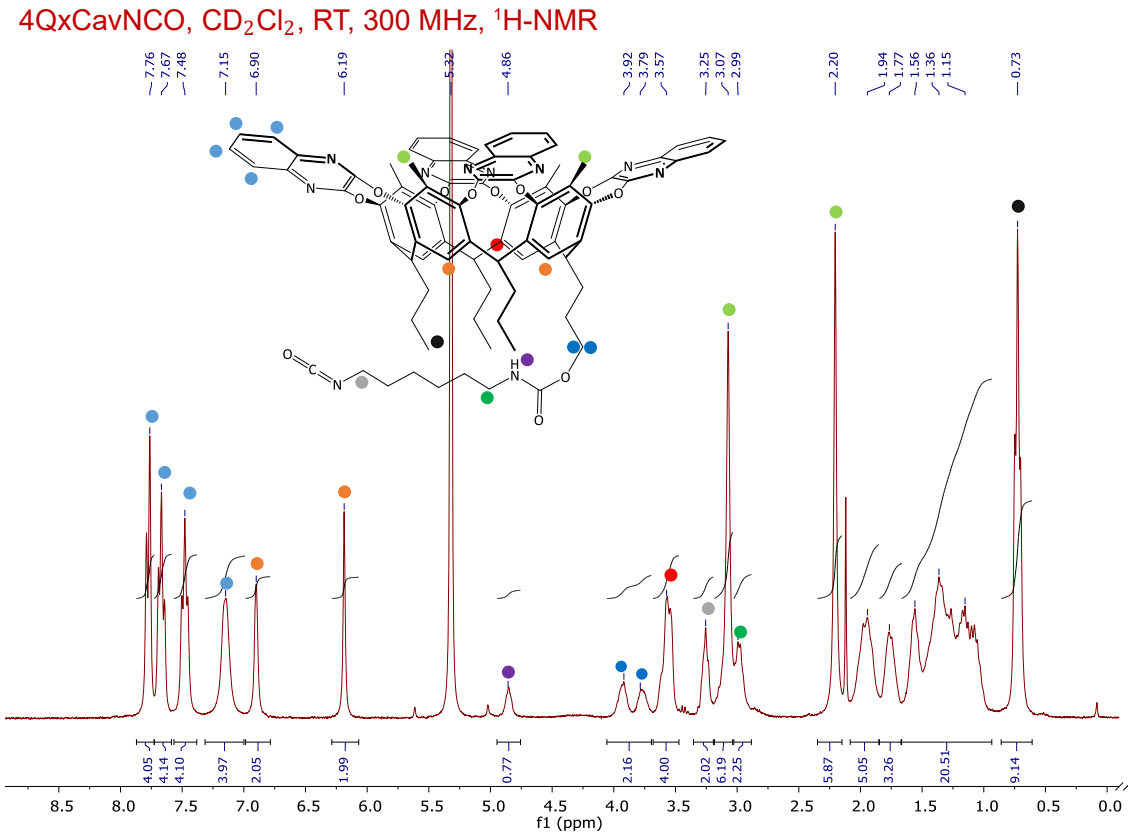

Figure C.4: ^{1}H-NMR spectrum of 4QxCavNCO in DMSO-d_6. The protons near the carbamate (blue dot) give two signals because in fact the dimer of the CAVITAND is observed and the two pairs of methylene signals have different shifts.

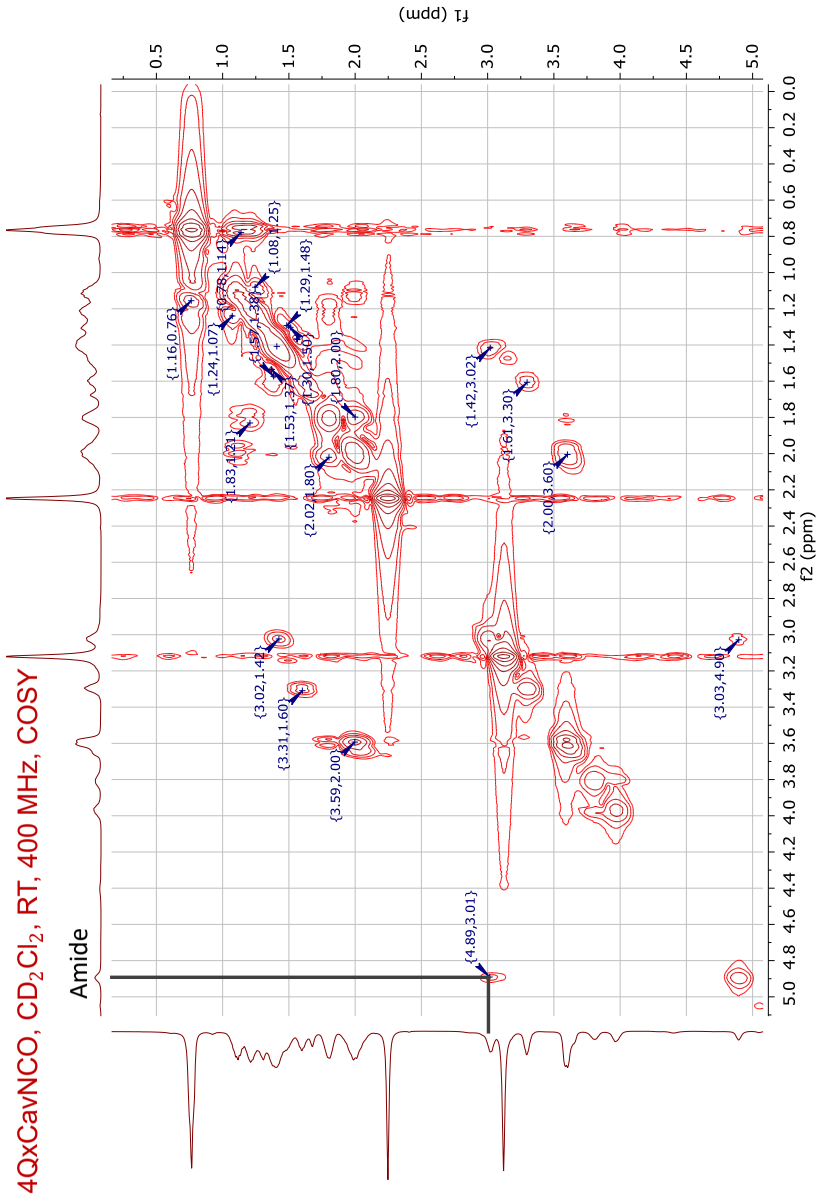

Figure C.5: COSY spectrum of 4QxCavNCO.

Chapter 5

Polyethylene Vitrimers

Abstract: Vitrimers are an emerging class of permanently cross-linked materials, where exchange reactions of cross-links provide malleability. The most promising application of these materials is to impart recyclability on thermoset materials such as cross-linked PE. Here, a facile and easy to up-scale method for the preparation of PE Vitrimers is presented by combining reactive extrusion and injection molding using exchange reactions of vinylogous urethanes and disulfide metathesis. It was found that for main chain polymers the amount of cross-links per chains is a critical parameter. Recyclability of the vinylogous urethane PE Vitrimer was demonstrated revealing minor degradation of the material. TOC-graphic: Recyclability of the vinylogous urethane PE Vitrimer.

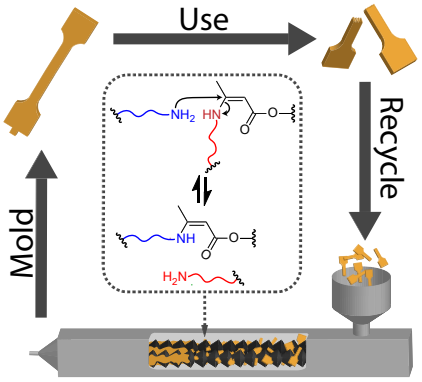

The contents of this chapter were partially adapted from: J. Tellers, M. Soliman, J. Vachon, R. Pinalli, and E. Dalcanale *In Preparation*.

As commented on in Section 3.1 PE, as the most widely employed synthetic polymer in the world,[1,2] is subject to widespread research interest to overcome some of its inherent flaws such as wear,[3,4] poor oxygen barrier properties,[5,6] low strength,[7–9] heat resistance,[9,10] and creep.[7,11] It is common practice to cross-link PE for demanding applications such as high voltage insulation and medical applications.[9,10,12,13] Cross-linking of PE results in material with superior mechanical performance and increased chemical-, thermal-, and creep resistance,[3,10,14–16] but at the cost of losing process- and recyclability.[10,17] An ideal material would retain these, combining properties offered by thermoplastic PE[18] with the properties of thermosets.[19] Here, an emerging sub-class of polymers called VITRIMERS for their glass like viscosity behavior presents great promise.[20,21]

VITRIMERS are a type of covalent adaptable network (CAN) (see Section 1.3.2), and altering the structure of PE so that it becomes VITRIMER-like will allow for macroscopic reshaping of a cross-linked PE. Few functionalities/types of reactions suitable for the preparation of VITRIMERS have been employed to functionalize commercial plastics,[22–24] and there is an ongoing need to advance the VITRIMER chemistry beyond the academic niche towards consumer ready materials.[25]

For flexible, low T_g polymers such as PE, exchange reactions with a high E_a are required to effectively freeze the network topology at room temperature, while being fast enough at elevated temperatures so that thermoplastic processing methods can be employed.[26] After evaluating some of the known types of exchange reactions, the vinylogous urethane chemistry was chosen because exchanges function without catalyst, are tunable, fast, and have a high E_a of 60 kJ·mol^{-1}, as DU PREZ *et al.* recently demonstrated.[19,27] Vinylogous urethanes are formed by reacting acetylacetonate (ACAC) moieties with primary amines, and an excess of amino groups is required to facilitate the exchange reactions.

In addition, another type of exchange chemistry, the disulfide metathesis, was explored mainly because of the commercially available cross-linker 4,4'-dithiodianiline (DTA). Aside from the disulfide group, this cross-linker bears two amino groups that can react with commercially available MA functionalized polymers such as polyethylene-*graft*-(maleic anhydride) (PE-MA)

and PP-MA. This allows for potentially easy access to large quantities of vitrimeric materials. The main disadvantages of this exchange chemistry are the strong yellow color of the disulfide group, and concerns about the long-term stability due to the radical intermediates occurring during the metathesis reaction.[28] Considering these drawbacks and given the abundance of commercial diamines, we focused our attention on PE with pendant ACAC groups.

In the subsequent Sections, the synthesis of suitable polymers with pendant ACAC groups obtained by post-functionalization of PE-HEMA and by direct copolymerization is presented. Then, a practical one step synthesis for PE VITRIMERS is demonstrated *via* reactive extrusion, by reacting terpolymer poly(ethylene-co-2-[methacryloyloxy]ethyl acetoacetate-co-2-hydroxyethyl methacrylate) (PACHE) (abbreviation originating from abbreviation of the individual comonomers PE-ACAC-HEMA, structure in Figure 5.1 **A**) with a slight excess of *m*-xylylenediamine (XYDIA) in the melt to obtain vinylogous urethane cross-links. In addition, a new route for vitrimeric PE by post-functionalization of PE-MA with the 4,4'-dithiodianiline (DTA) cross-linker is explored.

5.1 Functional Polyethylene for Vitrimer Synthesis

Several strategies are envisioned for the preparation of functional PE suitable to obtain VITRIMERS. As discussed earlier, PE with pending ACAC groups are required to make use of the vinylogous urethane chemistry, achieved by cross-linking of these groups with multifunctional amines. A functional PE was obtained by either transesterification of PE-HEMA with an acetoacetic ester, or by direct *co*-polymerization of ethylene with 2-(methacryloyloxy)ethyl acetoacetate. The polymers obtained from the latter route were prepared by SABIC. Even though no HEMA was employed during the *co*-polymerization, partial cleavage of ACAC unit resulted in a terpolymer referred to as PACHE (structure depicted in Figure 5.1 **A**). Despite that, the amount of ACAC can be controlled due to the linear relationship between the amount of incorporated ACAC and the ACAC feed

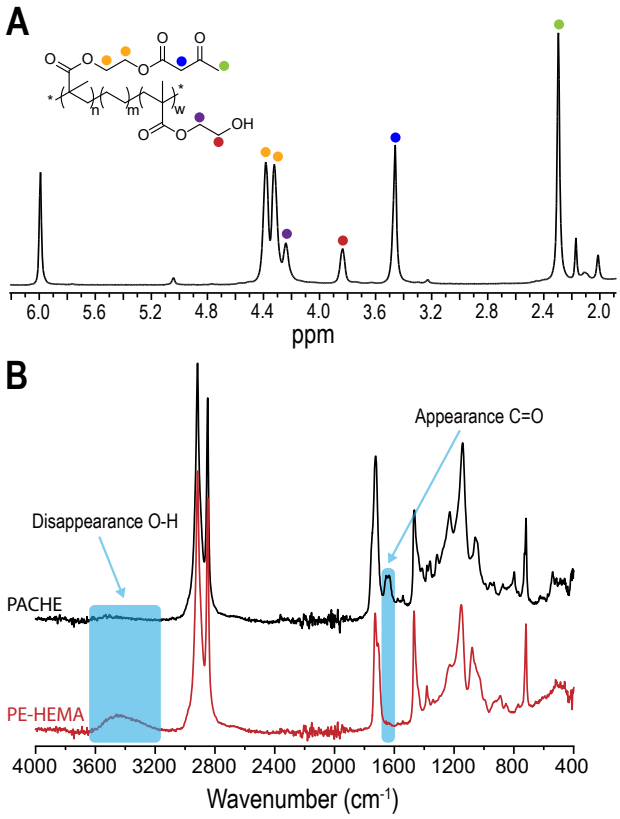

Figure 5.1: **A**: Portion of the ^{1}H NMR spectrum of solution prepared PACHE (120 °C, in TCE-d_2, excluding the PE backbone signals at low ppm). **B**: FTIR spectrum of PE-HEMA (red line) and of PACHE (black line). The light blue squares highlight the major changes before and after transesterification.

used in mol% and employing the PACHE terpolymer proved suitable to obtain PE VITRIMERS (*vide infra*).

The transesterification of PE-HEMA was carried out in solution, by first dissolving PE-HEMA polymers with varying amounts of HEMA in toluene, then adding methyl acetoacetate and 4-(dimethylamino)pyridine (DMAP), which was used as a transesterification catalyst. The reaction was carried out under atmospheric pressure to ensure that the developing methanol could evaporate. The polymers could be easily recovered *via* precipitation in isopropanol. By using PE-HEMA polymers with different amounts of HEMA, PACHE polymers with varying amounts of ACAC were be obtained. Three

Table 5.1: Overview of PACHE polymers obtained by transesterification of PE-HEMA polymers, their functional group content, and degree of functionalization.

Entry	Functional group content[a] (mol%)			T_m[b] (°C)	X_c[b,c] (%)	T_g[b] (°C)
	ACAC	HEMA	Et			
PACHEtr11	0.11	0.23	99.66	112.01	40.6	-16.24
PACHEtr96	0.96	0.69	98.35	107.41	35.0	-8.49
PACHEtr405	4.05	3.45	97.56	87.14	15.0	-17.09

[a] Determined *via* NMR, Et. short for ethylene; [b] det. *via* DSC; [c] X_c calc. with heat of fusion of PE = 286.2 J·g^{-1}.[29]

grades of PE-HEMA were used, obtaining a maximum degree of substitution of 58 % (determined *via* NMR). Table 5.1 contains an overview of the PACHE polymers obtained by transesterification. The conversion reached a maximum after ≈4 h, with further reaction time having no influence on the amount of substituted HEMA (see Figure D.1). The HTNMR of the ACAC functional polymers reveals that the methylene signals of the HEMA *co*-monomer shift after formation of the new ester (Figure 5.1 **A**), as well as showing new peaks belonging to the ACAC moiety. Additional proof for the success of the reaction is found in the FTIR spectra (Figure 5.1 **B**). After the transesterification, a new C=O band appears in the spectrum of the PACHE polymers at 1647 cm^{-1}, corresponding to the incorporated ACAC moiety. Furthermore, the broad OH band of the pristine PE-HEMA at 3444 cm^{-1} loses intensity, proving the successful reaction. Subsequently, PACHE polymers obtained *via* transesterification were explored for the preparation of VITRIMERS in solution.

5.2 Vinylogous Urethane PE Vitrimers

5.2.1 Solution synthesis of vinylogous urethane PE networks

In order to explore the concept, the preparation of vinylogous urethane PE VITRIMERS was first carried out in solution, following the scheme presented in Figure 5.2. Each of the PACHE polymers listed in Table 5.1 were dissolved

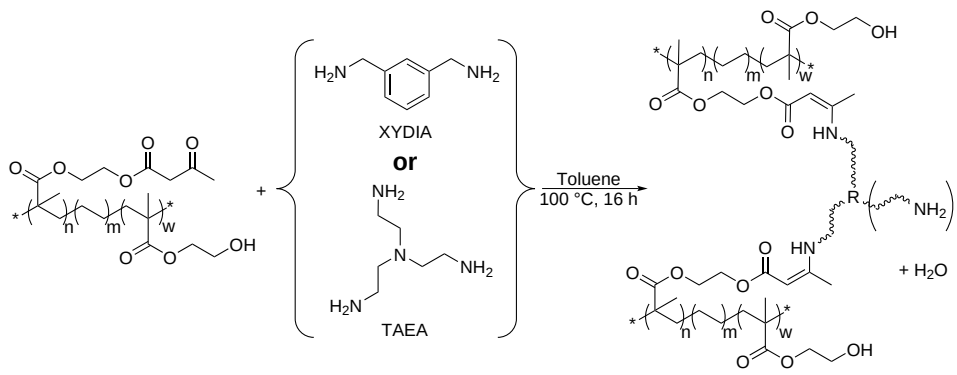

Figure 5.2: Reaction scheme for solution preparation of vinylogous urethane PE networks.

in dry toluene under inert conditions. Then, a multifunctional amine, either XYDIA or tris(2-aminoethyl)amine (TAEA), was added to cross-link the polymer. The amount of amino groups added was varied between 1.0 and 1.4 eq (accounting for di- and tri-functionality) to investigate the effect of varying amounts of free amino groups in the polymer matrix, which are required for the reshuffling reaction of vinylogous urethanes. During the reaction, solids precipitated from the solution when PACHEtr96 and PACHEtr405 were employed, which is a result of the cross-linking and a first indication for the successful network formation. The formation of the vinylogous urethane results in clear changes in the FTIR absorption spectrum of the material (Figure D.2). A new peak at 1599 cm^{-1} corresponds to the vibrations of the newly formed vinyl urethane group, and vibrations of the secondary amine appear in the fingerprint region at 781 cm^{-1} and at around 3276 cm^{-1} and 3369 cm^{-1}. Additionally, the shape of the C=O vibration peak found at 1655 cm^{-1} in the pristine polymer becomes more pronounced after the reaction. This change confirms the formation of the vinylogous urethanes. An overview of the performed reactions, starting polymers, equivalent of amino groups, and type of cross-linker used are given in Table 5.2. Three parameters were changed, specifically (i) the type of cross-linker, (ii) eq of amino groups added, and (iii) the amount of cross-links related to the varying ACAC content of the pristine PACHE polymers.

Table 5.2: Overview of VITRIMERS prepared in solution and the cross-linker and eq of amino groups used.

Entry	ACAC content[a] (mol%)	Cross-Linker	eq. amino groups[b]	T_m[c] (°C)		X_c[c,d] (%)		T_g[c] (°C)	
				Prist	Vit	Prist	Vit	Prist	Vit
VitX11-1.2	0.11	XYDIA	1.2	112.01	112.42	40.6	40.4	-16.24	-14.80
VitX96-1.2	0.96	XYDIA	1.2	107.41	103.96	35.0	33.3	-14.58	-11.15
VitX405-1.2	4.05	XYDIA	1.2	87.14	76.18	15.0	10.0	-17.09	-11.73
VitT11-1.2	0.11	TAEA	1.2	112.01	112.35	40.6	40.4	-16.24	-16.20
VitT96-1.0	0.96	TAEA	1.0	107.41	104.47	35.0	33.4	-14.58	-7.60
VitT96-1.2	0.96	TAEA	1.2	107.41	104.92	35.0	30.1	-14.58	-11.94
VitT96-1.4	0.96	TAEA	1.4	107.41	103.45	35.0	33.3	-14.58	-4.22
VitT405-1.0	4.05	TAEA	1.0	87.14	76.76	15.0	12.1	-17.09	9.28
VitT405-1.2	4.05	TAEA	1.2	87.14	80.19	15.0	11.7	-17.09	8.43
VitT405-1.4	4.05	TAEA	1.4	87.14	71.73	15.0	8.4	-17.09	9.25

[a] Determined *via* NMR; [b] With respect to ACAC groups; [c] Determined *via* DSC;
[d] X_c calc. with heat of fusion of PE = 286.2 $J \cdot g^{-1}$.[29]

For polymers with 1 eq of amino groups added we expected that compression molding will be unsuccessful due to the absence of free amino groups, and indeed the molding of sample VitT405-1.0 proved unsuccessful. Surprisingly, VitT96-1.0 could be compression molded into rectangular bars, albeit multiple cycles were required. Free amino groups are required for the reshuffling reaction of the vinylogous urethanes, and most likely small errors in the weighing process allow for some amino groups to be free in VitT96-1.0. Compression molded bars of VitT96-1.0, VitT96-1.2, and VitT96-1.4 were subjected to DMTA measurement to explore the influence of the different ratios of amino groups added. The plotted data is shown in Figure D.3. All samples appear to be cross-linked, showing a plateau modulus at high temperatures. With higher amount of amino groups added, the theoretical amount of cross-links between chains should be reduced, but the obtained data is inconclusive with only minuscule differences and no clear trend between samples. The main explanation is likely the harsh treatment during compression molding, partially degrading the sample. Similarly, the type of cross-linker used does significantly change the dynamic mechanical behavior. Polymer networks prepared from the same pristine polymer, but with different cross-linker, show no trend for tri- *vs* di-functional amine with respect to the relative occurrence of T_g or height of moduli (see Figure D.4).

Lastly, polymers with varying network density were compared, by starting with PACHE polymers with varying amounts of ACAC groups, the data of which are displayed in Figure 5.3. Naturally, there are large differences for the E' and the relative position of the α and β transition of the polymer networks due to the reduced degree of crystallinity (X_c) of the pristine polymers with higher ACAC content (see DSC data in Table 5.2). The most obvious influence of the cross-linking is evident after T_m, with the relative height of the plateau modulus increasing with increasing ACAC content in the pristine polymer. The plateau modulus of cross-linked materials corresponds directly to the cross-link density,[30] which is greater for polymers with a higher ACAC content, mirrored in the higher rubber modulus.

A feature of VITRIMERS is that a stress applied to the polymer can be relaxed at elevated temperatures due to exchange reaction adjusting the network topology. Stress relaxation measurements were performed

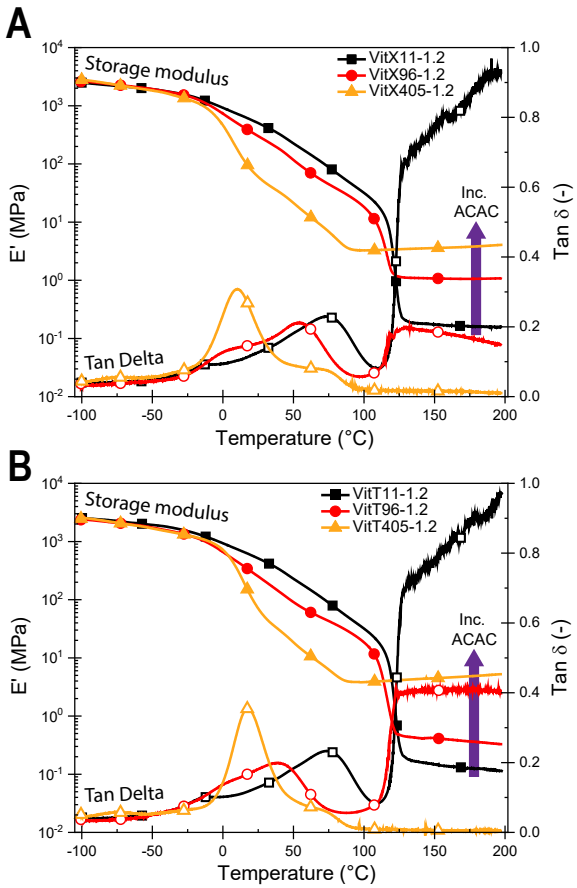

Figure 5.3: DMTA data of polymer networks grouped by the type of cross-linker used. **A**: XYDIA cross-linked, **B**: TAEA cross-linked. Purple arrows indicate the trend resulting from the increasing amount of ACAC in the respective pristine polymers and its influence on the plateau modulus.

for networks VitT96-1.2, VitX96-1.2, as well as VitX11-1.2 at elevated temperatures, monitoring an applied stress as a function of time. Networks with > 1 mol% of ACAC did not relax their stress. Only sample VitX11-1.2 with low ACAC content relaxed its stress at higher temperatures. However, the relaxation profile and obtained E_a reveals that relaxation is diffusion, not reaction-controlled, which is typical for a polymer melt (see Figure D.5).[31]

At this stage it was clear that vinylogous urethane PE networks can be obtained by reaction PACHE with multifunctional amines in solution. To move further, we wanted to move to an industrially applicable way to obtain

VITRIMERS and focus on networks with a lower cross-link density that can fully relax an applied stress. To prove that preparation of VITRIMERS on an industrial scale is feasible, techniques used in the processing of thermoplastic materials such as reactive extrusion and injection molding should be employed. By performing the reaction in the melt, the use of costly or harmful solvents is avoided and reactions should proceed faster without the need for long post curing steps which were previously employed.[19,32,33]

5.2.2 Solid-state synthesis of vinylogous urethane PE vitrimers

An industrial feasible method to prepare VITRIMERS would be to prepare them from suitable precursors using melt mixing or reactive extrusion. Such a precursor, the polymeric (LD)PE macromer PACHE with pendant ACAC groups, was provided by SABIC. This polymer was obtained by high pressure *co*-polymerization, where the amount of incorporated ACAC can be controlled by using its linear dependence on comonomer feed for sufficiently high feeds greater than 0.05 mmol (Figure D.6). For the preparation of VITRIMERS, PACHE polymers were first molten inside a twin-screw extruder at 150 °C, then reacted with 0.55 eq of diamine XYDIA (with respect to ACAC moieties) for ≈10 – 15 min, resulting in a cross-linked polymer network (Figure 5.4 **A**). We focused on XYDIA instead of TAEA because of the lower toxicity and less severe discoloration.

The slight excess of amino groups (0.05 eq) was employed to facilitate the exchange reactions, needed for the reshuffling of cross-links. The formation of vinylogous urethanes was confirmed by FTIR, revealing the characteristic bands of the vinyl urethane and ester groups at 1607 cm^{-1} and 1659 cm^{-1}, respectively (FTIR in Figure 5.4 **B**).[19,34] The reaction could be followed by monitoring the torque exerted on the screws (Figure D.7), which upon addition of cross-linker first spikes due to an initially unfavorable cross-linking. Then, facilitated by exchange reactions of vinylogous urethanes that promote network topology rearrangement (Figure 5.4 **C**), the torque decreases until a minimum equilibrium torque is reached, exceeding that of the molten pristine terpolymer.

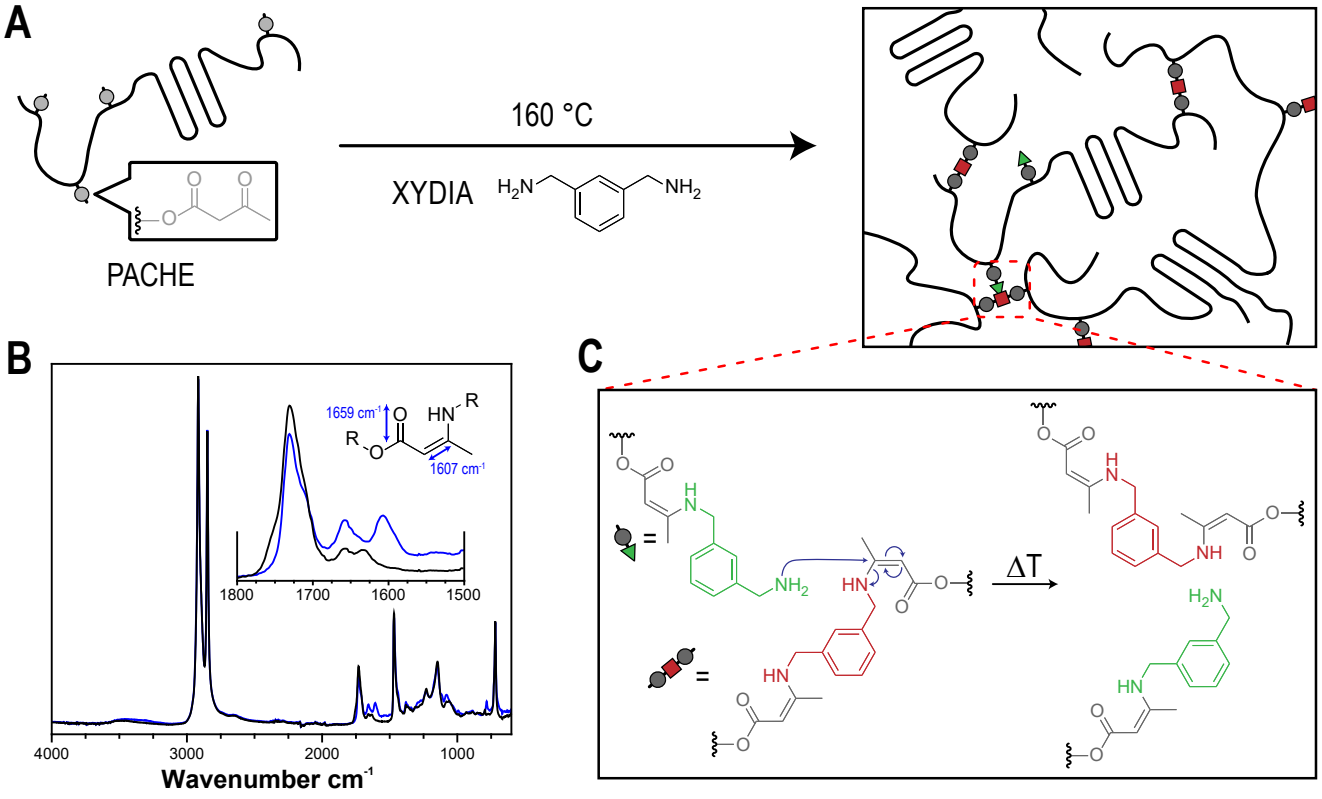

Figure 5.4: **A**: Synthesis scheme for vinylogous urethane PE-VITRIMERS. **B**: FTIR of pristine polymer (black line) and XYDIA cross-linked vitrimeric PE (blue line). **C**: Shuffling of cross-links *via* reaction of vinylogous urethanes and amino groups through MICHAEL addition of XYDIA cross-linked VITRIMERS.

Table 5.3: Overview of prepared polymers, their functional group content and molecular weight of the pristine polymers, thermal data of pristine and cross-linked polymers, and the average amount of cross-links per chain (LPC).

Entry	Functional group content[a] (mol%)			M_n[b] (Kg·mol^{-1})	Đ[b]	T_m[c] (°C)		T_c[c] (°C)		X_c[c,d] (%)		LPC[e]
	ACAC	HEMA	Et	Prist	Prist	Prist	Vit	Prist	Vit	Prist	Vit	
VitX0.5	0.12	0.53	99.35	12.9	5.8	110.2	111.0	97.1	99.7	40.8	40.3	0.5
VitX1.1	0.34	0.93	98.73	10.7	5.8	107.7	107.3	94.5	95.6	39.9	32.4	1.1
VitX1.9	0.66	1.34	98.00	9.7	4.06	105.7	105.5	89.6	89.2	33.9	30.1	1.9
VitX2.6	0.94	1.5	97.56	9.5	5.4	102.9	96.9	85.8	82.8	33.2	26.2	2.6

[a] Functional group content of pristine polymers before cross-linking, determined *via* NMR, Et. short for ethylene; [b] det. *via* GPC; [c] Determined *via* DSC, value for pristine (prist) left, for vitrimeric material (vit) right; [d] X_c calc. with heat of fusion of PE = 286.2 J·g^{-1}.[29] [e] LPC are calculated considering ACAC content, eq of cross-linker added, and M_n of pristine polymers.

Dog bones, DMTA bars and rheology disks were either directly obtained *via* injection molding by filling suitable molds with the hot polymers kept at >150 °C with a pressure of 5 – 10 bar, or cut from films obtained by compression molding of the pristine polymer powder or from VITRIMER pellets (pictures of transparent films and VITRIMER pellets in Figure D.8). An overview of the prepared polymers, functional group content, and molecular weight of the pristine polymers, thermal data of pristine and cross-linked polymers, and the theoretical average amount of cross-links per chain (LPC) (calculated for full functionalization with 0.55 eq of cross-linker), are given in Table 5.3.

5.2.3 Properties of vinylogous urethane PE vitrimers

Harsh conditions were employed trying to dissolve the VITRIMERS, keeping samples for 24 h at 100 °C in xylene. VitX0.5 dissolved within a couple of hours due to insufficient cross-linking, but already VitX1.1 stayed partially insoluble, leaving gel like residues that were sucked up by the needle during solvent removal step. VitX1.9 and VitX2.6 are insoluble in xylene at 100 °C, and gel fractions of 43.1±1.2 % (n = 8) and 65.3±4.4 % (n = 6) were determined respectively, showcasing the effect of the greater number of LPC. This presents a significant improvement over the recently reported (HD)PE VITRIMERS with an average gel fraction of ≈37 %.[24] The DSC and X-ray data (the wide-angle X-ray scattering (WAXD) spectra showing the characteristic PE diffraction maxima[35] are given in Figure D.9) reveal that the semi-crystalline nature of all materials was retained after cross-linking. The X_c was only slighly affected with almost no decrease for VitX0.5 and a ≈10 – 20 % decrease for VitX1.1, VitX1.9, and VitX2.6. The ACAC moiety needed for cross-linking is not part of the PE crystalline lattice and thus cross-linking only has a slight effect on crystallinity, an advantage over post-functionalization of a homo-polymer. All pristine polymers and VitX0.5 retained no rubbery plateau during DMTA measurements and melting of the crystalline lattice lead to measurement stop (see Figures D.10, D.11, D.12, and D.13), with VitX0.5 not having sufficient LPC to form a cross-linked or highly entangled network. However, cross-link density dependent plateau moduli of ≈0.1±0.03 MPa for VitX1.1, ≈0.4±0.1 MPa for VitX1.9, and

≈1.9±0.1 MPa for the denser VitX2.6 were observed (Figure 5.5 **A**).[30]

A similar dependency on LPC is uncovered from frequency sweeps of VitX0.5, VitX1.1, VitX1.9, and VitX2.6 performed at 160 °C (Figure 5.5 **B**). Whereas pristine polymers displayed the typical behavior of a low density polymer melt (G" > G' for all measured frequencies ω),[36] cross-linking resulted in a shift of the cross-over frequency of VitX0.5 to around 30 Hz due to chain extension.[37] This also reveals the reason for the failure during DMTA, where an oscillation frequency of 1 Hz was used, below the crossover point of VitX0.5. The higher cross-link density of VitX1.1 resulted in a predominantly solid behavior, with G' > G" over the available frequency range. In addition, an inversion of frequency dependence of the G' divided by the complex modulus (shear) (G*) (G'/G*(ω)), with respect to the polymer melt and VitX0.5, was observed (see Figure D.14: 0, 0.5, and 1.1 LPC), which is usually found for samples after their gel point.[37,38] However, due to the dissolution of VitX1.1 and thermoplastic like stress relaxation (*vide infra*), we surmise that VitX1.1 is not a fully cross-linked network. Raising the LPC to 1.9 (VitX1.9) further increases the elastic character of the network (Figure D.14 and Figure 5.5 **B**). The densest linked network with 2.6 LPC (VitX2.6) displays a frequency independent plateau G' over the available frequency range, with a dominating elastic character in the melt (G'/G* ≈ 1) for all ω at 160 °C (see Figure D.14), which is traditionally associated with fully cross-linked materials.[38] For true VITRIMERS only a single macromolecule is present at all times due to the consistent cross-link density, which contrasts other CANs like reversible DIELS ALDER networks, where frequency dependency of G' persists due to depolimerization occurring at higher temperatures.[21]

The same data is suitable to assess polymer melt strength using its established power law correlation with the zero-shear viscosity η_0 (Plot of complex viscosity (η^*) vs frequency at 160 °C in Figure D.15).[39,40] The terminal plateau was only observed for the pristine polymer within the available measurement range, but already for 0.5 LPC, despite the near liquid like behavior (G" > G' for most ω), η^* is nearly two orders of magnitudes larger than for the pristine melt at $\omega = 0.01$ rad·s^{-1} due to the increased M_n after linking. As expected, with increasing cross-link

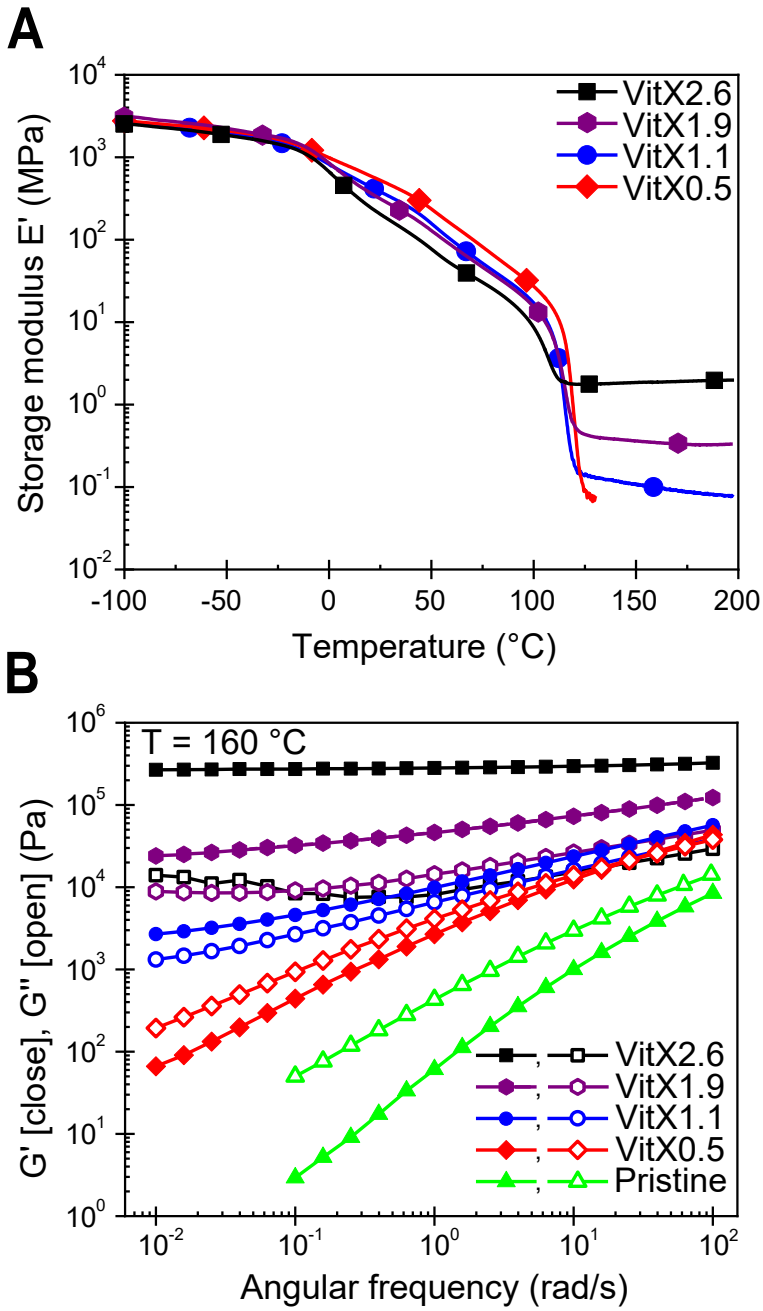

Figure 5.5: **A**: DMTA curves of VitX0.5, VitX1.1, VitX1.9, and VitX2.6 (heating rate = 3 °C·min^{-1} with ω = 1 Hz). **B**: Frequency sweeps of VitX0.5, VitX1.1, VitX1.9, and VitX2.6 at 160 °C; Pristine polymer of VitX1.1 displayed as reference for a typical (LD)PE melt.

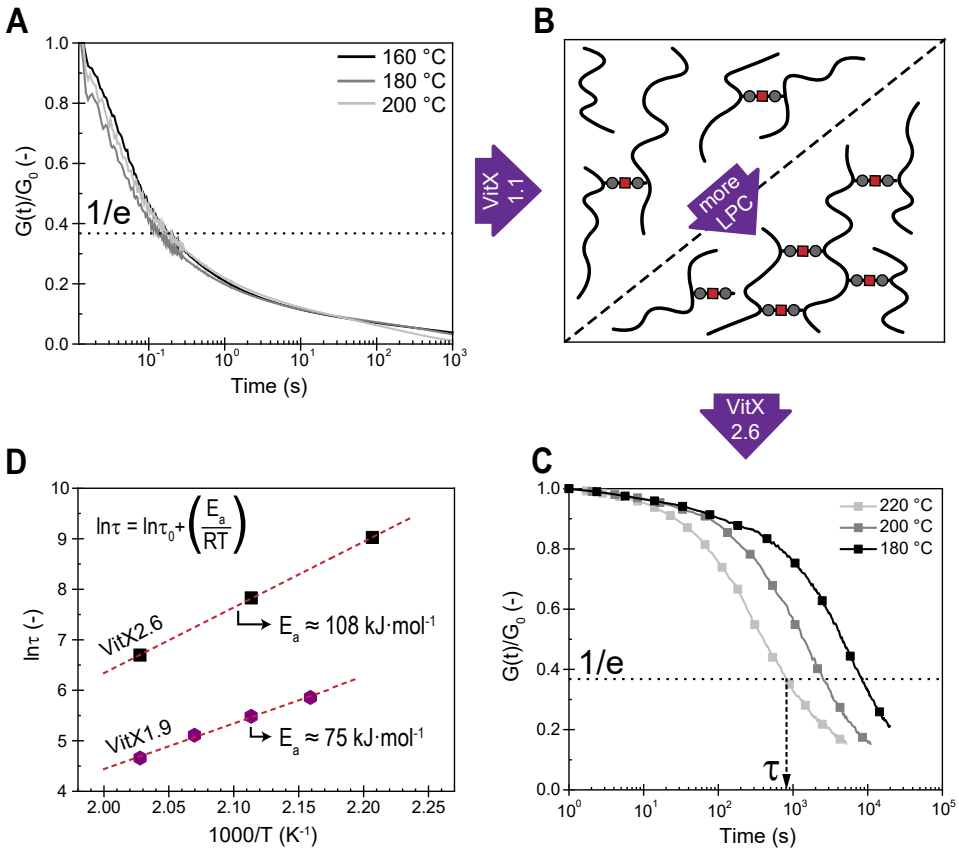

Figure 5.6: **A**: Normalized stress relaxation of VitX1.1 **B**: Illustration to show the importance of enough cross-links per chain for sufficient network formation, leading to exchange reaction-controlled stress relaxation. **C**: Normalized stress relaxation of VitX2.6. **D**: Plot of $\ln\tau$(T) versus inverse temperature obtained from stress relaxation of VitX1.9 and VitX2.6.

density, η^* further increases by three orders of magnitude between 0.5 LPC and 2.6 LPC. Additionally, an exponential relationship between η^* and the amount of LPC is found for varying shear rates (see Figure D.16), making it possible to predict the viscosity (η) of the vitrimeric PE from the ACAC feed used during synthesis of the pristine polymer. VITRIMERS are known as the first strong organic glass formers and as such their viscosity decreases linearly above T_g with increasing temperature.[17] For semi-crystalline materials that have crystallites, this phenomenon must be observed after T_m. Satisfyingly, the viscosity of VitX2.6 is found to decrease almost linearly with temperature above T_m (measured between 120 °C and 220 °C, see Figure D.17), but changes slower compared to other VITRIMERS scaled with T_g.

As mentioned earlier for the VITRIMER networks prepared in solution, it is characteristic that full stress relaxation is achieved at higher temperatures due to the isodesmic exchange reactions that reshuffle to accomodate the stress. Therefore, the evolution of an applied stress was measured as a function of time and temperature. Samples with 0.5 LPC and 1.1 LPC displayed very fast relaxation like that of lowly cross-linked or branched polymer melts, a consequence of the smaller number of cross-links (VitX0.5: Figure D.18; VitX1.1: Figure 5.6 **A**).[41] When sufficient LPC to form a proper network are employed (Figures 5.6 **B**), relaxation will be dominated by the exchange reactions, as movement can only occur when cross-links adapt. Indeed, samples VitX1.9 and VitX2.6 with an average 1.9 and 2.6 LPC show relaxation controlled by the exchange reactions (Figure 5.6 **C** for VitX2.6 and Figure D.20 for VitX1.9; Treatment of raw relaxation curves shown in Figure D.19). As a consequence, the characteristic relaxation time (τ), typically chosen when the initial stress relaxes to 1/e (≈37 %) according to the MAXWELL model,[19,42] follows ARRHENIAN dependence on temperature (eq 5.1). Thereby, an E_a of 75±4 kJ·mol^{-1} for VitX1.9 and an E_a of 108±2 kJ·mol^{-1} ($T(\tau = 60\ s) \approx 274$ °C) for VitX2.6 were calculated, obtained from the fit of lnτ versus inverse temperature (Figure 5.6 **D**).

$$\tau(T) = \tau_0 \cdot \exp\left\{\frac{E_a}{RT}\right\} \tag{5.1}$$

The E_a of VitX1.9 fits that of previously determined vinylogous urethane

systems (59±6 kJ·mol^{-1}, 69±2 kJ·mol^{-1}, and 73±12 kJ·mol^{-1}),[19,33,43] suggesting that the exchange pathway follows the therein reported iminium pathway and that exchanges are not inhibited by the polymer network structure. On the contrary, a near twofold E_a increase is observed for VitX2.6. From the time dependent rheology measurements, it is clear that chain mobility is significantly reduced in VitX2.6. Because of this, diffusion of functional groups within the polymer is significantly retarded, which is reflected in the E_a. Similar observations have been made for highly cross-linked silyl ether PS vitrimers,[44] where the E_a for exchange reactions in the polymer was greatly increased over the E_a obtained from small model compounds.

In reference [44] a neat way to calculate the T_v from the E' and the fit obtained from the plot of τ versus temperature (eq 5.2) is presented.

$$\textbf{VitX2.6} : \ln\tau(T) = 13.01 \cdot \frac{1000}{T} - 19.67 \iff \tag{5.2}$$

$$T = \frac{13010}{\ln\tau + 19.67} \tag{5.3}$$

The T_v is usually chosen when a η of 10^{12} Pa·s is reached,[42,45] and the relation between η, τ, and E' is given by Maxwell (eq 5.4):

$$\eta = \frac{E'}{2(1+\nu)} \cdot \tau \tag{5.4}$$

with ν being the Poisson's ratio, which for (LD)PE is 0.5 at low strain rates.[46] At 180 °C, a E' of 1.94 MPa was determined for VitX2.6 (Figure 5.5 **B**). At T_v, the η is 10^{12} Pa·s, and a τ of 1.55x10^6 s was calculated. Inserting this value into eq 5.3 yielded a T_v of 110.2±5.8 °C. The reported associative transamination of vinylogous urethane occurs in the temperature range of >80 °C – 110 °C.[47,48] The η of the vitrimer can only significantly decrease once the exchange reactions initiate, as the topology is otherwise frozen. The obtained T_v is thus within the expected temperature region, slightly above the onset of the transamination reactions. However, using the same method for VitX1.9 yields a T_v of 31.4±14 °C, which is significantly below that of VitX2.6. There are two things to consider. First, exchange reactions can

already become relevant for the less cross-linked system at lower temperature due to the larger degree of chain movement. But, considering the T_m of this VITRIMER it is unlikely that T_v is that low. More likely, this is a case where the limits of determining T_v from extrapolation of high temperature rheology become apparent, as was recently highlighted by DU PREZ *et al.* during their investigation of a dual temperature responsive VITRIMER.[33]
In order to assess the recyclability of the PE VITRIMERS, it is common practice to perform repeated mechanical tests of recycled material. Consequently, dog bones were obtained from extrusion and subjected to tensile testing, followed by successive extrusion and repeated breaking of the tested dog bones. The tensile strain curves and the average tensile strength for each of the cycles are given in Figure 5.7. For each step, four representative curves are plotted, whereas the inset shows the average obtained tensile strength after the first and subsequent cycling steps (n = 4 – 8). The obtained tensile strain curves do not directly overlap and usually two specimens give similar stress-strain curves. This is due to processing induced differences during the extrusion step and the fact that each step will produce two dog bones as a result of the employed mold. The tensile strength is found to slightly decrease between each step revealing minor degradation. To assess whether the cross-linked network is still intact after recycling, the gel fraction of samples that were recycled four times (Break 4) was investigated. For these samples a gel fraction of 63.6±2.2 % (n = 3) was determined, which is in line with the value obtained for the as synthesized VITRIMERS. Consequently, repeated extrusion of these PE VITRIMERS did not destroy the network structure revealing the potential to recycle the material.

5.3 DTA cross-linked PE-MA

There are many commercial grades of PP and PE materials available with maleic anhydride (MA) groups. These functional groups may be used for the preparation of VITRIMERS by employing suitable cross-linkers. However, these cross-linkers have to introduce the functionality that is able to exchange in order to impart vitrimeric properties. MA groups are known to readily react with amines to form a maleimide group. Using 4,4'-dithiodianiline

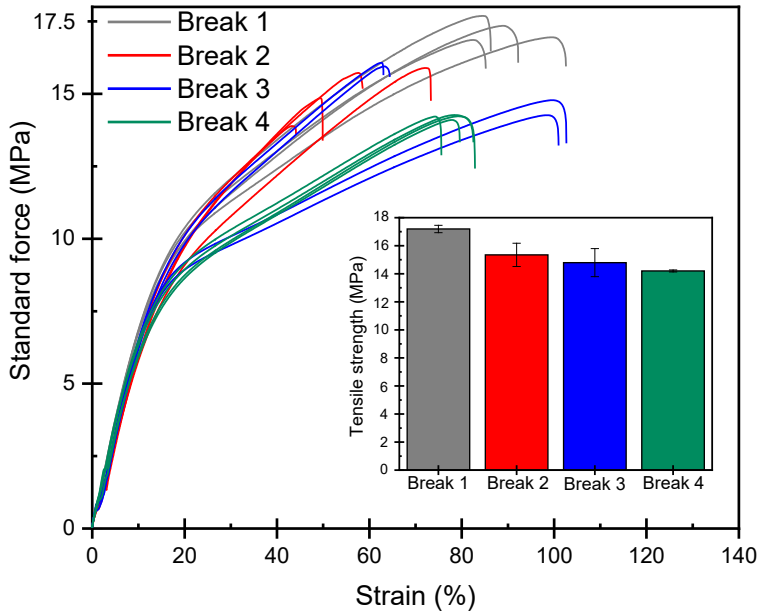

Figure 5.7: Repeated tensile tests of extruded dog bones of VitX2.6 as synthesized (break 1) and subsequent recycling steps (break 2 – 4). Inset shows the average tensile strength (n = 4 – 8) for each of the recycling steps.

(DTA), which is a diamine molecule that can react with two MA moieties, can be employed to form a cross-link. The VITRIMERIC properties then originate from the disulfide group of the DTA linker that can undergo a shuffling metathesis reactions.[49] A similar strategy was previously used to impart VITRIMER like properties to epoxide networks.[50] In order to obtain these DTA cross-linked PE networks, the previous strategy for the preparation of vinylogous urethane PE VITRIMERS, specifically the reactive extrusion of a suitable macromer with DTA, will be employed. A PE-MA available from SABIC with 0.4 mol% of MA groups (det. *via* NMR) was chosen initially. The amount of MA units is quite high for commercial MA functionalized polyolefins, but with a low M_n of 6000 g·mol^{-1} (M_w = 22300 g·mol^{-1}, dispersity (Đ) = 3.75) the amount of LPC is only about 0.8. This is assuming that all MA units react using 0.5 eq of di-functional cross-linker. This SABIC grade was chosen because of its availability, and because obtaining PP and PE grades with high MA content and reasonable M_n is difficult due to the scission of the polymer during grafting,[51,52] or

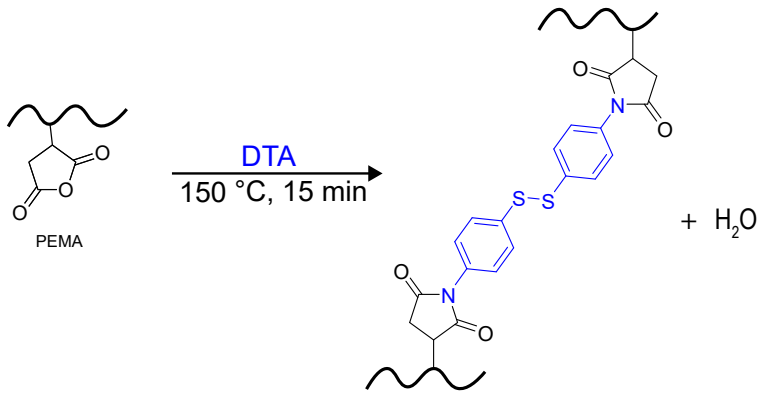

Figure 5.8: Synthesis scheme for DTA cross-linked PE-MA.

unwanted cross-linking.[53] It is possible to avoid scission, by grafting not directly on the carbon backbone, but instead grafting on suitable side groups at lower temperatures.[54]

The initial approach was therefore focused on investigating whether the cross-linking works on an easily accessible polymer, studying its influence on the polymer rheology. Afterwards, moving to polyolefins with greater MA content or higher M_n will provide a fully cross-linked system, as was demonstrated in the previous Section with vinylogous urethane PE VITRIMERS.

The aforementioned PE-MA was therefore reacted with 0.25 eq and 0.5 eq of DTA cross-linker (0.5 eq and 1 eq amino groups) according to the scheme depicted in Figure 5.8. This is achieved by first melting the polymer, then adding DTA as a solid. Also here the reaction could be followed by observing the torque exerted on the extruder screws, and reactions were carried out for 15 min to ensure that most MA groups react. Using FTIR spectroscopy, the disappearance of the MA C=O stretching vibrations at 1791 cm^{-1} and 1739 cm^{-1} could be followed (see Figure D.21), which provides evidence for the reaction of the MA moieties leading to a cross-linked material.[55]

Table 5.4 lists the prepared materials and thermal data of pristine and cross-linked material. Unsurprisingly, the introduction of DTA lead to a decrease in X_c, which corresponds to the amount of DTA added (see also Section 4.2). The T_m was not affected, but the peaks became broader with introduction of DTA detailing an increased distribution of crystal sizes, a result of the cross-linking with DTA.[56] To assess the effect of the cross-

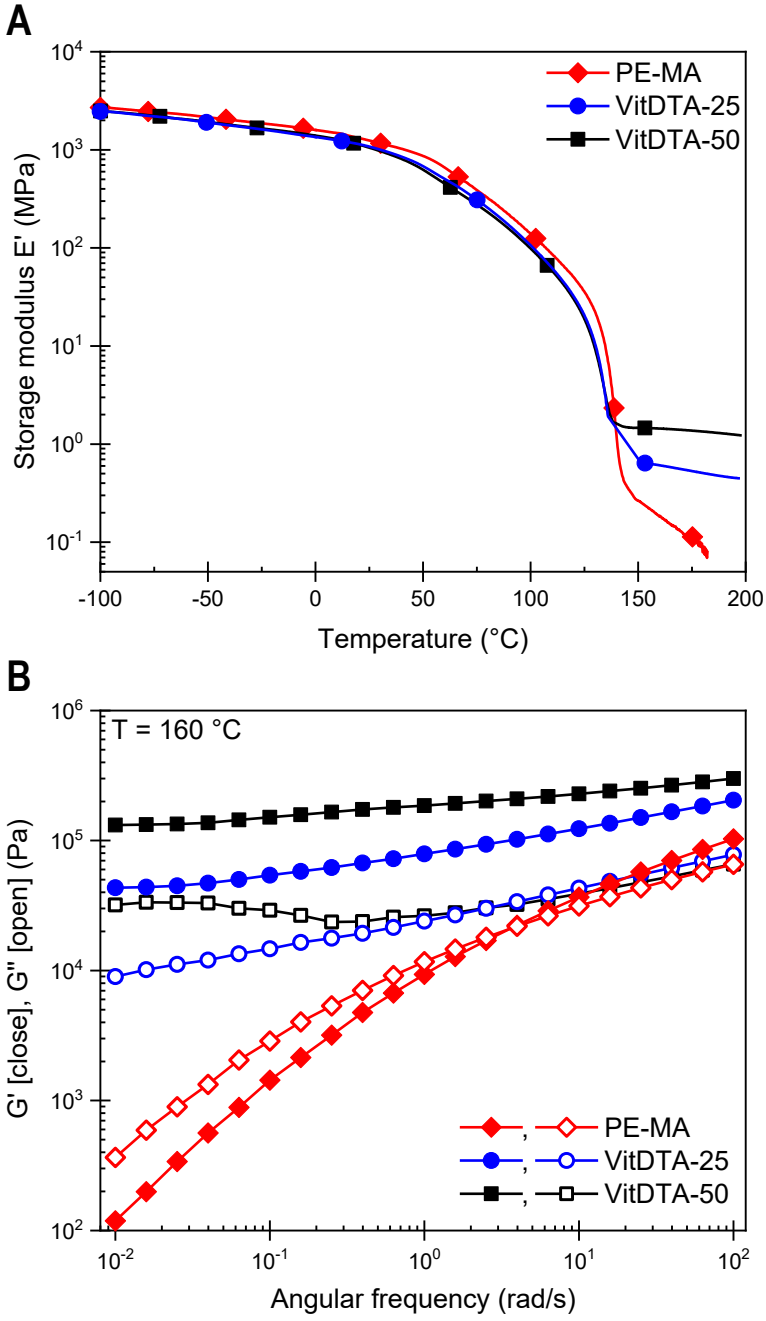

Figure 5.9: **A**: DMTA curves of VitDTA-50, VitDTA-25, and the pristine PE-MA (heating rate = 3 °C·min^{-1} with ω = 1 Hz). **B**: Frequency sweeps of VitDTA-50, VitDTA-25, and the pristine PE-MA at 160 °C.

Table 5.4: Overview of DTA cross-linked PE materials.

Entry	MA content[a] (mol%)	Eq. DTA[b]	T_m[c] (°C)	X_c[c,d] (%)	T_g[c] (°C)
PE-MA	0.4	-	126.67	58.9	n.d.
VitDTA-25	0.4	0.25	129.23	54.9	n.d.
VitDTA-50	0.4	0.5	127.14	52.0	n.d.

[a] Determined *via* NMR; [b] With respect to MA groups; [c] Determined *via* DSC. [d] X_c calc. with heat of fusion of PE = 286.2 $J \cdot g^{-1}$.[29]

linking, the time and temperature dependent rheology was investigated performing DMTA and parallel plate measurements. The obtained data is illustrated in Figure 5.9. The pristine PE-MA is a type of (HD)PE, reflected in the relatively high T_m. The pristine polymer has a significant amount of entanglements, which is reflected in the observed modulus after T_m (≈127 °C) of the polymer (see Figure 5.9 **A**), as entanglements will lead to a rubber plateau for certain materials dependent on the oscillation frequency used (in this case 1 Hz).[30] Eventually, at higher temperatures the time dependent behavior of the pristine polymer changes and measurement failure occurs at ≈180 °C. Both samples cross-linked with DTA retain a modulus over the entire temperature range (up to ≈200 °C), a result of the interchain linkage that increases the amount of entanglements and cross-links.[30] The height of the plateau modulus corresponds directly to the amount of cross-links and consequently to the amount of DTA added. At 180 °C a E'(VitDTA-25) of 0.51 MPa and E'(VitDTA-50) of 1.35 MPa were obtained, corroborating the theory.

In Figure 5.9 **B** the time dependent data is presented. A frequency sweep was conducted of the polymer melt at 160 °C. As expected for an entangled polymer melt, a crossover point at 3.5 Hz was observed for the PE-MA sample, and the observed moduli are strongly frequency dependent. Cross-linked sample VitDTA-25 showed no crossover point over the available frequency range and G' was above G", showing that the material does not flow. Further increasing the cross-link density (VitDTA-50) increased the plateau modulus and the frequency dependency of the G' further decreased, a prominent fea-

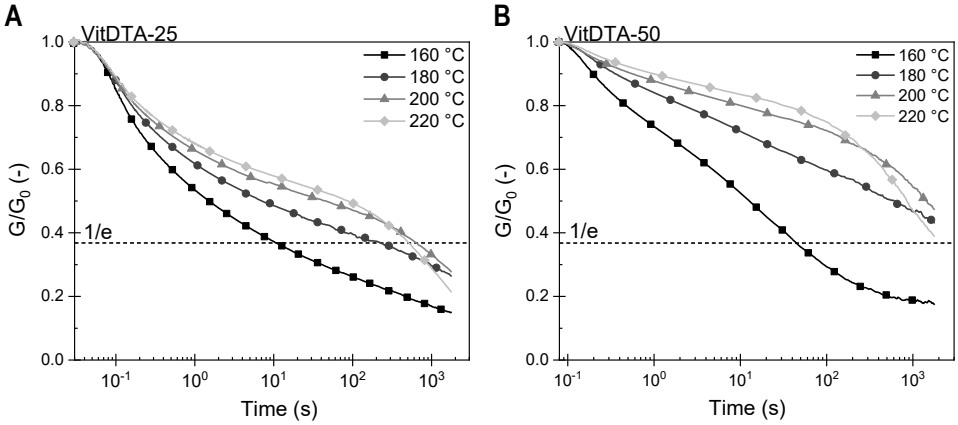

Figure 5.10: Plots of the normalized stress relaxation of **A**: VitDTA-25 and **B**: VitDTA-50.

ture of cross-linked polymer matrices.[36] Clearly, the rheology data supports the claim that a cross-linked, or at least significantly entangled polymer matrix was obtained. It was possible to shape the material using compression molding, indicating that an applied stress can be relaxed. Subsequently, the relaxation behavior of these materials was investigated.

In particular, the evolution of a constant stress was measured as a function of time and temperature using the parallel plate rheology setup. The treated relaxation curves (G_0 is taken at the maximum of G) are plotted in Figure 5.10. As expected, at all temperatures the stress relaxes over time. There is no clear correlation between temperature and relaxation time, and the stress relaxes slower at higher temperatures. The more highly cross-linked sample VitDTA-50 relaxes its stress slower on average, due to the higher cross-link density. Likely, there are not sufficient LPC to form a fully cross-linked network, and two stages of relaxation occur. An initial fast one as a result of polymer chains followed by a reaction-controlled mechanism which is more apparent for the curves taken at 200 °C and 220 °C. This system was not further pursued due to its strong discoloration and expensive cross-linker, but provides in principle another route to PE VITRIMERS.

5.3.1 Conclusions

To conclude, we demonstrated an industrially relevant, easy to up-scale pathway to PE VITRIMERS using the established vinylogous urethane chemistry. Proper network formation was revealed through solubility and mechanical tests. Only for samples with a sufficient number of LPC, the relaxation is controlled by the exchange reactions and τ_0 shows an ARRHENIAN dependence on temperature. It is becoming increasingly evident that when macromers are employed, the E_a is significantly higher for the same type of exchange chemistry, a fact that needs to be considered in the design of future main chain polymer VITRIMERS. Going forward, the long-term stability of the reactive groups needs to be evaluated, and at least 3 – 4 cycles of lasting use and remolding outside of the lab environment (after longer periods of actual use) should be possible before moving on to landfill or incendiary disposal.

In addition, a facile pathway to cross-linked PE was demonstrated by using di-amine cross-linker DTA, avoiding the use of solvents or catalysts. The reaction was confirmed by FTIR and the effects of cross-linking on polymer were rheology elucidated *via* DMTA and time dependent measurements, revealing increased melt strength. The disulfide moiety present in the cross-linker can impart VITRIMER like properties to the material, given that sufficient LPC are used. The strong discoloration and potential degradation of the disulfide groups may hamper the use of this system in applications where colorless materials are preferred.

5.4 Experimental Section

Gel permeation chromatography (GPC). GPC was performed at 160 °C on a POLYMER LABORATORIES *PLXT-20* Rapid GPC Polymer Analysis System (refractive index detector and viscosity detector) with three PLgel OLEXIS (300 mm x 7.5 mm, POLYMER LABORATORIES) columns in series. 1,2,4-Trichlorobenzene was used as eluent at a flow rate of 1 $mL \cdot min^{-1}$. The molecular weights were calculated with respect to polyethylene standards (POLYMER LABORATORIES). A POLYMER LABORATORIES *PL XT-220* robotic sample handling system was used as auto-sampler.

High Temperature Nuclear Magnetic Resonance (HTNMR). The HTNMR spectra were recorded on a Bruker AVANCE *III* (500 MHz) equipped with a cryogenically cooled probe head at 120 °C in TCE-d_2. ^{1}H NMR chemical shifts are given in ppm in reference to the residual solvent peak of TCE at 6.00 ppm.

Fourier *Transformed Infrared Spectroscopy* (FTIR). FTIR-spectra were recorded on a Perkin Elmer *Spectrum One* equipped with a *Golden Gate accessory* (diamond ATR).

Rheology. Injection molded disks for rheology (diameter 25 mm, thickness 1 mm) were measured using a TA Instruments *DHR 2*, equipped with a parallel plate geometry. The G' and G" were monitored during a frequency sweep from 100 rad·s^{-1} – 0.01 rad·s^{-1} at 160 °C using a strain amplitude of 0.4 %. Stress relaxation measurements were performed at multiple temperatures between 160 °C and 220 °C, applying a step strain of 1 %, then monitoring the stress until at least 75 % of the initial stress relaxed or until a constant stress value was observed.

Dynamic Mechanical Thermal Analysis (DMTA). Rectangular samples suitable for DMTA were cut to dimension of 3 x 5 x 0.5 mm (length x width x thickness) from injection molded bars or directly compression molded to size. Samples were measured on a TA Instruments *Q800* in tensile mode. The E' and E" were monitored while screening the samples during a temperature sweep from -100 °C to 200 °C at 3 K·min^{-1}. An oscillation frequency of 1 Hz with an oscillation amplitude of 10 µm were applied.

Determination of Gel fraction. Extruded pieces with a weight of ≈190 mg were first placed in a 50 mL vial, then 10 mL of xylene was added, the vial closed, heated to 100 °C and kept for 24 h. After cooling to room temperature, the liquid is decanted, and the solid residue washed at least three times with isopropanol. The samples were dried in a vacuum oven (80 °C) until the weight was constant. The gel fraction was determined according to equation 5.5.

$$\text{Gel fraction}(\%) = \frac{\mathrm{m}_{final}}{\mathrm{m}_{initial}} \cdot 100\ \% \tag{5.5}$$

Differential scanning calorimetry (DSC). All DSC measurements were performed on a TA Instruments *Q20* equipped with a *RCS 90* cooling system. About 2 – 5 mg of polymeric sample was weighed inside an aluminum pan and subjected to DSC measurements under nitrogen atmosphere. Unless otherwise noted, polymers were screened twice from 90 °C to 200 °C at a constant heating/cooling rate of 10 K·min^{-1}. The H_m, T_g, T_m, and T_c were determined from the second heating and cooling cycle.

Tensile tests. Tensile tests were performed with a Zwick type *Z020* tensile tester equipped with a 1 kN load cell. The tests were performed on injection molded dog bones with dimensions of 75 mm x 4 mm x 2 mm. A grip-to-grip separation of 30 mm was used. The samples were prestressed to 0.5 N and then loaded with a constant cross-head speed of 50 mm·min^{-1}.

Calculation of LPC. The number of LPC was calculated assuming every ACAC moiety reacts according to equation 5.6, with LPC as cross-links per chain (LPC), M_n as he number average molecular weight of the pristine polymer, M as the average molecular weight of a repeating unit (calculated using mol% determined by NMR), $mol\%_{ACAC}$ as the NMR determined content of ACAC in mol%, and considering the 0.55 eq excess of cross-linker loosing roughly every tenth possible cross-link (1.1 eq of amino groups).

$$\text{LPC (sample)} = \frac{M_n \cdot \text{mol }\%_{ACAC}}{M \cdot \text{eq}_{\text{amino groups}}} \tag{5.6}$$

5.4.1 Synthesis

The PE-HEMA and PACHE polymers with varying amounts of HEMA and ACAC were provided by SABIC and used as received. The PACHE polymers provided by SABIC were used exclusively for the solid-state preparation of PE vitrimers. XYDIA 99 %, methyl acetoacetate 99 %, and DMAP 99 % were purchased from Sigma-Aldrich and used as received.

Synthesis of PACHE polymers via transesterification of PE-HEMA.

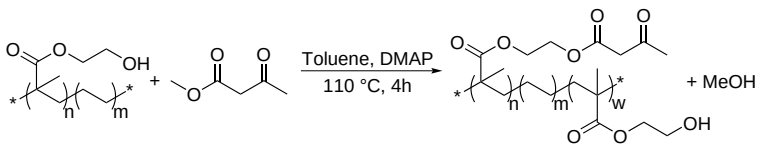

All PACHE polymers obtained from transesterification of PE-HEMA were obtained following the following general procedure: First, PE-HEMA *co*-polymer (30 g) was dissolved in toluene (400 mL) at 100 °C inside a glass reactor equipped with mechanical stirring. Then, methyl acetoacetate (34 mL, 5 eq) and DMAP (7.7 g, 1 eq) were added, the temperature raised to 120 °C, and the mixture stirred for 4 h. The polymers were recovered by precipitating the hot solution into methanol (1 L), stirring for 1 h, filtering off the precipitate, and drying at high vacuum yielding the polymers as white solids.

Solution synthesis of vinylogous urethane PE VITRIMERS.

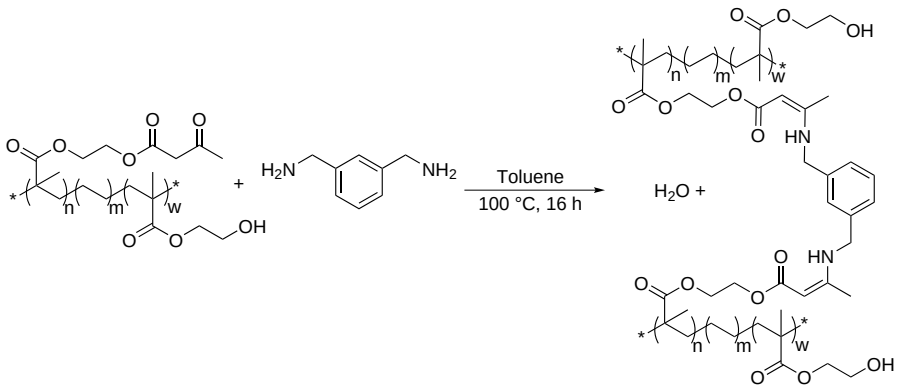

Only PACHE polymers obtained from transesterification of PE-HEMA were used for the prepration of vinylogous urethane PE VITRIMERS in solution, using this general procedure: Reaction was carried out under dry conditions. First, PACHE *co*-polymers were dissolved in toluene (50 mL) at 100 °C inside a glass reactor equipped with mechanical stirring. Then, the diamine cross-linker (0.6 eq with respect to ACAC units) was added drop wise *via* syringe. The reactor was closed with a septum and stirred overnight at 100 °C resulting in precipitation of a polymeric solid. The contents of the reactor were dropped into a beaker with methanol (200 mL) and stirred for 1 h. Filtering and drying of the solids gave the polymers as white to yellow

solids.

Reactive extrusion of vinylogous urethane PE VITRIMERS.

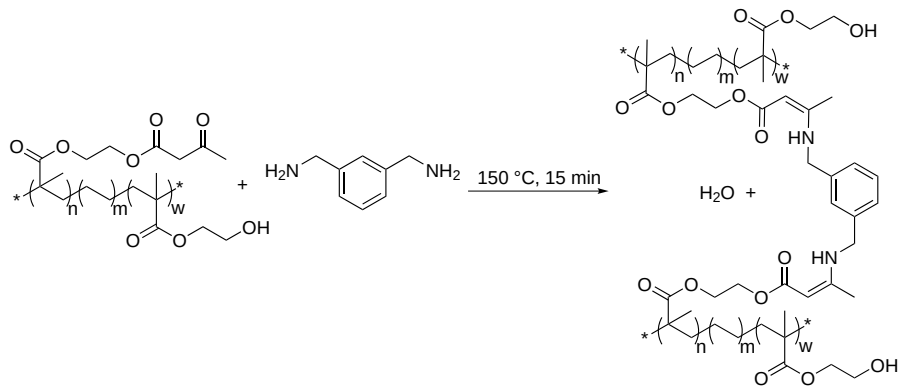

The PACHE *co*-polymers were fed inside a nitrogen flushed co-rotating twin-screw mini-extruder set to 150 °C, rotating at 100 rpm and molten until the observed torque exerted on the screws was constant (≈4 – 5 min). Then, the diamine cross-linker (0.55 eq with respect to ACAC units) was added drop wise *via* syringe and the combined materials were mixed until the observed torque remained constant (usually ≈10 min – 15 min). The hot polymer melt was then injection molded into suitable molds to prepare rectangular bars for DMTA, disks for rheology, and dog bones for tensile tests.

Reactive extrusion of DTA cross-linked PE.

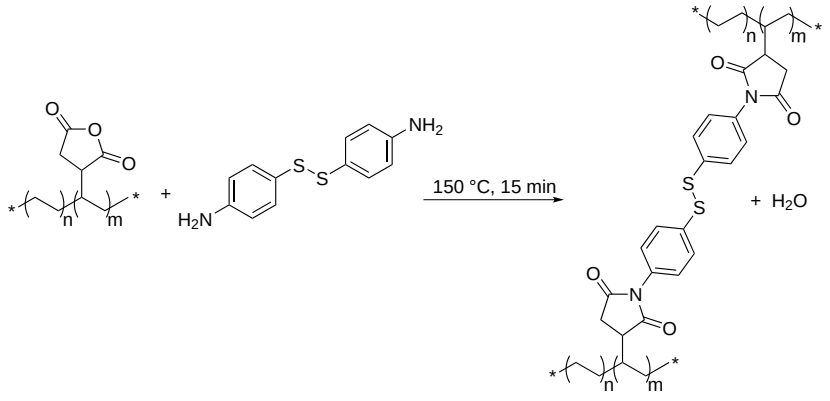

The synthesis for DTA cross-linked PE followed exactly the same approach used for vinylogous urethane PE VITRIMERS. Since DTA is a solid, it was added with a spatula instead of using a syringe. Suitable tests specimens for

DMTA and rheology were prepared by compression molding of the reacted polymer.

References

[1] G. B. Kauffman, *J. Chem. Educ.* **1986**, *63*, A181, DOI 10.1021/ed063pA181.1.

[2] R. Geyer, J. R. Jambeck, K. L. Law, *Sci. Adv.* **2017**, *3*, 1–5, DOI 10.1126/sciadv.1700782.

[3] L. A. Pruitt, *Biomaterials* **2005**, *26*, 905–915, DOI 10.1016/j.biomaterials.2004.03.022.

[4] S. Wannasri, S. V. Panin, L. R. Ivanova, L. A. Kornienko, S. Piriyayon, *Procedia Eng.* **2009**, *1*, 67–70, DOI 10.1016/j.proeng.2009.06.018.

[5] Y. Zhong, D. Janes, Y. Zheng, M. Hetzer, D. De Kee, *Polym. Eng. Sci.* **2007**, *47*, 1101–1107, DOI 10.1002/pen.20792.

[6] A. M. Walker, Y. Tao, J. M. Torkelson, *Polymer* **2007**, *48*, 1066–1074, DOI 10.1016/j.polymer.2006.12.038.

[7] A Bhattacharyya, S Chen, M Zhu, *Express Polym. Lett.* **2014**, *8*, 74–84, DOI 10.3144/expresspolymlett.2014.10.

[8] Y. Pietrasanta, J. J. Robin, N. Torres, B. Boutevin, *Mech. Time-Dependent Mater.* **1998**, *2*, 85–95, DOI 10.1023/a:1009756818443.

[9] M. Mauri, N. Tran, O. Prieto, T. Hjertberg, C. Müller, *Polymer* **2017**, *111*, 27–35, DOI 10.1016/j.polymer.2017.01.010.

[10] D. R. Paul, J. W. Barlow, *J. Macromol. Sci. Part C* **2007**, *18*, 109–168, DOI 10.1080/00222358008080917.

[11] B. Xu, J. Simonsen, W. E. Rochefort, *J. Appl. Polym. Sci.* **2000**, *76*, 1100–1108, DOI 10.1002/(SICI)1097-4628(20000516)76:7<1100::AID-APP14>3.0.CO;2-B.

[12] M. Lazar, R. Rado, J. Rychly in *Polym. physics. Adv. Polym. Sci. Vol. 95*, (Ed.: H. J. Cantow), Springer, Berlin, Heidelberg, **1990**, pp. 149–197, DOI 10.1007/3-540-52159-3_8.

[13] M. Mauri, L. Svenningsson, T. Hjertberg, L. Nordstierna, O. Prieto, C. Müller, *Polym. Chem.* **2018**, *9*, 1710–1718, DOI 10.1039/C7PY01840A.

[14] M. G. Teeter, X. Yuan, L. E. Somerville, S. J. MacDonald, R. W. McCalden, D. D. Naudie, *Can. J. Surg.* **2017**, *60*, 212–216, DOI 10.1503/cjs.005216.

[15] R. W. McCalden, S. J. MacDonald, C. H. Rorabeck, R. B. Bourne, D. G. Chess, K. D. Charron, *J. Bone Jt. Surgery-American Vol.* **2009**, *91*, 773–782, DOI 10.2106/JBJS.H.00244.

[16] C. A. Engh, A. S. Stepniewski, S. D. Ginn, S. E. Beykirch, C. J. Sychterz-Terefenko, R. H. Hopper, C. A. Engh, *J. Arthroplasty* **2006**, *21*, 17–25, DOI 10.1016/j.arth.2006.05.002.

[17] W. Denissen, J. M. Winne, F. E. Du Prez, *Chem. Sci.* **2015**, *7*, 30–38, DOI 10.1039/c5sc02223a.

[18] D. S. Achilias, C. Roupakias, P. Megalokonomos, A. A. Lappas, V. Antonakou, *J. Hazard. Mater.* **2007**, *149*, 536–542, DOI 10.1016/j.jhazmat.2007.06.076.

[19] W. Denissen, G. Rivero, R. Nicolaÿ, L. Leibler, J. M. Winne, F. E. Du Prez, *Adv. Funct. Mater.* **2015**, *25*, 2451–2457, DOI 10.1002/adfm.201404553.

[20] L. Imbernon, S. Norvez, *Eur. Polym. J.* **2016**, *82*, 347–376, DOI 10.1016/j.eurpolymj.2016.03.016.

[21] C. J. Kloxin, C. N. Bowman, *Chem. Soc. Rev.* **2013**, *42*, 7161–7173, DOI 10.1039/C3CS60046G.

[22] Y. Zhou, J. G. Goossens, R. P. Sijbesma, J. P. Heuts, *Macromolecules* **2017**, *50*, 6742–6751, DOI 10.1021/acs.macromol.7b01142.

[23] A. Demongeot, R. Groote, H. Goossens, T. Hoeks, F. Tournilhac, L. Leibler, *Macromolecules* **2017**, *50*, 6117–6127, DOI 10.1021/acs.macromol.7b01141.

[24] M. Röttger, T. Domenech, R. Van Der Weegen, A. Breuillac, R. Nicolaÿ, L. Leibler, *Science* **2017**, *356*, 62–65, DOI 10.1126/science.aah5281.

[25] W. Zou, J. Dong, Y. Luo, Q. Zhao, T. Xie, *Adv. Mater.* **2017**, *29*, 1606100, DOI 10.1002/adma.201606100.

[26] O. R. Cromwell, J. Chung, Z. Guan, *J. Am. Chem. Soc.* **2015**, *137*, 6492–6495, DOI 10.1021/jacs.5b03551.

[27] F. Du Prez, J. Winne, W. Denissen, L. Leibler, R. Nicolaÿ, COMPOSITIONS COMPRISING A POLYMERIC NETWORK (WO2016097169), **2016**.

[28] L. Zhou, G. Zhang, Y. Feng, H. Zhang, J. Li, X. Shi, *J. Mater. Sci.* **2018**, *53*, 7030–7047, DOI 10.1007/s10853-018-2015-z.

[29] C. M. Cormier, B. Wunderlich, *J. Polym. Sci.* **1967**, *5*, 987–988, DOI 10.1002/pol.1967.160050514.

[30] S. F. Edwards, H. Takano, E. M. Terentjev, *J. Chem. Phys.* **2000**, *113*, 5531–5538, DOI 10.1063/1.1290134.

[31] J. P. Brutman, P. A. Delgado, M. A. Hillmyer, *ACS Macro Lett.* **2014**, *3*, 607–610, DOI 10.1021/mz500269w.

[32] W. Denissen, I. De Baere, W. Van Paepegem, L. Leibler, J. Winne, F. E. Du Prez, *Macromolecules* **2018**, *51*, 2054–2064, DOI 10.1021/acs.macromol.7b02407.

[33] M. Guerre, C. Taplan, R. Nicolay, J. M. Winne, F. E. Du Prez, *J. Am. Chem. Soc.* **2018**, DOI 10.1021/jacs.8b07094.

[34] T. Stukenbroeker, W. Wang, J. M. Winne, F. E. Du Prez, R. Nicolaÿ, L. Leibler, *Polym. Chem.* **2017**, *8*, 6590–6593, DOI 10.1039/c7py01488k.

[35] L. Fontana, D. Q. Vinh, M. Santoro, S. Scandolo, F. A. Gorelli, R. Bini, M. Hanfland, *Phys. Rev. B - Condens. Matter Mater. Phys.* **2007**, *75*, 174112, DOI 10.1103/PhysRevB.75.174112.

[36] S. Goodyer, Measuring Polymers using a Rotational Rheometer in Oscillatory Mode Product Manager for Rheology, **2013**.

[37] H. H. Winter, *Macromol. Symp.* **2017**, *374*, 1600113, DOI 10.1002/masy.201600113.

[38] H. H. Winter, F. Chambon, *J. Rheol. (N. Y. N. Y).* **1986**, *30*, 367–382, DOI 10.1122/1.549853.

[39] J. Ghijsels, A.; Ente, J. J. S. M. and Raadsen, *Int. Polym. Process.* **1990**, *5*, 284–286, DOI 10.1017/CBO9781107415324.004.

[40] J. Ghijsels, A. and De Clippeleir, *Int. Polym. Process.* **1994**, *9*, 252–257, DOI 10.3139/217.940252.

[41] L. Imbernon, S. Norvez, L. Leibler, *Macromolecules* **2016**, *49*, 2172–2178, DOI 10.1021/acs.macromol.5b02751.

[42] D. Montarnal, M. Capelot, F. Tournilhac, L. Leibler, *Science* **2011**, *334*, 965–968, DOI 10.1126/science.1212648.

[43] W. Denissen, M. Droesbeke, R. Nicola, L. Leibler, J. M. Winne, F. E. Du Prez, *Nat. Commun.* **2017**, *8*, 14857, DOI 10.1038/ncomms14857.

[44] Y. Nishimura, J. Chung, H. Muradyan, Z. Guan, *J. Am. Chem. Soc.* **2017**, *139*, 14881–14884, DOI 10.1021/jacs.7b08826.

[45] J. C. Dyre, *Rev. Mod. Phys.* **2006**, *78*, 953–972, DOI 10.1103/RevModPhys.78.953.

[46] N. H. Ladizesky, I. M. Ward, *J. Macromol. Sci. Part B* **1971**, *5*, 661–692, DOI 10.1080/00222347108224781.

[47] R. J. Friary, V. Seidl, J. H. Schwerdt, T. M. Chan, M. P. Cohen, E. R. Conklin, T. Duelfer, D. Hou, M. Nafissi, R. L. Runkle, P. Tahbaz, R. L. Tiberi, A. T. Mc Phail, *Tetrahedron* **1993**, *49*, 7179–7192, DOI 10.1016/S0040-4020(01)87197-0.

[48] K. Ostrowska, M. Ciechanowicz-Rutkowska, T. Pilati, G. Zżuchowski, *Monatshefte für Chemie / Chem. Mon.* **1999**, *130*, 555–562, DOI 10.1007/PL00010234.

[49] H. Otsuka, S. Nagano, Y. Kobashi, T. Maeda, A. Takahara, *Chem. Commun.* **2010**, *46*, 1150–1152, DOI 10.1039/B916128G.

[50] A. Ruiz de Luzuriaga, R. Martin, N. Markaide, A. Rekondo, G. Cabañero, J. Rodríguez, I. Odriozola, *Mater. Horiz.* **2016**, *3*, 241–247, DOI 10.1039/C6MH00029K.

[51] N. G. Gaylord, M. K. Mishra, *J. Polym. Sci. Polym. Lett. Ed.* **1983**, *21*, 23–30, DOI 10.1002/pol.1983.130210104.

[52] R. M. Ho, A. C. Su, C. H. Wu, S. I. Chen, *Polymer* **1993**, *34*, 3264–3269, DOI 10.1016/0032-3861(93)90400-5.

[53] N. G. Gaylord, M. Mehta, *J. Polym. Sci. Part C Polym. Lett.* **1982**, *20*, 481–486, DOI 10.1002/pol.1982.130200903.

[54] M. Zhang, R. H. Colby, S. T. Milner, T. C. Chung, T. Huang, W. Degroot, *Macromolecules* **2013**, *46*, 4313–4323, DOI 10.1021/ma4006632.

[55] M. Abbasian, M. Shahparian, S. E. S. Bonab, *J. Elastomers Plast.* **2013**, *45*, 317–331, DOI 10.1177/0095244312452271.

[56] L. Feng, M. R. Kamal, *Can. J. Chem. Eng.* **2004**, *82*, 1239–1251, DOI 10.1002/cjce.5450820611.

Appendix D

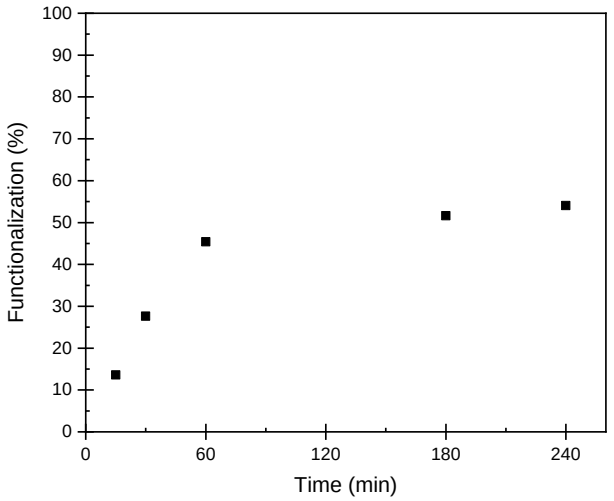

Figure D.1: Degree of functionalization of PACHEtr96 (determined by NMR) for the transesterification of PE-HEMA with methyl acetoacetate as a function of reaction time.

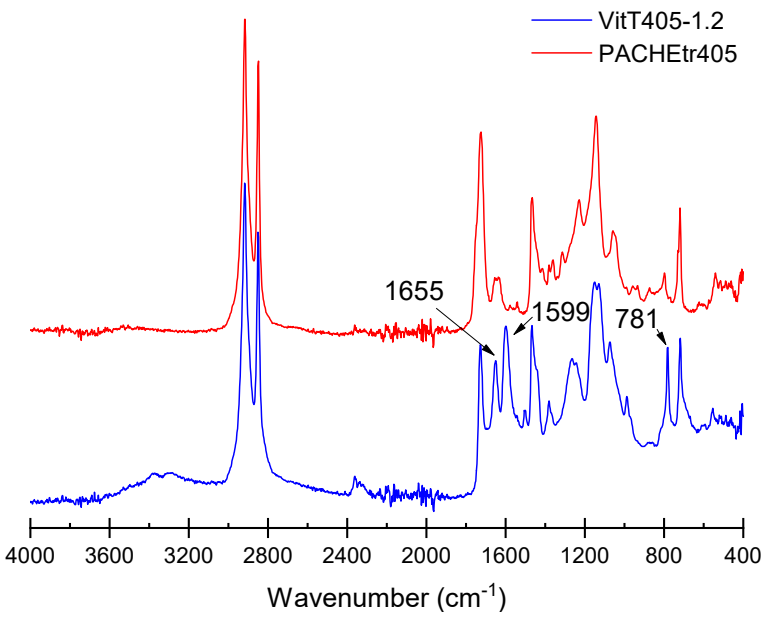

Figure D.2: FTIR absorption spectrum of VitT405-1.2 (blue line) and PACHEtr405 (red line).

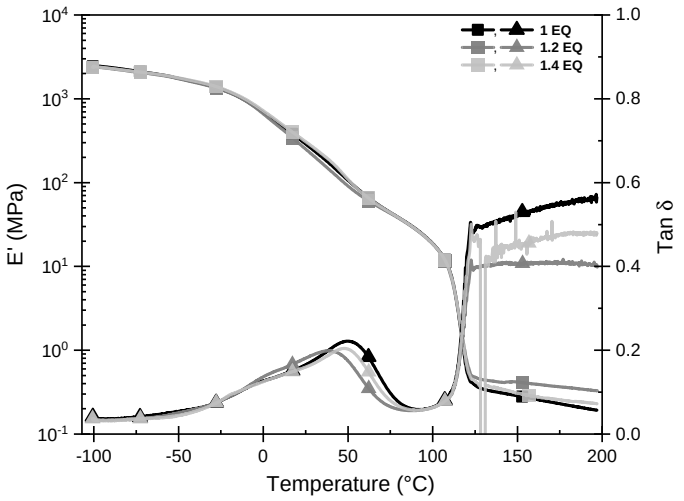

Figure D.3: DMTA screening of VitT96-1.0 (black line), VitT96-1.2 (grey line), and VitT96-1.4 (light grey line) between 100 °C and 200 °C. Square symbols represent data points for E', triangle symbols data points for Tan δ.

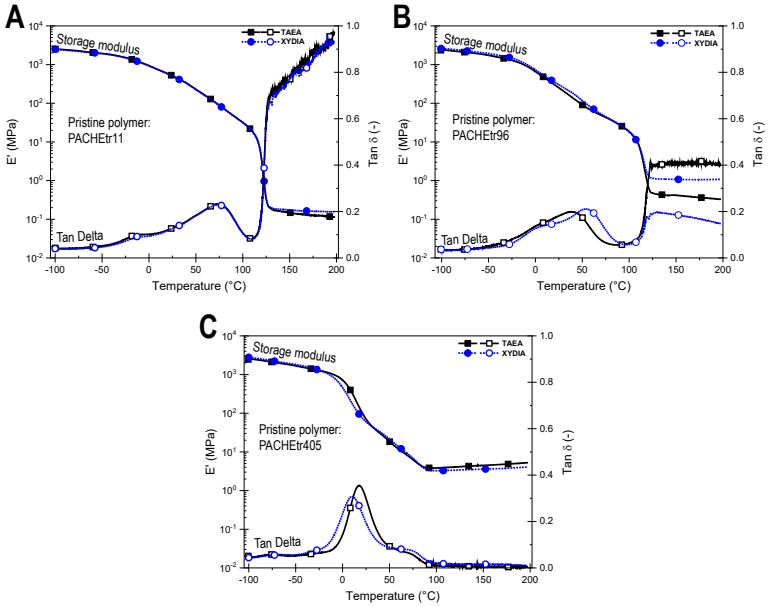

Figure D.4: DMTA comparison of XYDIA and TAEA cross-linked PACHEtrans polymers. Specifically, **A**: VitX11-1.2 and VitT11-1.2, **B**: VitX96-1.2 and VitT96-1.2, and **C**: VitX405-1.2 and VitT405-1.2. Closed symbols represent data points for E', open symbols data points for Tan δ.

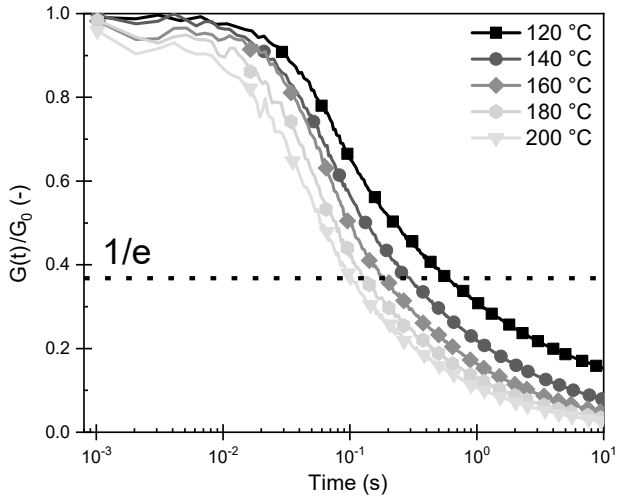

Figure D.5: Normalized stress-relaxation data of VitX11-1.2 as function of time and temperature.

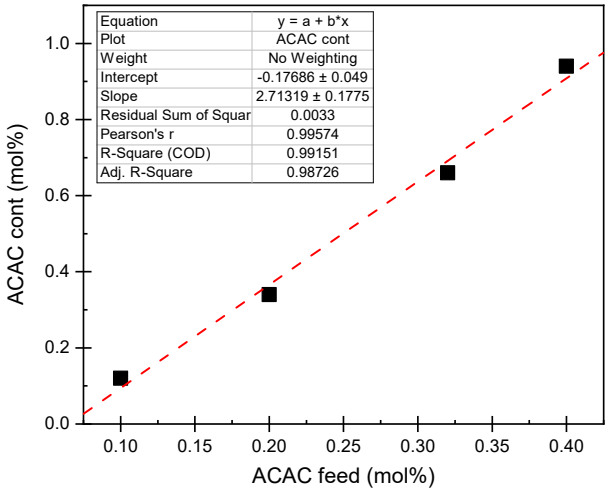

Figure D.6: Plot of incorporated ACAC (in mol%) as function of *co*-monomer feed (in mol%). The linear relationship is revealed by the fit represented by the red line.

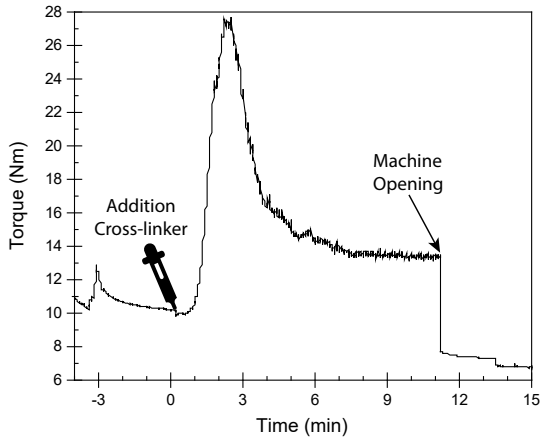

Figure D.7: Torque exerted on extruder screws as a function of reaction time. At 0 min, indicated by the syringe, the cross-linker was added to the polymer melt. Opening of the extruder leads to a sudden torque drop highlighted by the arrow.

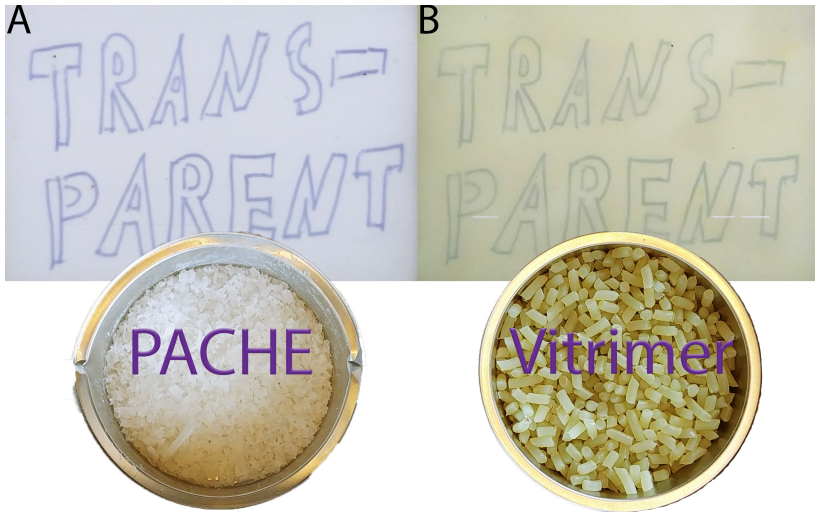

Figure D.8: Examples of compression molded films over poorly sketched spelling of "transparent" on the top and picture of powdered and pelletized polymer samples (**A**: PACHE polymers; **B**: VITRIMER samples).

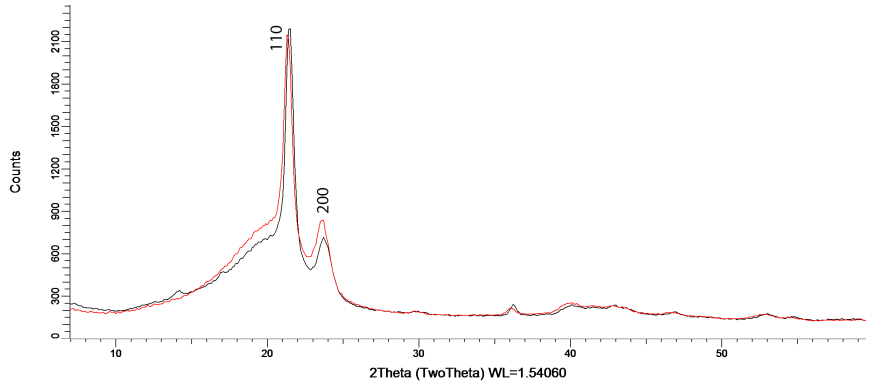

Figure D.9: WAXD patterns recorded from (LD)PE (black line) and VitX2.6 (red line). In both cases the characteristic (110) and (200) diffraction maxima are present,[35] corroborating that the crystalline parts of the VITRIMER are made up solely of PE and that the crystalline character is retained.

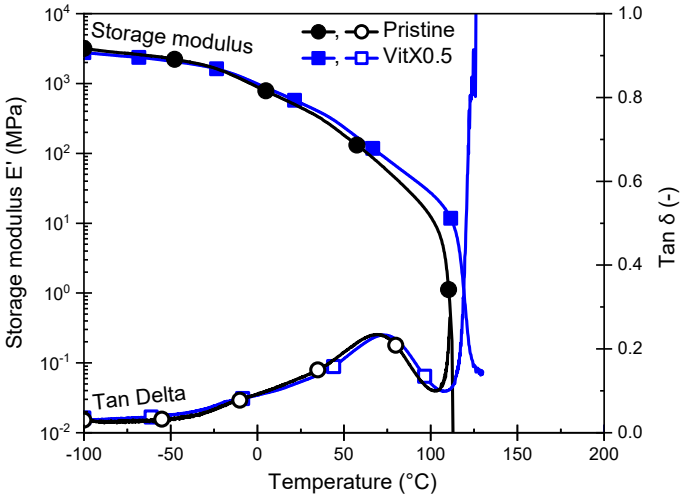

Figure D.10: DMTA screening of pristine (black lines) and VitX0.5 (blue lines) between -100 °C and 200 °C. Close symbols represent data points for E', open symbols data points for Tan δ.

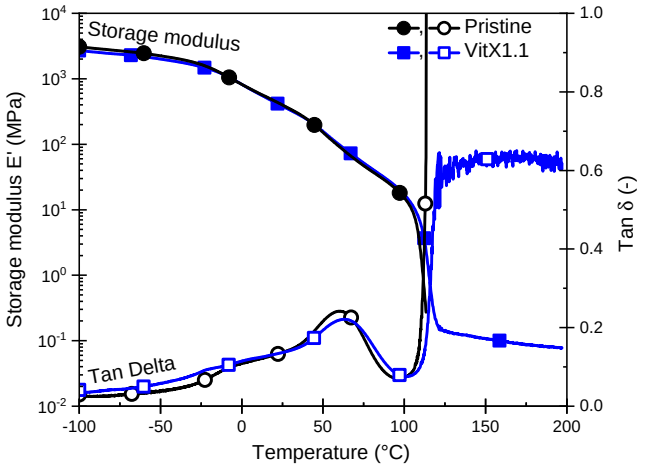

Figure D.11: DMTA screening of pristine (black lines) and VitX1.1 (blue lines) between -100 °C and 200 °C. Close symbols represent data points for E', open symbols data points for Tan δ.

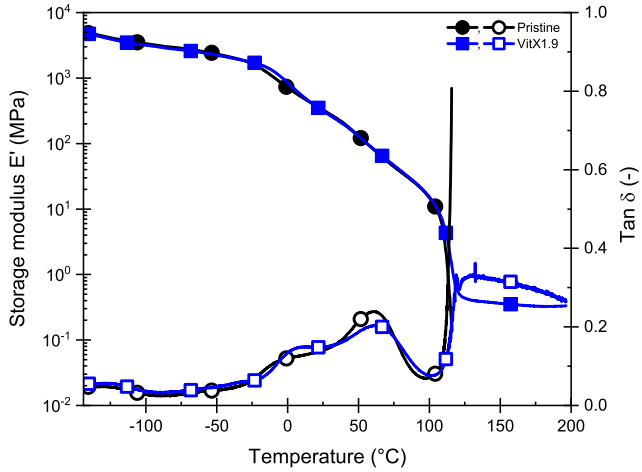

Figure D.12: DMTA screening of pristine (black lines) and VitX1.9 (blue lines) between -140 °C and 200 °C. Close symbols represent data points for E', open symbols data points for Tan δ.

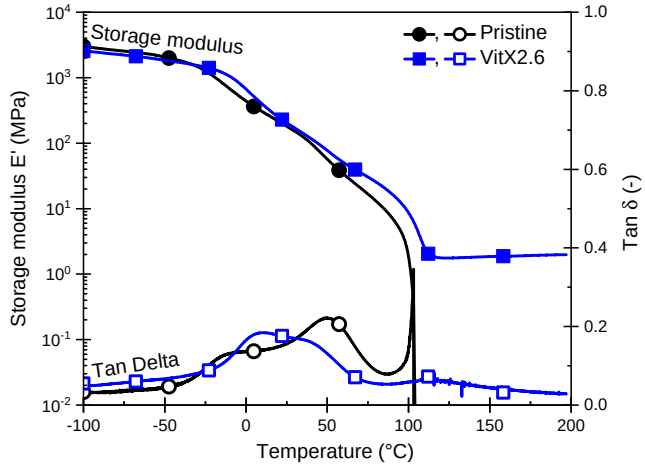

Figure D.13: DMTA screening of pristine (black lines) and VitX2.6 (blue lines) between -100 °C and 200 °C. Close symbols represent data points for E', open symbols data points for Tan δ.

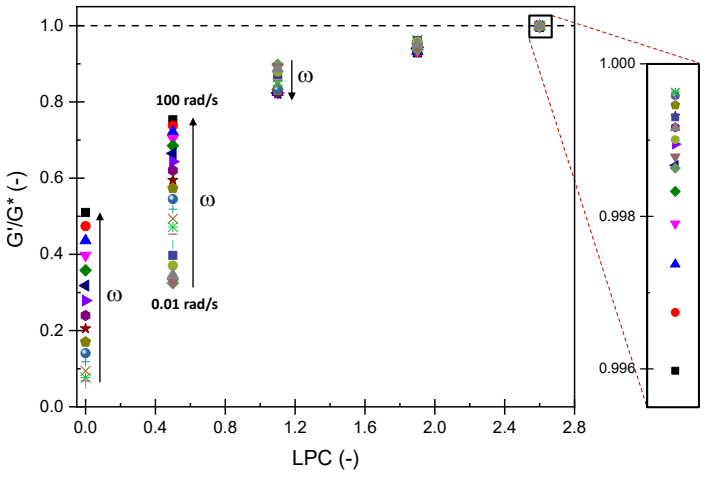

Figure D.14: Plot of the normalized storage modulus (G' divided by G*, or G'/G*) at different frequencies (0.01 rad·s^{-1} → 100 rad·s^{-1}) versus LPC of VITRIMER samples VitX0.5, VitX1.1, VitX1.9, and VitX2.6. Pristine sample of VitX1.1 displayed as reference (0 LPC). Arrows highlight the direction of frequencies. Black box on the right depicts the enlarged view of data points for VitX2.6.

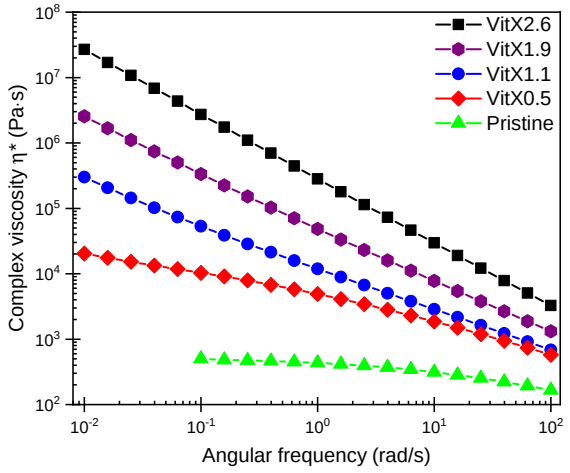

Figure D.15: Plot of the complex viscosity versus angular frequency for VITRIMERS VitX0.5 (red line), VitX1.1 (blue line), VitX1.9 (purple line), and VitX2.6 (black line). The pristine polymer of Vit1.1 is displayed as a reference for a typical polymer melt (in green).

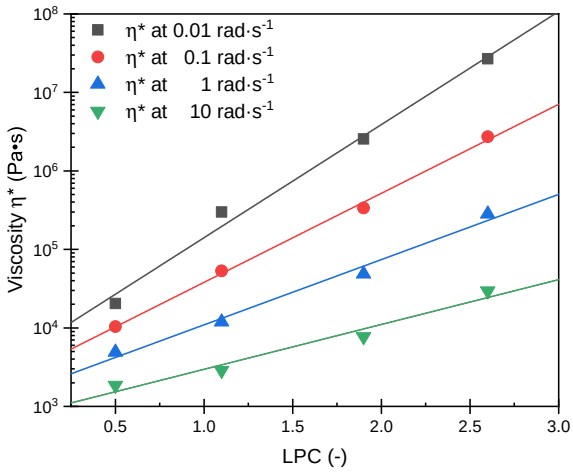

Figure D.16: Complex viscosity η^* as function of LPC for different shear rates.

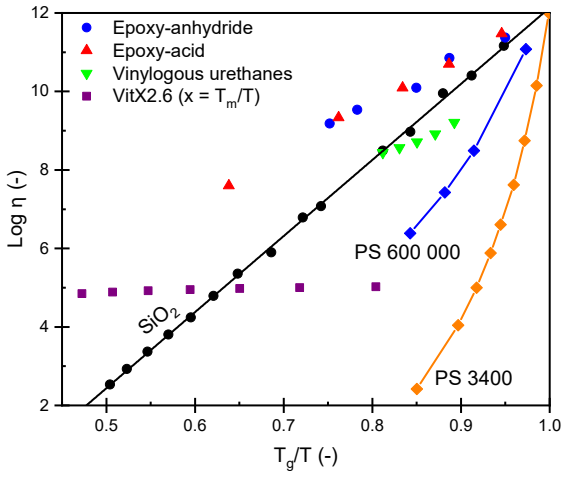

Figure D.17: Viscosity data of VitX2.6 inserted into the Angell fragility plot presented in Section 1.3.2. Data obtained between 120 °C and 220 °C at a constant frequency of 1 rad·s^{-1} and a strain amplitude of 0.4 %. Temperature of VitX2.6 is scaled with T_m instead of T_g because of the semi-crystalline nature of the polymer.

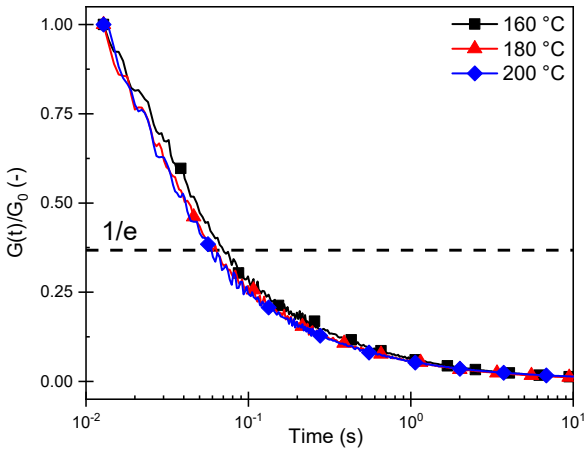

Figure D.18: Normalized stress relaxation of VitX0.5 as function of time and temperature.

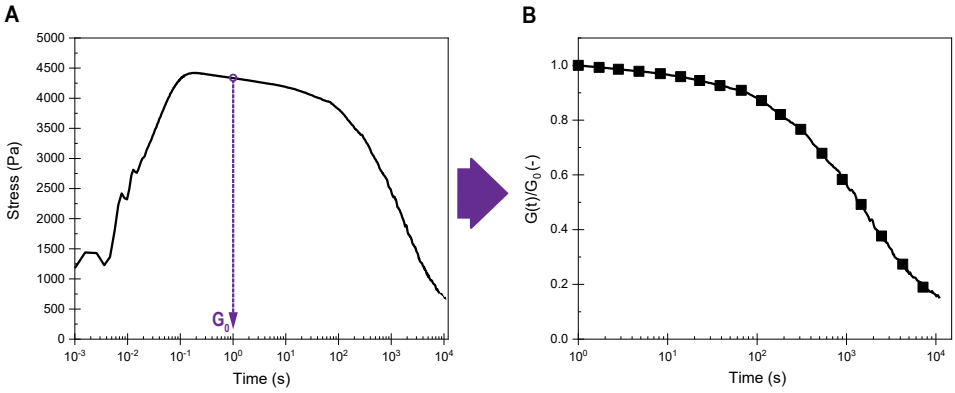

Figure D.19: **A**: Treatment of raw stress-relaxation curves to obtain normalized spectrum. G_0 selected at t = 1 s for exchange reaction-controlled relaxation. **B**: Normalized treated relaxation curve.

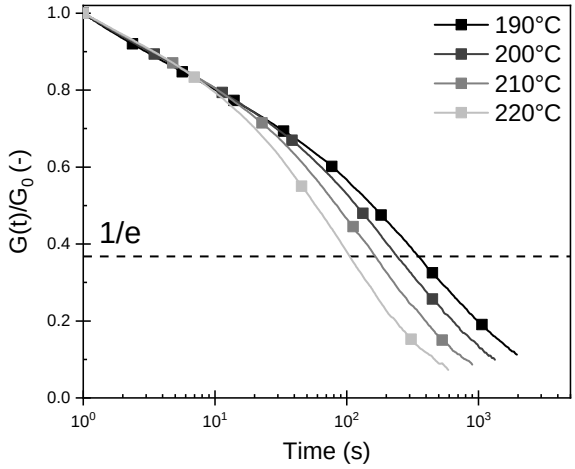

Figure D.20: Normalized stress relaxation of VitX1.9 as function of time and temperature.

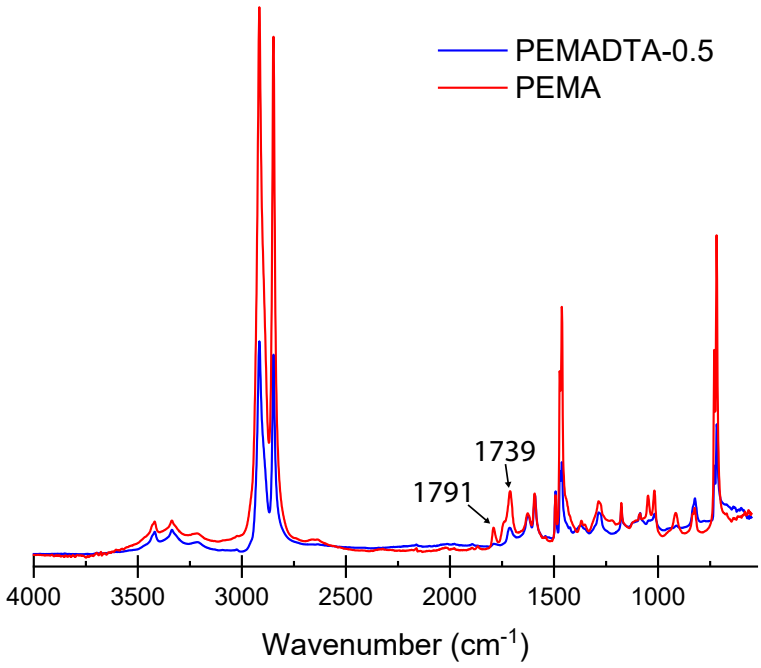

Figure D.21: FTIR absorption spectrum of PEMADTA-0.5 (blue line) and PE-MA (red line).

Chapter 6

Epilogue

6.1 Afterword

Within the scope of this thesis, alternative methods to the static cross-linking of polymers (thermosets) were to be explored. Thermosets find application in demanding applications such as aerospace and automotive due to their solvent resistance, thermal stability, and their superior mechanical properties. However, due to the presence of irreversible cross-links in the legacy systems, they lose the ability to be reprocessed. Here is where dynamic cross-links could provide an advantage. No matter the type, all dynamic cross-links share that polymer networks build up from these cross-links are able to adapt to external stresses. Commonly, certain conditions are met such as temperature triggered exchange reactions or reversible supramolecular bonds to initiate the adaptation.[1]

Three methods were investigated, multiple hydrogen bonding, solvophobic, and covalent adaptable networks. Out of these, we will only highlight the multiple hydrogen bonding and dynamic covalent exchange, due to the limited data-set of the material employing solvophobic interactions. In Figure 6.1 the DMTA data of VitX1.9 and VitX 2.6 from Chapter 5 are plotted together with the data of ODIN functionalized PE-HEMA polymer **P2** from Chapter 3. Naturally, the graphs look very different due to the different X_c between the polymers. However, after melting of the polymers the main difference is the type of cross-linking, as their molecular weight is similar with 9.7 (VitX1.9), 9.5 (VitX2.6), and 13.5 Kg·mol^{-1} (**P2**). Consequently,

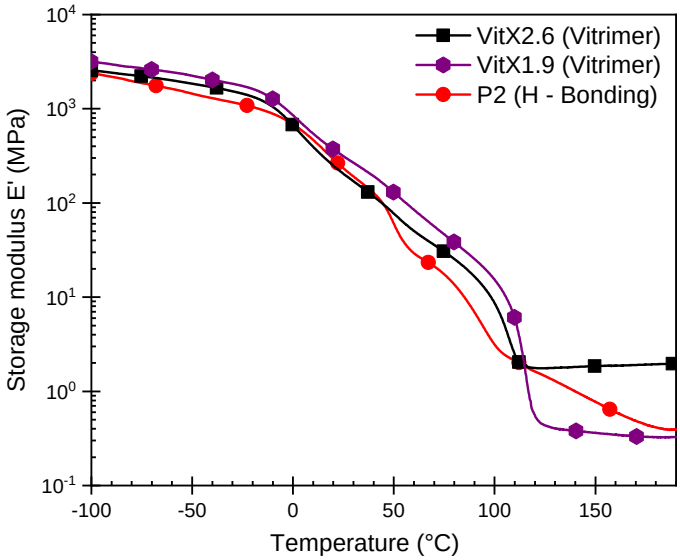

Figure 6.1: Comparison of DMTA data of VitX1.9, VitX 2.6, and ODIN functionalized PE-HEMA polymer **P2**.

the following discussion of the main differences between the two focuses on the moduli observed after melting of the polymer crystals.

Even though the cross-links are adaptable, a constant plateau modulus is observed for the VITRIMER networks VitX1.9 and VitX2.6, because the network density is constant at all times (excluding degradation). As mentioned in Chapter 5, this is because new cross-links can only be formed after association of another species to an existing cross-link moiety. On the contrary, due to the progressive dissocation of the multiple hydrogen bonding moieties with temperature,[2] the modulus of **P2** is found to drop from the level of VitX2.6 directly after melting to the value of VitX1.9. This trend was elegantly illustrated choosing the data of **P2**, because the observed E' nicely fits within that of the VITRIMER samples. However, generally the polymers cross-linked with multiple hydrogen bonding show a decrease in E' with increasing temperature in a similar manner to **P2**.

The network characteristics using those cross-linking methods are therefore fundamentally different. Using CAN chemistry results in networks with

all the characteristics of a classical thermoset (insolubility, mechanical properties), but with the added advantage that specimens made thereof can be reprocessed. However, because the network density is constant it is unlikely or significantly more difficult to design a system that can be processed at the same rate as a conventional thermoplastic, simply because on top of chain diffusion there is the additional requirement for a reaction to take place for chains to adapt.

Here, depolymerization networks such as those comprised of cross-links using DIELS-ALDER chemistry or non-covalent interactions have an advantage, because in principle the network can be completely reversed so that chain diffusion will control the polymer flow behavior. This comes at a cost of properties, as these systems should be soluble at higher temperature in solvents that are good for the base polymer (the polymer that makes up the backbone).

6.2 Way forward

Within this thesis, it was demonstrated that polymer networks with dynamic cross-links can be processed using conventional thermoplastic processing methods. In the previous section, we briefly discussed the fundamental differences between covalent adaptable and supramolecularly cross-linked networks. Going forward, actual products need to be benchmarked versus adaptable cross-linked polymers. Investigating the long term stability of the cross-linking types will play a key role. For example, an average lifetime of polymer tubing, which is generally cross-linked (HD)PE, or PEX, is given to be at ≈40 – 50 years. Although most manufacturers give a warranty of 25 years.[3] During its lifetime, these tubes are constantly subjected to water and even chlorinated cleaning chemicals.[4] The effect of actual long term use has thus far been neglected. Clearly, materials made from these adaptable networks need to be subjected to experiments that mimic long term exposure to the environment of actual use. If the material holds up, the resilience of the functional groups to these long term stress tests needs to be investigated by confirming the processability. Only if that is guaranteed, will using this new technology really be feasible.

That being said, from a producer standpoint it might already be lucrative to sell a cross-linked polymer that can be processed into a desired shape, eliminating the need for an additional post curing step to obtain a cross-linked material. Especially for PE this is of interest in order to avoid long degassing times required after cross-linking with peroxides.[5]

References

[1] L. Imbernon, S. Norvez, *Eur. Polym. J.* **2016**, *82*, 347–376, DOI 10.1016/j.eurpolymj.2016.03.016.

[2] R. P. Sijbesma, F. H. Beijer, L Brunsveld, B. J. Folmer, J. H. Hirschberg, R. F. Lange, J. K. Lowe, E. W. Meijer, *Science* **1997**, *278*, 1601–1604, DOI 10.1126/science.278.5343.1601.

[3] PEX Tubing: Myths and Facts, https://www.pexuniverse.com/pex-myth-and-facts (visited on 11/06/2018).

[4] T. Gill, R. Knapp, S. Bradley, W. Bradley, *ANTEC 1998 Plast. Plast. My Mind* **1998**, *3*, 1–5, DOI 10.1179/146580199101540448.

[5] M. Mauri, N. Tran, O. Prieto, T. Hjertberg, C. Müller, *Polymer* **2017**, *111*, 27–35, DOI 10.1016/j.polymer.2017.01.010.

Acknowledgements

I would like to acknowledge the European Union for funding this Ph.D. under the European Union's Horizon 2020 research and innovation programme (Marie Skłodowska-Curie grant agreement No. 642929 – SUPRABARRIER project). The opportunities provided by these types of grants are plentiful and this particular one provided an excellent experience and education for me.

I would also like to thank my supervisors for their outstanding contribution to this thesis and to my personal development. Specifically, I would like to thank my supervisors from the University of Parma, Enrico Dalcanale and Roberta Pinalli, for their management of the project, guidance, discussions, always having an open door, and great group dinners. Then, I would like to thank my supervisors from SABIC Maria Soliman and Jérôme Vachon. Maria for her great suggestions, guidance, and for demanding just a little bit more. Jérôme, thank you for all the tips, suggestions, jokes, all the tedious paperwork that you have done, and for being an all around great person.

I would like to thank the many people at SABIC that provided a great body of work over these last three years. Doing a lot of the groundwork, I would like to thank Estelle Poulet and Deliani Lovera for their direct support and management at Sabic. I would like to thank Peter Neuteboom, Diego Castaneda, and Jan Duchateau from the (LD)PE team for providing the *co*-polymers used in this thesis. Also, the support from the analytical team from BOZ is greatly appreciated. I would also like to acknowledge Brian Marwi, Maurice Wijers, Peter Streutjens, Maurice Dohmen, and Jos Verhaeren from the processing laboratory. I would like to thank Anantharaman Dhanabalan, Rukmini Khatokar, Abbas Alli G Shaikh, and Earath Sunil from STC Bangalore for taking excellent care of my colleague Arek and I during our

two months stay in Bangalore.

I would like to thank the Group of Prof. Rint Sijbesma for their hospitality during my two Months stay at the Eindhoven University of Technology. I would like to especially thank my "colleague in crime" from the SUPRABARRIER project Arkadiusz Zych for all his help, amazingly dry humor, and deeply philosophical discussion at the Oasis of STC Bangalore.

Then, I would like to acknowledge all the other people from the University of Parma. First, I want to acknowledge Stefano for his excellent work on elucidating the crystal structure of ODIN that led to our joint publication. I would like to acknowledge all the fun Ph.D. students from the other groups, especially those fortunate enough to work with Prof. Secchi who is not shy to join an aperitivo or two. I want to thank my group for all the fun moments we shared. Especially Federico, who showed me around Parma and provided me with countless ridiculous moments. You made my first weeks especially easy. I want to thank Elisa for giving me tips on how to make that beast of a cavitand during my initial months of the Ph.D.. I want to thank you Alessandro for all your help and top notch volleyball matches. A huge thanks goes to you Andreas for all the pies, Swiss jokes, and provision of amazing stories. May you always be able to avoid Durian and indecent behavior.

Lastly, my thanks goes out to my girls Anjali and Francesca. You truly made these years some of the best in my life. All the evenings trying to find out who the best Geisha is, eating amazing home cooked Italian and Indian food (I am still waiting for the "fusion"), watching stupid movies, and discussing the gossip of the month were extremely fun. I loved going on vacation with you guys and cannot wait for the next one. I could not have hoped for funnier, kinder, and better friends.

Outreach

Until now, the contents of this thesis contributed to the following publications:

Peer-reviewed journal publications:

- **Tellers, Jonathan**; Canossa, Stefano.; Pinalli, Roberta; Soliman, Maria; Vachon, Jérôme; Dalcanale, Enrico, *Macromolecules* **2018**, *51* (19), 7680–7691, DOI: 10.1021/acs.macromol.8b01715.
- **Tellers, Jonathan**; Zych, Arkadiusz; Neuteboom, Peter; Pinalli, Roberta; Soliman, Maria; Vachon, Jérôme; Dalcanale, Enrico. PE-HEMA as adhesion coating. In preparation.
- **Tellers, Jonathan**; Pinalli, Roberta; Soliman, Maria; Vachon, Jérôme; Dalcanale, Enrico. Polyethylene Vitrimers *via* Reactive Extrusion. To be submitted.

Patents and Patent applications

- Jérôme Vachon, Estelle Julie Mathilde Poulet, Maria Soliman, Arkadiusz Zych, Enrico Dalcanale, Roberta Pinalli, and **Jonathan Tellers**. GAS BARRIER FILM. PCT/EP2018/072316. patent pending.
- Jérôme Vachon, Peter Neuteboom, Maria Soliman, Enrico Dalcanale, Roberta Pinalli, and **Tellers, Jonathan**. POLYOLEFIN TERPOLYMERS, VITRIMERS MADE THEREFROM, AND METHOD OF MAKING THE POLYOLEFIN TERPOLYMERS AND VITRIMERS. SABA.P0349US.P1. patent pending.

Conferences

- Dynamic Cross-Linking of Polyethylene *via* Sextuple Hydrogen Bonding Array. **Jonathan Tellers**, Stefano Canossa, Roberta Pinalli, Maria Soliman, Jérôme Vachon, and Enrico Dalcanale. *Frontiers in Chemistry* ARCHEMFRONT, Armenia, Oct. **2018**. The poster won the 1st prize poster award (sponsored by the journal *molecules*).

Schools

- TBU Summer School – Polymer functionalization and processing, Tomas Bata University in Zlín, Czech Republic **2017**.
- School – Amherst Rheology Course, University of Luxembourg, Campus Limpertsberg in Luxembourg City, Luxembourg **2018**.
- Ph.D. Summer School – Scientists have to be great communicators, Kaunas University of Technology in Palanga, Lithuania **2018**.